IRE Transactions

n Microwave Theory and Techniques

Volume MTT-5 **OCTOBER, 1957** Number 4

In This Issue

For complete Table of Contents, see page 221.

PUBLISHED BY THE

fessional Group on Microwave Theory and Techniques

IRE PROFESSIONAL GROUP ON MICROWAVE THEORY AND TECHNIQUES

The Professional Group on Microwave Theory and Techniques is an association of IRE members with professional interest in the field of Microwave Theory and Techniques. All IRE members are eligible for membership and will receive all Group publications upon payment of the prescribed annual assessment of $3.00. Members of the American Physical Society may become affiliated with PGMTT and receive all Group publications upon payment of the Affiliate assessment of $7.50 per year.

IRE TRANSACTIONS®

on Microwave Theory and Techniques

Published by the Institute of Radio Engineers, Inc., for the Professional Group on Microwave Theory and Techniques, at 1 East 79th Street, New York 21, New York. Responsibility for the contents rests upon the authors, and not upon the IRE, the Group, or its members. Price per copy: IRE PGMTT members, $1.20; IRE members, $1.80, nonmembers, $3.60. Annual subscription price: IRE members, $8.50; colleges and public libraries, $12.75; nonmembers, $17.00.

Address all manuscripts to K. Tomiyasu, PGMTT Editor, General Electric Microwave Laboratory, 601 California Ave., Palo Alto, Calif. Submission of three copies of manuscripts, including figures will expedite the review.

IRE Transactions on Microwave Theory and Techniques

Published by the Professional Group on Microwave Theory and Techniques

Volume MTT-5 OCTOBER, 1957 Number 4

TABLE OF CONTENTS

Message from the Editor

In the preceding issue Herbert F. Engelmann, past Chairman of the PGMTT, expressed indebtedness to and congratulated Theodore S. Saad who for three years as editor devoted tireless efforts in building up the IRE TRANSACTIONS ON MICROWAVE THEORY AND TECHNIQUES to a highly technical and valuable publication. I wish to take this opportunity to endorse heartily this congratulation and to express hope that the high publication standard can be maintained.

We are particularly pleased to present and to honor in this issue Dr. Wilmer L. Barrow as our distinguished microwave personality. His numerous contributions to microwave theory and techniques are well known and his interesting editorial speaks for itself.

During the past few months we have increased the staff of our Editorial Board from 12 to 28. With this increase we have been able to decrease the paper reviewing load per member and to devote more time to each review. It is intended that the Board represent a cross section of the PGMTT membership in matters of editorial policy. Any comments or criticisms you may have are always welcome. On behalf of the PGMTT, I wish to express appreciation to the Board members who have generously accepted these responsibilities.

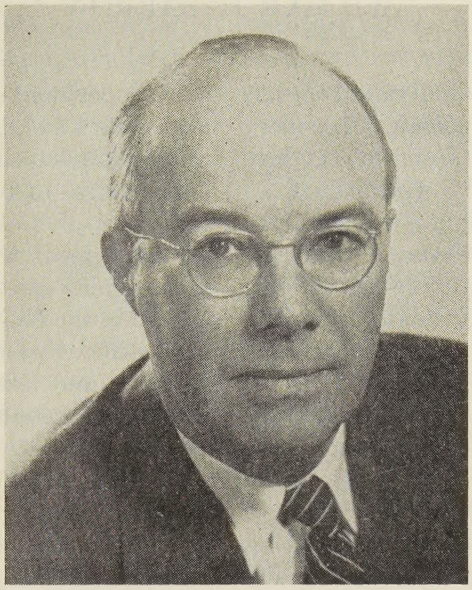

Wilmer L. Barrow

Wilmer L. Barrow is Vice-President for Research and Development of the Sperry Gyroscope Company, following previous appointments as Sperry's Chief Engineer in 1947 and as Vice-President in 1952. Formerly, he was on the faculty of Massachusetts Institute of Technology under wartime emergency as Director of Fire Control in 1943, and Director of Armament Engineering in 1945.

Dr. Barrow was born in Baton Rouge, La., on October 25, 1903. He received the B.S.E.E. degree from Louisiana State University and the M.S. degree in electrical communications from M.I.T. He was a Redfield Proctor Fellow in physics at the Technische Hochschule in Munich, Germany where he received the Sc.D. degree in 1931.

For the next twelve years he was on the staff of the Electrical Engineering Department at M.I.T. where he taught courses in electrical communications and did research principally in microwave technology and its applications. He was also Director of the M.I.T. Radar School.

From his research activities at M.I.T. and at Sperry have come twenty-four American and several foreign patents. He has published a number of papers, some jointly with his students.

Dr. Barrow served in advisory capacities to the armed forces and the National Defense Research Committee during World War II. His duties included membership in committees on fire control, bombing, and air traffic control under the Secretary of War. He was also Chairman of the Radar Panel, Research and Development Board, and a member and later Chairman of the Technical Consulting Group Committee on Guided Missiles. He was awarded the Certificate for Merit by the President for wartime contributions to radar.

Dr. Barrow has been active in the IRE since 1928. He has held membership in many committees, has served on the Board of Directors, and was Chairman of the IRE Convention in Boston in 1940. He was awarded the Morris Liebmann Memorial Prize in 1943, for his contributions to the waveguide and microwave art.

He is a Fellow of the American Academy of Arts and Sciences, and Sigma Xi, and an active member of the American Management Association, American Ordnance Association, American Rocket Society, Armed Forces Communications and Electronics Association, Association of Research Directors, Industrial Research Institute, and Institute of Aeronautical Sciences.

Yesteryear—Tomorrow

WILMER L. BARROW

IT IS an exciting experience for an individual to participate in the birth of a new technological discovery and then to live to see it develop from infancy into a mature and important factor in the world. Such an experience comes unexpectedly to only a few lucky individuals and then usually once in a lifetime. I have always considered myself fortunate to have shared this kind of experience with a few other fortunate persons in the opening up and growth of the modern microwave industry.

Classical electromagnetic theory was established by Maxwell and transmission and reception at microwave frequencies had been demonstrated by Hertz prior to the year 1900. Nonetheless, the practical possibilities of this region of the spectrum were not appreciated during the early part of the twentieth century. Interest, development, and commercialization were then completely in the lower frequency region. Those of us who directed our scientific careers at that time toward the vacant land of microwaves had to go it pretty much alone.

There was, of course, good reason for the lack of interest and activity in the applications of microwaves. Although there were a few ideas that certain applications would be worthwhile, such as point-to-point communication and aids to air navigation, certain others could not be fully visualized, or if foreseen, could not be properly evaluated. But a really practical solution seemed far away indeed.

There were no satisfactory generators of microwave power. The receiver art was no further advanced than that of the simple detector. Means of conducting energy about, or of radiating it into space, or receiving it, were in a preprimitive state. And the equivalents of circuit elements, bridges, filters, and so on, that make sophisticated communications systems possible, were totally missing. Thus, a complete new technology had to emerge in order for the many applications to change from the dream stage to one of practical and economic reality.

The decade from *1930 to 1940* might well be termed the *Period of Discovery* of the modern microwave technology. It is largely in this period that the basic contributions were made on which later progress was built.

How did one get started in this Period of Discovery of microwaves? I had best give you some personal experiences here, but I suspect that the situation was more or less the same for Southworth, Schelkunoff, Hansen, the Varians, Hahn, Metcalf, Wolf, Chu, and the others.

Firstly, there was *the scientific urge*. For me, this was a burning desire to understand thoroughly and basically the theory of radio wave propagation. I am sure that such a personal urge must be present in anyone who undertakes Columbus-like voyages into uncharted and unpopulated technological areas.

Secondly, there was *the preparation*. More than the teachings of undergraduate courses was necessary. It did not appear, when my education was under way, that the teaching of electromagnetic theory was done nearly as well in the United States as it was in Germany. Thus, it was that I went to the latter country to study under Zenneck and Sommerfeld. Today, or at any time, a sound and careful preparation is a necessary task for anyone who sets his sails on a voyage of discovery. It may be carried out in any of several ways, but certainly today more than ever before, a sound theoretical background is necessary for advanced work in microwaves.

Finally, there was *discovery productivity*. Back at M.I.T. in 1931, the problem of why electromagnetic waves could not be sent from a horn of metal—the corresponding device to an acoustical horn—appeared to me to be an important unanswered scientific question. The first attack on this problem was theoretical and because of the complexities, no solution was obtained immediately. However, these efforts suggested the query as to why could not electromagnetic waves that might radiate from the large end of the horn be led into its small end through a conducting hollow metal pipe—corresponding to an acoustical speaking tube. The mathematics here were easier and in 1932, the answer was found to be *yes*, they could be transmitted through a pipe with finite losses, provided a certain critical frequency was exceeded. Shortly, thereafter, the horn problem also gave a favorable answer.

Today, it is hard to realize that at that time only a few individuals were prepared to accept the reality of waveguide transmission and horn radiation, largely because of the absence of a second conductor, theretofore considered essential in any electrical circuit or transmission line. It was clear that a demonstration would be necessary before much attention could be attracted to this new transmission technique.

It proved to be harder to demonstrate than it had been to solve the mathematics. There followed a waiting period during which the development of suitable power sources took place. W. W. Hansen and his colleagues at Stanford University were then laying the groundwork for successful microwave amplifiers and oscillators. Finally, in March, 1936, the first experiments were performed at M.I.T. in a cast-off galvanized-iron air duct 18 inches in diameter. By this demonstration the earlier theoretical conclusions were confirmed and a new tech-

nology for handling microwaves was opened up. The period of discovery was now well under way.

During this same time, Southworth and his associates at the Bell Telephone Laboratories had been striving for the same ends industriously, effectively, and quietly. With the greater manpower and facilities available to them they made an even greater contribution than we did at M.I.T. to pioneering this new technique, and were often ahead. I feel sure, however, that dismay was equally shared when each first learned that the other was scheduled to present his first paper on the subject at the Spring Meeting of the IRE and the American Physical Society in Washington, D. C. on May 1, 1936. This emotion was promptly dissipated by a cordial pre-meeting interchange of papers that was but the beginning of continued close and friendly relations.

The early days at M.I.T. were characterized by simple equipment and modest effort. For example, the first several years of work were done with about $100 a year and to a great extent on "extra-curricular" time. Think what a small effort that would be today! It was important for its future growth that this infant technology get into the hands of many others and that real "push" be put behind it.

This push was supplied by wartime necessity. The need for microwave airborne and gun-laying radars supplied almost unlimited manpower and funds. The M.I.T. Radiation Laboratory was organized as a governmental activity and several commercial organizations such as Sperry Gyroscope, General Electric, RCA, Raytheon, and many others, either expanded their efforts greatly or joined the parade. The results were astounding, and every branch of microwave technology advanced rapidly beyond the fondest dreams of the Period of Discovery.

Thus, starting with the World War II effort we might designate a *Period of Development* of microwaves. Mathematicians, physicists, and engineers in considerable numbers and with great talents have developed this field into a highly sophisticated science supported by a vast amount of engineering know-how. Applications now encompass line-of-sight and scatter communication links, marine and air transport navigation and weather radars, particle accelerators for research, medical, and industrial uses, equipment for measuring the properties of materials and controling industrial processes, and many others besides. The modern microwave specialist has available an extensive array of power sources, test equipment, resonators, fixtures, and plumbing components. He employs elaborate and advanced procedures and methods of construction that make him among the most competent of contemporary engineers. He may even consider that his is a separate profession.

The frontier that was invaded in the early 1930's has only been pushed back, not vanquished. There is still virgin ground to be explored by the daring and significant contributions to be made by the industrious. Preceding editorials by G. C. Southworth and Ernst Weber have illuminated very well the future technical challenge that lies ahead.

Within the industrial complex surrounding contemporary microwave specialists are other rewarding opportunities for personal growth. I refer to the opportunities for men with technical backgrounds in executive and managerial positions. The need for individuals possessing both technical and administrative abilities is now great and it will become even more so in the expanding future of our profession. Although it is easiest to move into technical administration, there are other attractive avenues. Manufacturing, sales, and management in many of our companies, both small and large, also offer exciting and rewarding challenges to the exceptional individual ready to risk another kind of exploratory voyage on the industrial sea.

The horizon of the microwave professional of today is indeed wide and enticing. It would be wonderful to start all over again.

Microwave Prize

The Professional Group on Microwave Theory and Techniques has established the Microwave Prize to recognize annually a significant paper which appeared in the IRE TRANSACTIONS ON MICROWAVE THEORY AND TECHNIQUES. *In selecting the paper, consideration is given primarily to the subject of the contribution and secondarily to its presentation. The award consists of a certificate, a monetary sum of $100, and a feature publication in these* TRANSACTIONS. *If the paper has more than one author, the monetary sum is to be divided equally among the authors.*

—The Editor

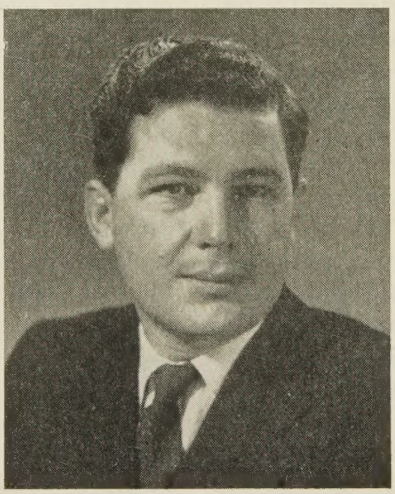

ROBIN I. PRIMICH
Radio Physics Laboratory
Defence Research Board
Ottawa, Canada

"A Semi-Infinite Array of Parallel Metallic Plates of Finite Thickness for Microwave Systems"

IRE TRANSACTIONS ON MICROWAVE THEORY AND TECHNIQUES
Vol. MTT-4, pp. 156–166; July, 1956

We are pleased to announce that the Microwave Prize for 1956 has been awarded to Dr. Robin I. Primich for the subject paper. The paper deals with the reflection at the flat face of a "metal lens" of the phase-advancing type. The treatment is a skillful application of the variational method of approximation. The theory predicts an unobvious advantage in using plate thicknesses of up to about two-thirds as great as the intervening air thickness to minimize the reflection, and this is verified by experiment. This paper is one of a series of contributions by Dr. Primich relating to this subject.

We commend Dr. Primich on this fine contribution and hope that subsequent recipients of the prize will continue this high standard.

W. L. PRITCHARD, *Chairman*
PGMTT Administrative Committee

A Variable-Ratio Microwave Power Divider and Multiplexer*

W. L. TEETER† AND K. R. BUSHORE‡

Summary—A microwave circuit is presented which provides continuous variation of microwave power between two outputs in any desired ratio. A typical device utilizing the circuit is described, and other uses of the circuit are discussed. An *X*-band power divider was constructed which had a vswr of less than 1.2 at all times over the frequency range of 8.6 to 9.6 kmc, divided the total input energy between the outputs in any ratio from 1/10,000 to 1, and had less than 0.4-db total insertion loss. No other losses were present. Adjustment could be made under maximum power levels of the waveguide. Another use of the circuit is to couple two high-power transmitters into one output, thus providing a dual frequency antenna coupler or diplexer. By cascading diplexers, multiplexing can be accomplished.

Introduction

THIS PAPER primarily describes theory and operation of a microwave power divider which can be adjusted so that microwave power is divided between two outputs in any desired ratio. Used conversely, the device has other applications, such as coupling two frequencies into one output.

During the past decade many power dividers have been developed by various organizations. Usually, each device was designed for a specific application and was not adaptable as a general laboratory tool because of such characteristics as limited bandwidth, high vswr, limited power handling capacity, high insertion losses, critical adjustment, or complicated construction.[1]

The device described herein obtains variable power division by controling the phase of one half of the incoming rf energy relative to the other half. Few, if any, of the limitations found in using other power dividers have been encountered in this device.

Operation

The basic power divider circuitry uses two broadband short-slot waveguide hybrids,[2] a convenient method of phase control such as a line stretcher or ferrite phase controller and connecting waveguides. A typical installation is shown in Figs. 1 and 2. The input microwave power is divided equally by hybrid *A-B* and establishes a 90° phase relationship between A_0 and B_0. Waveguide no. 1 is of constant electrical length, while the length of waveguide no. 2 can be varied with a line stretcher. Varying the line stretcher varies the phase

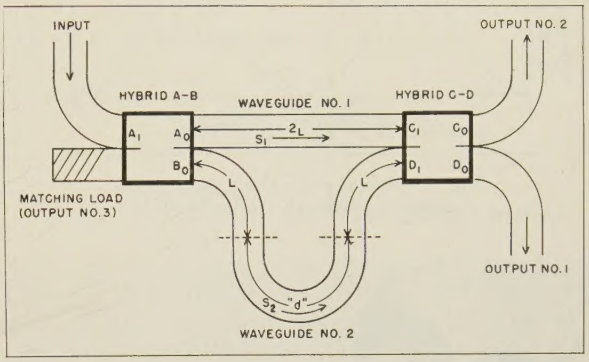

Fig. 1—Power divider circuitry.

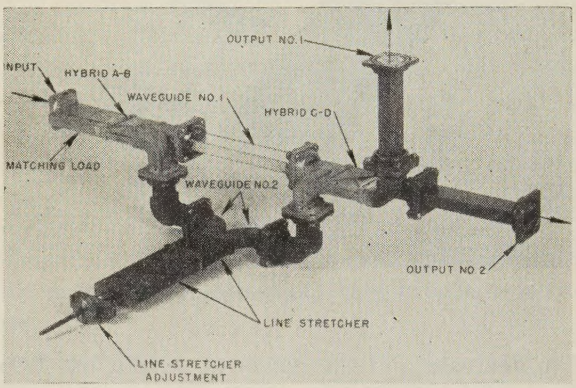

Fig. 2—Complete power divider (test model).

relationships of the power arriving at C_i and D_i of hybrid *C-D*. The relative phase of the power arriving at C_i and D_i determines the ratio of power coupling to output no. 1 and to output no. 2. Power at output no. 3 of Fig. 1 is 30 to 40 db below the input level regardless of the line stretcher adjustment, therefore a low-power matching load is placed at output no. 3 merely to terminate that particular arm of the hybrid properly.

When waveguides no. 1 and no. 2 are the same electrical length ($d=0$) or if the difference length d is an exact multiple of the guide wavelength, the power from A_0 adds to the power from B_0 and proceeds to output no. 1.

As d is changed to one-fourth guide wavelength, the phase relationships at C and D are such as to cause an equal amount of power to appear at each output, no. 1 and no. 2.

When d is made equal to one-half guide wavelength, all power will proceed to output no. 2.

As d is increased further, the changing relative phases of the signals in hybrid *C-D* cause the power at output

* Manuscript received by the PGMTT, September 17, 1956; revised manuscript received, June 27, 1957.

† Lockheed Missile Systems Div., Palo Alto, Calif.; formerly with U. S. Navy Electronics Lab., San Diego, Calif.

‡ U. S. Navy Electronics Lab., San Diego, Calif.

[1] No specific devices will be mentioned here, since numerous texts and technical series carry descriptions of the various existing methods of power division.

[2] H. J. Riblet, "The short-slot hybrid junction," PROC. IRE, vol. 40, pp. 180–184; February, 1952.

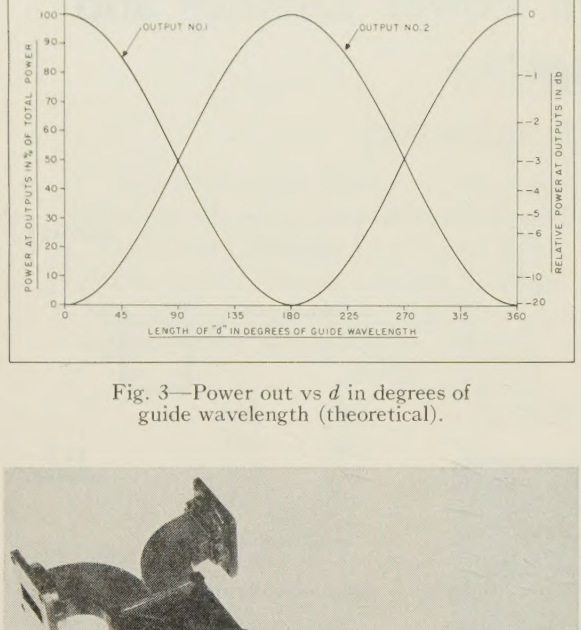

Fig. 3—Power out vs d in degrees of guide wavelength (theoretical).

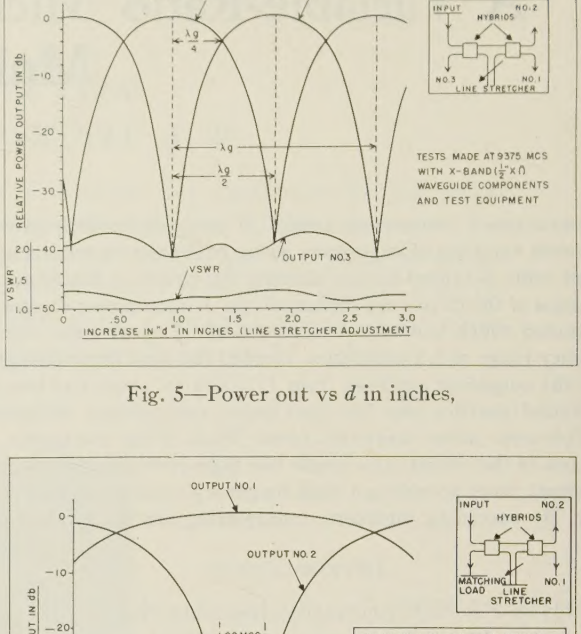

Fig. 5—Power out vs d in inches,

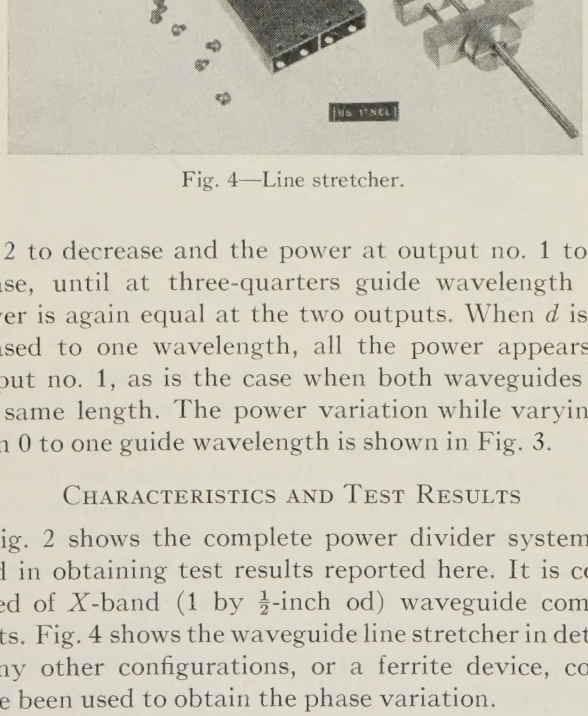

Fig. 4—Line stretcher.

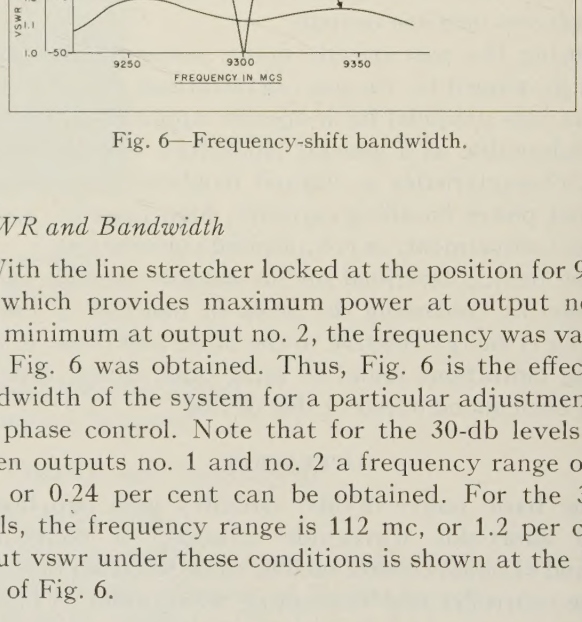

Fig. 6—Frequency-shift bandwidth.

no. 2 to decrease and the power at output no. 1 to increase, until at three-quarters guide wavelength the power is again equal at the two outputs. When d is increased to one wavelength, all the power appears at output no. 1, as is the case when both waveguides are the same length. The power variation while varying d from 0 to one guide wavelength is shown in Fig. 3.

Characteristics and Test Results

Fig. 2 shows the complete power divider system as used in obtaining test results reported here. It is composed of X-band (1 by $\frac{1}{2}$-inch od) waveguide components. Fig. 4 shows the waveguide line stretcher in detail. Many other configurations, or a ferrite device, could have been used to obtain the phase variation.

Power Variation

Fig. 5 shows the variation of power at outputs no. 1, and no. 2, and no. 3 vs movement of the line stretcher. Zero db in Fig. 5 represents the input power minus the 0.4-db copper losses in the waveguide circuitry.

The circuit shown in Fig. 2 performed satisfactorily with power in excess of 275-kw peak total without breakdown. Thus the power handling capability is essentially that of the waveguide and hybrids.

VSWR and Bandwidth

With the line stretcher locked at the position for 9300 mc which provides maximum power at output no. 1 and minimum at output no. 2, the frequency was varied and Fig. 6 was obtained. Thus, Fig. 6 is the effective bandwidth of the system for a particular adjustment of the phase control. Note that for the 30-db levels between outputs no. 1 and no. 2 a frequency range of 22 mc, or 0.24 per cent can be obtained. For the 3-db levels, the frequency range is 112 mc, or 1.2 per cent. Input vswr under these conditions is shown at the bottom of Fig. 6.

Other Uses

The power divider circuit may be used in many other applications. The circuit may be used, for example, for diplexing to couple two high-power transmitters into one output[3] and to provide a dual frequency antenna coupler. Cascading the diplexers results in multiplexing of any number of frequencies. The transmitter with the

[3] Although the dual frequency development discussed herein was accomplished before 1953 at the U. S. Navy Electronics Lab., the author has recently been notified of a basic circuit patent #2,702,371 issued in February, 1955 (filed February, 1949) to D. E. Sunstein, "Hybrid network for continuing and separating electromagnetic wave signals." This patent uses magic tees and covers the combining of signals of two differing frequencies into a common transmission line.

frequency (f_1) would be placed at the input of Fig. 1, and the transmitter with the other frequency (f_2) would be placed where the matching load is shown. When the line stretcher is properly set, the total power from both transmitters would be coupled into output no. 1. To provide maximum coupling of both frequencies into output no. 1, the line stretcher must be set so that for frequency f_1 the difference length d is an integral number of wavelengths, and for frequency f_2 the difference length d is an odd multiple of a half guide wavelength. By using the following equation the distance d can be calculated which must be used to provide the proper phasing for both frequencies:[4,5]

$$d = \left(\frac{\lambda g_2}{2}\right)\left(\frac{\lambda g_1}{\lambda g_2 - \lambda g_1}\right) \tag{1}$$

where

d = loop distance (see Fig. 1).
λg_1 = guide wavelength of f_1, and
λg_2 = guide wavelength of f_2.

An example of the use of (1) follows: where

$$f_1 = 9385 \text{ mc } (\lambda g_1 = 4.467 \text{ cm})$$

and

$$f_2 = 9273 \text{ mc } (\lambda g_2 = 4.574 \text{ cm})$$

$$d = \frac{(4.574)\ (4.467)}{2(0.107)} \times \frac{1}{2.54} = 37.478 \text{ inches.}$$

Thus, by using $d = 37.478$ inches in the line stretcher, maximum coupling of inputs with frequencies of 9385 and 9273 mc would be obtained. When using a ferrite line stretcher, d could be measured in electrical phase or current.

Any number of frequencies may be combined and hence filtered by cascading couplers. The power capacity would be essentially the full power of the waveguide as it would be largely determined by the hybrid couplers and phase shifter.

Other possible uses might be a broad frequency selective device for use in a receiver input, a variable ratio waveguide switch, etc.

The authors are indebted to K. Tomiyasu who made many helpful suggestions in the preparation of this paper.

[4] W. L. Teeter and K. R. Bushore, "A Dual-Frequency Microwave RF Head," U. S. Navy Electronics Lab., Rep. 556; January 12, 1955.

[5] Eq. (1) of Teeter and Bushore, *ibid.*, is derived by stating the conditions described in the foregoing text. The distance d may also be expressed in more general terms from the following:

Let λg be the guide wavelength for the mean frequency f between f_1 and f_2 and λ, the air wavelength; λc is the cutoff wavelength.

V = velocity of light.

Then let

$$\phi = 2\pi \frac{d}{\lambda g}$$

substitute for λg,

$$\phi = 2\pi d \sqrt{\frac{1}{\lambda^2} - \frac{1}{\lambda_c{}^2}}$$

$$= 2\pi d \sqrt{\frac{f^2}{V^2} - \frac{1}{\lambda_c{}^2}}$$

and

$$\frac{d\phi}{df} = 2\pi d \quad \frac{1}{\sqrt{\frac{f^2}{V^2} - \frac{1}{\lambda_c{}^2}}} \left(\frac{1}{2}\right)\left(\frac{2f}{V^2}\right) = \frac{\Delta\phi}{\Delta f}. \tag{3}$$

For the condition $\Delta\theta = \pi$ and where Δf is small; that is, both f_1 and f_2 are within the frequency of the hybrid slots and the waveguide, ($\Delta f = f_1 - f_2$).

Substitute for $\Delta\theta$ in (3)

$$\frac{\pi}{\Delta f} = \frac{2\pi d f}{V^2} \lambda g$$

and solve for d

$$d = \frac{V^2}{2f\lambda g \Delta f} = \frac{V}{2\Delta f} \frac{(V)}{(f)} \frac{(1)}{(\lambda g)}.$$

Since $f\lambda = V = 3 \times 10^{10}$ cm/sec, substitute for f, to get

$$d = \frac{V}{2\Delta f} \frac{(\lambda)}{(\lambda g)} \tag{4}$$

or

$$d = \frac{V}{2(f_1 - f_2)} \frac{(\lambda)}{(\lambda g)}. \tag{5}$$

Eq. (5) is plotted by Teeter and Bushore, *ibid.*

High-Power Ferrite Circulators*

PETER A. RIZZI†

Summary—The Faraday rotation and insertion loss of various ferrite-loaded waveguide structures have been studied in order to determine their power-handling capacities. A method of measuring insertion loss to within ±0.05 db is described. Two figures of merit containing this information are defined for the various configurations. The first, defined as the rotation per attenuation, indicates for a given value of rotation the efficiency of power transmission through the device, while the second, defined as the dissipative area per power loss, indicates the power handling capacity of the structure. By utilizing this information, the author has described an *X*-band ferrite circulator which is capable of handling an average power of 1000 watts. In addition, the design of a 2000-watt gyrator type circulator is indicated.

Introduction

When a dc magnetic field is applied to a waveguide containing a ferrite material, the ferrite responds anisotropically to the rf field. Because of the gyroscopic nature of the electrons which determine the magnetization of the ferrite, a nonsymmetrical tensor is required to describe its rf permeability. This lack of symmetry coupled with the high resistivity of the ferrite implies the possibility of realizing microwave circuit elements which do not obey the law of reciprocity. In recent years, many useful devices have been developed which employ this property. Some of these use the Faraday rotation of an electromagnetic wave in a cylindrical waveguide to obtain their nonreciprocal behavior. For example, Hogan[1] described two types of circulators which employ the ferrite's nonreciprocal property. In many applications, however, the losses in these devices are prohibitively large. Consequently, the associated temperature rise adversely affects the power handling capacity of the device.

Kales[2] has investigated the case of solid ferrite rods in a cylindrical waveguide and obtained characteristic equations which, when solved, determine the propagation constants for the various modes. More recently, Suhl and Walker[3] have studied the propagating modes in a cylindrical ferrite waveguide structure and have also employed perturbation techniques to obtain the propagation constants for a waveguide containing either a very thin pencil of ferrite or a ferrite which was only weakly magnetized. In addition to the above investigations, Sakiotis and Chait[4,5] and Fox, Miller, and Weiss[6] have made an extensive study of the properties of ferrites in waveguides.

The present work considers the case of a cylindrical rod magnetized in the direction of propagation for which curves of rotation and insertion loss have been obtained for various diameters and lengths of ferrite. From this information a figure of merit, defined as the rotation per attenuation, was calculated for the various ferrite diameters. This revealed the ferrite diameter which gave the greatest efficiency of power transmission through the ferrite-loaded guide.

An analysis of a hollow ferrite cylinder in a cylindrical waveguide has been made. Theoretical values of rotation for both the solid and hollow rod case have been calculated. Experimental values of rotation and attenuation have also been obtained. From this data a figure of merit, defined as the dissipative or surface area of the ferrite rod per attenuation, has been determined. This enables one to determine the ferrite geometry for maximum power handling capacity.

Theoretical Results

Polder[7] and Hogan[1] have demonstrated that when an electromagnetic wave is propagated in a ferrite medium which has been magnetized to saturation in the z direction, the rf components of B and H are related by a tensor permeability. By considering the case of uniform plane wave propagating through a ferrite medium magnetized in the direction of propagation, the above investigators showed that the plane of polarization of the wave was rotated as it propagated through the ferrite. The rotation per unit length is related to the propagation constants in the following manner:

$$\theta = \frac{\beta_- - \beta_+}{2} \tag{1}$$

where β_+ and β_- are the propagation constants for the right, and left-hand circularly-polarized waves, respectively.

Using the waveguide analysis described by Kales,[2] the author[8] has derived characteristic equations for the

* Manuscript received by the PGMTT, November 19, 1956; revised manuscript received, June 28, 1957. This paper is based in part on a dissertation submitted in partial fulfillment of the requirements for the Doctor of Eng. degree, Yale University, New Haven, Conn.

† Raytheon Manufacturing Co., Missile Systems Div., Bedford, Mass.

[1] C. L. Hogan, "The microwave gyrator," *Bell Sys. Tech. J.*, vol. 31, pp. 1–31; January, 1952.

[2] M. L. Kales, "Modes in waveguides that contain ferrites," *J. Appl. Phys.*, vol. 24, pp. 604–608; May, 1953.

[3] H. Suhl and L. R. Walker, "Topics in guided wave propagation through gyromagnetic media," *Bell Sys. Tech. J.*, vol. 33, pp. 579–659, and 1133–1194; May and September, 1954.

[4] H. N. Chait and N. G. Sakiotis, "Ferrites at microwaves," PROC. IRE, vol. 41, pp. 87–93; January, 1953.

[5] N. G. Sakiotis and H. N. Chait, "Properties of ferrites in waveguides," IRE TRANS., vol. MTT-1, pp. 11–16; November, 1953.

[6] A. G. Fox, S. E. Miller, and M. T. Weiss, "Behavior and applications of ferrites in the microwave region," *Bell Sys. Tech. J.*, vol. 34, pp. 5–103; January, 1955.

[7] D. Polder, "On the theory of ferromagnetic resonance," *Phil. Mag.*, vol. 40, pp. 99–115; January, 1949.

[8] P. Rizzi, "The electromagnetic field in composite dielectric and ferrite waveguide structures," D.Eng. dissertation submitted to Yale School of Eng., pp. 36, 43; 1955.

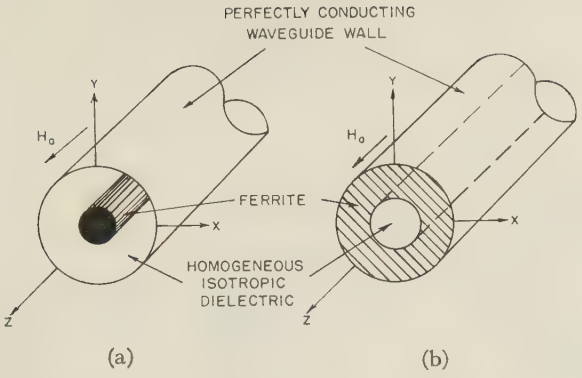

Fig. 1—Composite ferrite and dielectric waveguide structures.

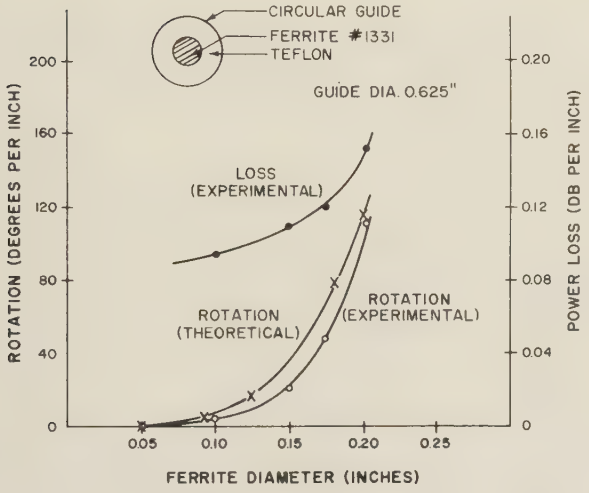

Fig. 2—Saturation rotation and loss for the teflon and ferrite structure shown in Fig. 1(a).

two waveguide configurations shown in Fig. 1. A brief outline of the analysis is given in the Appendix.

Because of the complexity of the characteristic equations, graphical methods were used to solve for the propagation constants of the circularly-polarized waves. Then by use of (1), the rotation per unit length for various ferrite diameters was determined. For the structure shown in Fig. 1(a), the following materials were used:

Ferrite MF-1331[9]

Relative dielectric constant $= \epsilon = 13$.
Saturation magnetization $= M_a = 2200$ Gauss.
(The dc magnetic field was set at 300 oersteds.)

Teflon

Relative dielectric constant $= \epsilon_1 = 2.08$.

Fig. 2 shows the theoretical values of saturation rotation at X band for various ferrite diameters.

For the structure shown in Fig. 1(b), a hollow MF-1331 ferrite cylinder was assumed in the calculations.

[9] Ferrite MF-1331, now designated as R-1, is produced by the General Ceramics Corp., Keasbey, N. J. The above values of dielectric constant and saturation magnetization are typical for MF-1331.

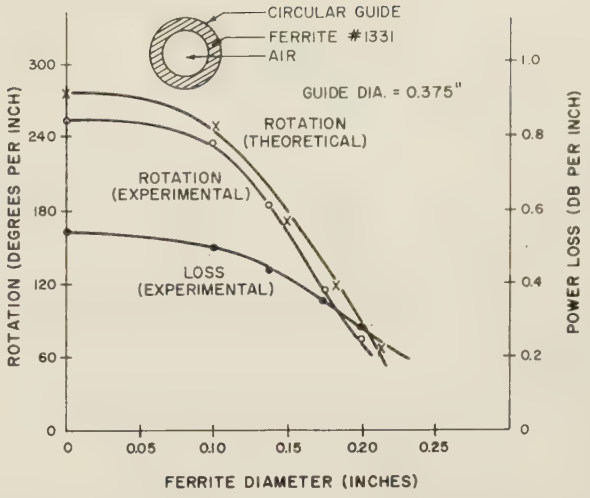

Fig. 3—Saturation rotation and loss for the hollow ferrite structure shown in Fig. 1(b).

The center section contained air so that the relative dielectric constant in this region was unity. Fig. 3 shows the theoretical values of saturation rotation at X band for various inside ferrite diameters. It is interesting to note that with a hole in the center of the ferrite equal to approximately half the waveguide diameter (Fig. 3), one obtains the same amount of rotation as from a solid rod 0.20 inch in diameter placed at the center of the teflon-loaded guide (Fig. 2). This implies that if the losses are of the same order of magnitude in the two structures, the hollow cylinder with its larger dissipative area should be capable of handling much higher amounts of microwave power without having to increase the length of the Faraday rotator. The hollow cylinder has an additional advantage in that the ferrite touches the metallic waveguide wall and consequently can conduct the generated heat away more readily than the solid ferrite rod which is imbedded in teflon.

In order to determine theoretically the attenuation in the ferrite structures, tables of the various type Bessel functions for complex arguments are required. However, since the available tables are not complete enough for our purpose, we must turn to an experimental study of the loss characteristics for the various ferrite configurations.

Experimental Techniques and Results

For the purpose of studying the rotation and loss characteristics in composite ferrite and dielectric waveguide structures, the measuring apparatus shown in Fig. 4 was assembled.

In order to measure the Faraday rotation in the circularly symmetric ferrite structures, a rotary joint and protractor combination was employed. By gradually increasing the magnetic field, the rotation, due to the ferrite, also increased. Thus, by turning the circular-to-rectangular transition at the output of the ferrite section so that the rotation meter always reads a maximum, the rotation can be "followed" as it increases due to the

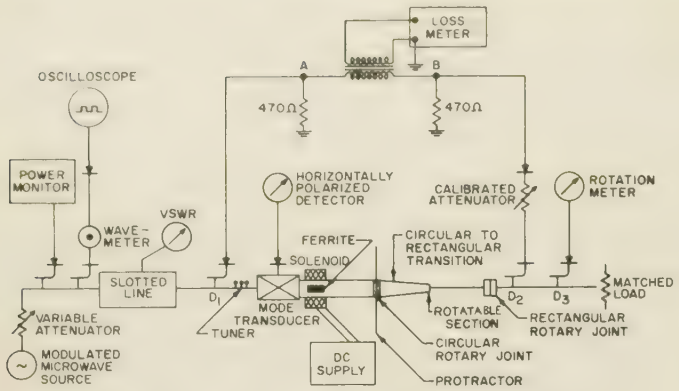

Fig. 4—Apparatus for measuring rotation and loss in ferrites at X band.

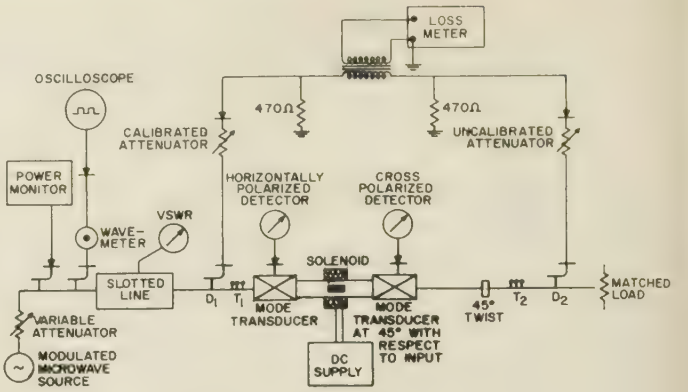

Fig. 5—Improved loss measurement apparatus.

increasing magnetic field. By continuing this process until the ferrite is saturated, the saturation rotation of the sample can be determined. With the circular-to-rectangular transition set for a maximum reading on the rotation meter, the insertion loss due to the ferrite-loaded waveguide structure can be measured. This is accomplished by sampling the input and output energy from directional couplers D_1 and D_2, respectively. The difference between the crystal outputs is fed to a transformer and amplified. The output signal thus indicates the amount of attenuation in the structure between D_1 and D_2. To calibrate the output or loss meter, a calibrated attenuator was inserted in the second or output branch of the circuit as shown in Fig. 4. By placing an air-filled waveguide section between the two directional couplers, the calibrated attenuator was varied until a null was obtained on the loss meter. Thus, with this attenuator setting, the circuit was balanced for zero loss. The loss meter was then calibrated by introducing known amounts of loss with a standard attenuator. With the calibrated attenuator returned to its setting for zero loss and the air-filled waveguide section replaced by the ferrite-loaded guide, the insertion loss for both solid and hollow rod ferrite structures was obtained.

Since the ferrite structures were cylindrical in cross section, a mode transducer was employed to change the dominant TE_{10} mode in rectangular guide to TE_{11} mode in circular guide. In addition to its transducing properties, this device also contains an output terminal which accepts any horizontally-polarized reflections[10] from the ferrite structure. Because of the horizontally-polarized detector's position in the measurement setup, the loss meter actually measures the power absorbed by the ferrite structure plus that absorbed by the horizontally-polarized detector. In order to obtain the actual power loss in the ferrite structure, the apparent power loss due to horizontally-polarized reflections was subtracted from the loss meter reading. Fig. 2 and Fig. 3 show the insertion loss and the measured saturation rotation at X Band for various diameters of solid and holly cylinders of ferrite No. 1331. Comparison with the theoretical curves shows that the measured and computed values of rotation are in agreement to within 10 per cent. The variation in saturation magnetization from the value of 2200 Gauss assumed in the calculations accounts for most of this discrepancy.

By using the improved measurement technique described below, some of the above data were checked. In addition, measurements were made on hollow rod samples with larger inside and outside diameters. The improved loss measurement system is shown in Fig. 5. With a section of essentially lossless waveguide between the directional couplers D_1 and D_2 and the calibrated attenuator set at zero attenuation, the uncalibrated attenuator is adjusted so that the loss meter reads zero. Next, the ferrite section and mode transducers are placed between the directional couplers. By increasing the magnetic field, the rotation is increased to the value of $(N\pi+\pi/4)$ nearest the saturation rotation. A slight adjustment of magnetic field and tuner T_2 will yield nulls in the cross-polarized and horizontally-polarized detectors, respectively. The tuner T_1 is then used to minimize the input vswr. Since the system has been tuned for maximum transmission, the only significant loss is that due to the ferrite section. The final step of the procedure is to adjust the calibrated attenuator so as to renull the loss meter. The amount of loss required to renull is equal to the loss through the ferrite-loaded waveguide section. In all the ferrite structures which were investigated, the cross-polarized detector null was at least 40 db down from the input power level. Thus, the ellipticity introduced by the ferrite section was negligible. The horizontally-polarized detector null was at least 50 db down from the input so that its effect on the loss measurements was also negligible. An analysis of this system and the data obtained from it indicated that the measurement errors were less than ± 0.05 db. Fig. 6 shows some of the loss data obtained on large diameter hollow ferrite rods using the above technique.

From the data in Figs. 2, 3, and 6 curves of Q_T, defined as the rotation per attenuation, and Q_D, defined as the dissipative area per power loss, can be plotted for the various configurations.[11] These are given in Fig. 7–

[10] All reflections were reduced, in part, by use of quarter-wave dielectric transformers on each end of the ferrite cylinders.

[11] The total cylindrical surface of the ferrite is considered as the dissipative area. That is, the dissipative area per unit length is equal to πd for solid cylinder and $\pi(d_{\text{inside}}+d_{\text{outside}})$ for hollow cylinder.

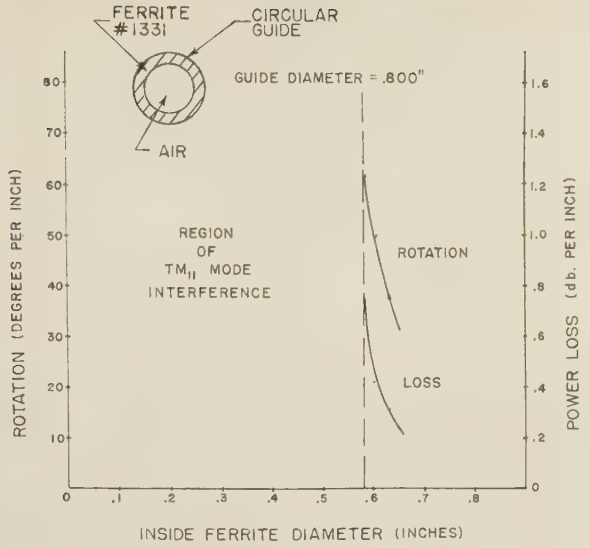

Fig. 6—Saturation rotation and loss for large hollow cylinders.

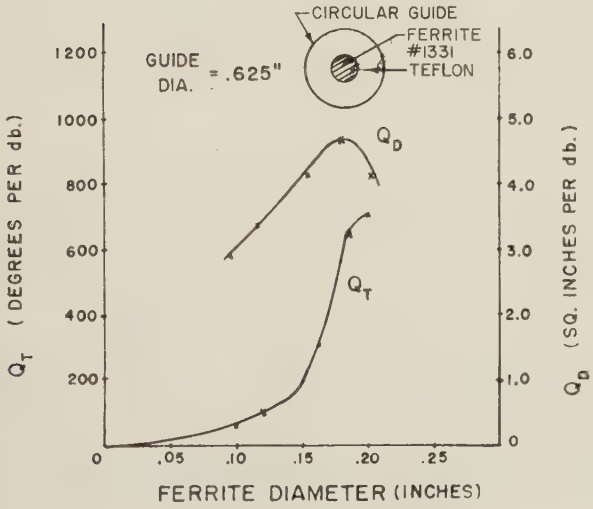

Fig. 7—Figures of merit for teflon and ferrite structures.

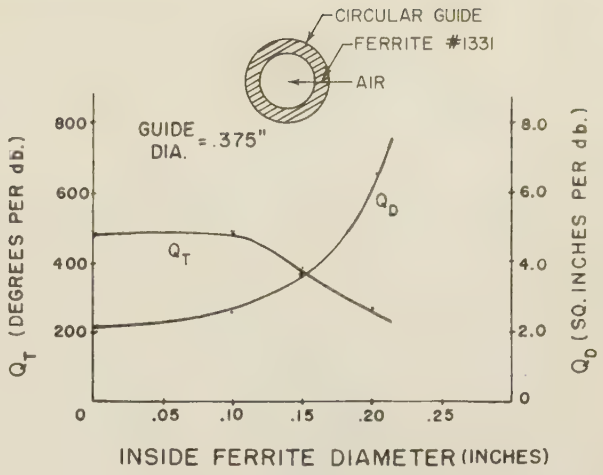

Fig. 8—Figures of merit for small hollow ferrite cylinders.

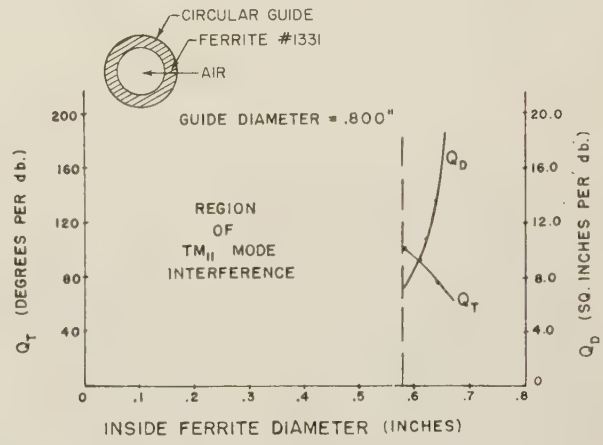

Fig. 9—Figures of merit for large hollow ferrite cylinders.

Fig. 9. Inspection of the Q_T curves for the various configurations indicate that if one is concerned with efficiency of power transfer, the solid rod structures are obviously better. However, more often the problem is one of obtaining a structure with a very large power handling capacity while maintaining the insertion loss reasonably low, but not necessarily at a minimum. For example, if 0.5 db were set as the maximum allowable loss for a ferrite structure with a saturation rotation of 45°, one would be free to choose any structure with a Q_T greater than 90°/db. Since large power handling capacity is desired, one would consequently choose the structure with the highest Q_D. At this point it should be mentioned that the values of Q_D for teflon and ferrite cannot be compared directly with Q_D for the hollow rod case. First of all, the loss curve in Fig. 2, and consequently Q_D in Fig. 7, contains the losses due to the teflon. Secondly, the efficiency of heat transfer from the ferrite to the waveguide wall is different for the two geometries. Therefore, strictly speaking, the Q_D curves are only valuable in determining what dimensions of a given ferrite geometry yield greatest power handling capacity.

Description of High-Power Circulators

A study of the data in the previous section resulted in the choice of the structure in Fig. 10 for use in high-power ferrite circulators. This choice, as previously discussed, amounted to a compromise between high-power handling capacity (Q_D) and low insertion loss(Q_T).

One type of circulator described in the literature[1] employs a pair of two-mode transducers and a ferrite section which gives 45° of Faraday rotation. This type is shown in Fig. 11. Due to the ferrite's rotation, energy entering port 1 travels to port 2 practically unattenuated. Similarly, energy entering port 2 travels to port 3 while energy entering port 3 travels to port 4. This type of circulator has been built at X band with an insertion loss of less than 0.4 db between successive ports and a reverse loss of greater than 20 db over a 5 per cent frequency band. The reverse loss is limited by the frequency sensitivity of the saturation rotation which varies from 40° to 50° over the 5 per cent frequency band. High-power tests have shown this circulator capable of handling at least an average power of 1000 watts with no forced cooling of the ferrite section. Since a higher power

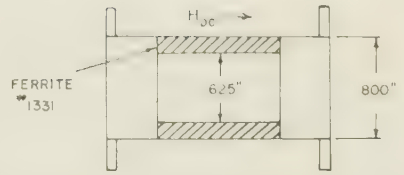

Fig. 10—Hollow ferrite cylinder used in high-power ferrite circulators.

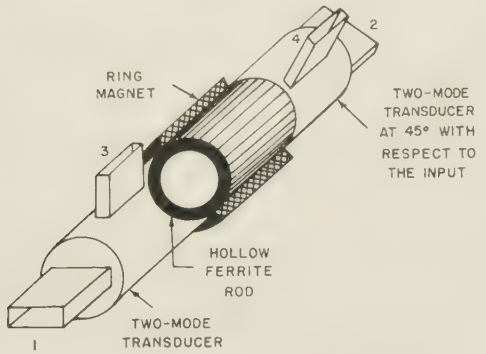

Fig. 11—Polarization-type circulator.

source was not available, the actual power required to cause the ferrite to lose its magnetic properties could not be determined. For 1000 watts input, the temperature of the ferrite was only 100°C as compared to its Curie temperature of 215°C. The insertion loss at this power level was approximately 0.7 db. Since it was found that the change in loss due to the increased temperature was less than 0.1 db, the 0.3 db increase in loss was attributed to the nonlinear attenuation characteristic of the ferrite. Sakiotis, Chait, and Kales[12] have shown that for power levels greater than about 1000 watts this characteristic becomes important. Under these conditions, the power handling capacity of the ferrite structure is limited not only by the heat dissipation but also by the power level at which the nonlinear effects become appreciable. Thus, from the above temperature data, it is doubtful if the circulator shown in Fig. 11 can retain its properties at cw powers of greater than 2000 watts.

A second type of ferrite circulator has been described by Hogan[1] which employs two magic-tees and a gyrator. This type is shown in Fig. 12. By using a hollow ferrite rod which has 90° rotation and a 90° twist section, a difference in phase shift of 180° for the two directions of propagation through the ferrite-twist combination can be obtained. Since any energy which enters port 1 splits between the two branches of the circulator, only half of the input power passes through the ferrite. Therefore, by using a 90° hollow rod section with the same inside and outside diameters as the one used in the 45° circulator, the high-power insertion loss between successive ports would still be 0.7 db while the power handling capacity should be doubled (*viz.*, 2000 watts).

[12] N. Sakiotis, H. N. Chait, and M. L. Kales, "Nonlinearity of propagation in ferrite media," PROC. IRE, vol. 43, p. 1011; August, 1955.

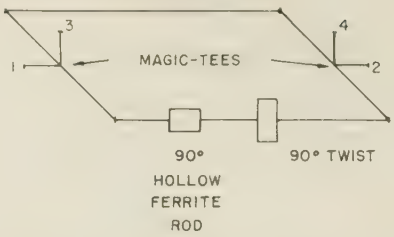

Fig. 12—Gyrator-type circulator.

Conclusion

The insertion loss and Faraday rotation for various ferrite configurations have been studied by use of a system capable of measuring microwave loss to within ± 0.05 db. By defining both a power handling and transmission figure of merit, a ferrite structure capable of handling large amounts of microwave power was chosen. With this structure a polarization type circulator was constructed with a power handling capacity of at least 1000 watts and an insertion loss of less than 0.7 db at the high-power level. In addition, a gyrator type circulator has been suggested which should have a 2000 watts power handling capacity with a high-power insertion loss of less than 0.7 db.

Appendix

When a ferrite is magnetized in the z direction, the rf components of $\vec{B}$ and $\vec{H}$ are related in the following manner:

$$\vec{B} = \mu\vec{H}_t + jK\vec{i}_z \times \vec{H}_t + \mu_z H_z \vec{i}_z \qquad (2)$$

where the subscript t denotes the projection of a vector on the xy plane and $\vec{i}_z$ denotes the unit vector in the z direction.

Assuming an $e^{j\omega t+\gamma z}+\gamma z$ dependency, Maxwell's equations may be written as follows:

$$\nabla_t \times \vec{E} + \gamma\vec{i}_z \times \vec{E} = -j\omega\vec{B}$$
$$\nabla_t \times \vec{H} + \gamma\vec{i}_z \times \vec{H} = j\omega\epsilon\vec{E}$$

where ϵ is the dielectric constant of the ferrite.

Using (2) and the divergence relations, the above equations may be rewritten in the following form:

$$\nabla_t^2 E_z + aE_z + bH_z = 0$$
$$\nabla_t^2 H_z + cH_z + dE_z = 0$$

where

$$a = g^2 - g_0^2 \frac{K}{\mu}, \qquad b = -\omega\gamma K \frac{\mu_z}{\mu},$$
$$c = g^2 \frac{\mu_z}{\mu}, \qquad d = \omega\gamma\epsilon \frac{K}{\mu}$$

and

$$g_0^2 \equiv \omega^2 K\epsilon \qquad g^2 \equiv \omega^2\mu\epsilon + \gamma^2.$$

Transforming the above equations into a pair of scalar wave equations we obtain

$$\nabla_t^2 u_1 + S_1 u_1 = 0$$
$$\nabla_t^2 u_2 + S_2 u_2 = 0 \tag{3}$$

where

$$E_z = S_1 u_1 + S_2 u_2$$
$$H_z = S_1 \frac{S_1 - a}{b} u_1 + S_2 \frac{S_2 - a}{b} u_2 \tag{4}$$

and

$$S_1 S_2 = ac - bd \qquad S_1 + S_2 = a + c.$$

Since u_1 and u_2 are related to E_z and H_z, and E_t and H_t are related to E_z and H_z through the curl relations, we can write E_t in terms of u_1 and u_2. These equations are

$$\vec{E}_t = \gamma \nabla_t (u_1 + u_2) - \frac{j\mu}{\gamma K} \vec{i}_z \times \nabla_t \{(S_1 - a)u_1 + (S_2 - a)u_2\}$$

$$\vec{H}_t = \frac{1}{\omega K} \nabla_t \{(g^2 - S_1)u_1 + (g^2 - S_2)u_2\}$$
$$- j\omega\epsilon \vec{i}_z \times \nabla_t (u_1 + u_2). \tag{5}$$

Since u_1 and u_2 are the solutions to (3), then (4) and (5) define the electromagnetic field in the ferrite region of a waveguide structure.

Because of the circular symmetry, we solve the scalar wave equations in cylindrical coordinates. Thus

$$u_1 = [A_1 J_n(\sqrt{S_1} r) + B_1 N_n(\sqrt{S_1} r)] e^{jn\phi}$$

$$u_2 = [C_1 J_n(\sqrt{S_2} r) + D_1 N_n(\sqrt{S_2} r)] e^{jn\phi}$$

where A_1, B_1, C_1, and D_1 are constants and J_n and N_n represent the Bessel functions of the first and second kind, respectively. In the waveguide region containing a homogeneous isotropic dielectric ϵ_2, the solution of the wave equation yields

$$E_{z_2} = [A_2 J_n(kr) + B_2 N_n(kr)] e^{jn\phi}$$
$$H_{z_2} = [C_2 J_n(kr) + D_2 N_n(kr)] e^{jn\phi}$$

where

$$k^2 = \gamma^2 + \omega^2 \mu_2 \epsilon_2.$$

Having the various field components, we can now solve for the propagation constants in ferrite structures similar to those in Fig. 1. Since the tangential components of E and H must be continuous across the boundary between the ferrite and the dielectric, this leads to four equations involving the field distribution in both the ferrite and dielectric regions. In order to obtain a nontrivial solution, we require that the determinant of their coefficients must equal zero. From this condition we obtain the equation which when solved yields the propagation constants for the various modes in the circularly-symmetric ferrite-loaded waveguide.

For the structure shown in Fig. 1(a) the equation is

$$P_1 Q_2 = P_2 Q_1 \tag{6}$$

where for $i = 1, 2$

$$P_i = \left[\left\{ \frac{\mu_2 \mu}{\mu_z K} S_i (S_i - a) r_1 G_1'(r_1) + n\gamma^2 (k^2 - S_i) G_1(r_1) \right\} J_n(\sqrt{S_i} r_1) - \frac{\mu}{K} k^2 (S_i - a) \sqrt{S_i} r_1 J_n'(\sqrt{S_i} r_1) G_1(r_1) \right]$$

$$Q_i = \left[\left\{ nF_1(r_1) \left[k^2 (g^2 - S_i) + \frac{\mu}{\mu_z} S_i (S_i - a) \right] + \omega^2 K \epsilon_2 S_i r_1 F_1'(r_1) \right\} J_n(\sqrt{S_i} r_1) - k^2 \omega^2 K \epsilon \sqrt{S_i} r_1 J_n'(\sqrt{S_i} r_1) F_1(r_1) \right]$$

and

$$F_1(r) \equiv \left\{ \frac{J_n(kr)}{J_n(kr_0)} - \frac{N_n(kr)}{N_n(kr_0)} \right\}.$$

$$G_1(r) \equiv \left\{ \frac{J_n(kr)}{J_n'(kr_0)} - \frac{N_n(kr)}{N_n'(kr_0)} \right\}.$$

$r_1 \equiv$ radius of the ferrite rod,

$r_0 \equiv$ radius of the circular waveguide.

In all these equations the primes signify differentiation with respect to the complete argument.

For the structure shown in Fig. 1(b), the eigenvalue equation is

$$P_1 Q_2 = P_2 Q_1 \tag{7}$$

where

$$P_1 \equiv \left\{ \begin{array}{l} [nK\mu_z\gamma^2(S_1 - k^2) J_n(kr_1) - \mu\mu_2 S_1 (S_1 - a) kr_1 J_n'(kr_1)] F(\sqrt{S_1} r_1) \\ + [nK\mu_z\gamma^2(S_2 - k^2) J_n(kr_1) - \mu\mu_2 S_2 (S_2 - a) kr_1 J_n'(kr_1)] m_3 N_n(\sqrt{S_2} r_1) \\ + \mu\mu_z k^2 r_1 J_n(kr_1) [\sqrt{S_1}(S_1 - a) F'(\sqrt{S_1} r_1) + \sqrt{S_2}(S_2 - a) m_3 N_n'(\sqrt{S_2} r_1)] \end{array} \right\}$$

$$P_2 \equiv \left\{ \begin{array}{l} [nK\mu_z\gamma^2(S_2 - k^2) J_n(kr_1) - \mu\mu_2 S_2 (S_2 - a) kr_1 J_n'(kr_1)] G(\sqrt{S_2} r_1) \\ + [nK\mu_z\gamma^2(S_1 - k^2) J_n(kr_1) - \mu\mu_2 S_1 (S_1 - a) kr_1 J_n'(kr_1)] m_2 N_n(\sqrt{S_1} r_1) \\ + \mu\mu_z k^2 r_1 J_n(kr_1) [\sqrt{S_2}(S_2 - a) G'(\sqrt{S_2} r_1) + \sqrt{S_1}(S_1 - a) m_2 N_n'(\sqrt{S_1} r_1)] \end{array} \right\}$$

$$Q_1 \equiv \left\{ \begin{array}{l} [n\{\mu S_1(S_1 - a) + \mu_z k^2(g^2 - S_1)\}J_n(kr_1) + \omega^2\epsilon_2 K\mu_z S_1 kr_1 J_n'(kr_1)]F(\sqrt{S_1}r_1) \\ + [n\{\mu S_2(S_2 - a) + \mu_z k^2(g^2 - S_2)\}J_n(kr_1) + \omega^2\epsilon_2 K\mu_z S_2 kr_1 J_n'(kr_1)]m_3 N_n(\sqrt{S_2}r_1) \\ - \omega^2\epsilon K\mu_z k^2 r_1 J_n(kr_1)[\sqrt{S_1}F'(\sqrt{S_1}r_1) + \sqrt{S_2}m_3 N_n'(\sqrt{S_2}r_1)] \end{array} \right\}$$

$$Q_2 \equiv \left\{ \begin{array}{l} [n\{\mu S_2(S_2 - a) + \mu_z k^2(g^2 - S_2)\}J_n(kr_1) + \omega^2\epsilon_2 K\mu_z S_2 kr_1 J_n'(kr_1)]G(\sqrt{S_2}r_1) \\ + [n\{\mu S_1(S_1 - a) + \mu_z k^2(g^2 - S_1)\}J_n(kr_1) + \omega^2\epsilon_2 K\mu_z S_1 kr_1 J_n'(kr_1)]m_2 N_n(\sqrt{S_1}r_1) \\ - \omega^2\epsilon K\mu_z k^2 r_1 J_n(kr_1)[\sqrt{S_2}G'(\sqrt{S_2}r_1) + \sqrt{S_1}m_2 N_n'(\sqrt{S_1}r_1) \end{array} \right\}$$

and

$$F(\sqrt{S_1}r) \equiv J_n(\sqrt{S_1}r) + m_1 N_n(\sqrt{S_1}r), \qquad G(\sqrt{S_2}r) \equiv J_n(\sqrt{S_2}r) + m_4 N_n(\sqrt{S_2}r)$$

$$m_1 \equiv \frac{\left\{ \begin{array}{l} [S_1 J_n(\sqrt{S_1}r_0)]\left[\frac{n\gamma}{r_0} N_n(\sqrt{S_2}r_0) - \frac{\mu}{\gamma K}\sqrt{S_2}(S_2 - a)N_n'(\sqrt{S_2}r_0)\right] \\ - [S_2 N_n(\sqrt{S_2}r_0)]\left[\frac{n\gamma}{r_0} J_n(\sqrt{S_1}r_0) - \frac{\mu}{\gamma K}\sqrt{S_1}(S_1 - a)J_n'(\sqrt{S_1}r_0)\right] \end{array} \right\}}{\left\{ \begin{array}{l} [S_2 N_n(\sqrt{S_2}r_0)]\left[\frac{n\gamma}{r_0} N_n(\sqrt{S_1}r_0) - \frac{\mu}{\gamma K}\sqrt{S_1}(S_1 - a)N_n'(\sqrt{S_1}r_0)\right] \\ - [S_1 N_n(\sqrt{S_1}r_0)]\left[\frac{n\gamma}{r_0} N_n(\sqrt{S_2}r_0) - \frac{\mu}{\gamma K}\sqrt{S_2}(S_2 - a)N_n'(\sqrt{S_2}r_0)\right] \end{array} \right\}}$$

$$m_2 \equiv \frac{\left\{ \begin{array}{l} [S_2 J_n(\sqrt{S_2}r_0)]\left[\frac{n\gamma}{r_0} N_n(\sqrt{S_2}r_0) - \frac{\mu}{\gamma K}\sqrt{S_2}(S_2 - a)N_n'(\sqrt{S_2}r_0)\right] \\ - [S_2 N_n(\sqrt{S_2}r_0)]\left[\frac{n\gamma}{r_0} J_n(\sqrt{S_2}r_0) - \frac{\mu}{\gamma K}\sqrt{S_2}(S_2 - a)J_n'(\sqrt{S_2}r_0)\right] \end{array} \right\}}{\left\{ \begin{array}{l} [S_2 N_n(\sqrt{S_2}r_0)]\left[\frac{n\gamma}{r_0} N_n(\sqrt{S_1}r_0) - \frac{\mu}{\gamma K}\sqrt{S_1}(S_1 - a)N_n'(\sqrt{S_1}r_0)\right] \\ - [S_1 N_n(\sqrt{S_1}r_0)]\left[\frac{n\gamma}{r_0} N_n(\sqrt{S_2}r_0) - \frac{\mu}{\gamma K}\sqrt{S_2}(S_2 - a)N_n'(\sqrt{S_2}r_0)\right] \end{array} \right\}}$$

$$m_3 \equiv \frac{\left\{ \begin{array}{l} [S_1 N_n(\sqrt{S_1}r_0)]\left[\frac{n\gamma}{r_0} J_n(\sqrt{S_1}r_0) - \frac{\mu}{\gamma K}\sqrt{S_1}(S_1 - a)J_n'(\sqrt{S_1}r_0)\right] \\ - [S_1 J_n(\sqrt{S_1}r_0)]\left[\frac{n\gamma}{r_0} N_n(\sqrt{S_1}r_0) - \frac{\mu}{\gamma K}\sqrt{S_1}(S_1 - a)N_n'(\sqrt{S_1}r_0)\right] \end{array} \right\}}{\left\{ \begin{array}{l} [S_2 N_n(\sqrt{S_2}r_0)]\left[\frac{n\gamma}{r_0} N_n(\sqrt{S_1}r_0) - \frac{\mu}{\gamma K}\sqrt{S_1}(S_1 - a)N_n'(\sqrt{S_1}r_0)\right] \\ - [S_1 N_n(\sqrt{S_1}r_0)]\left[\frac{n\gamma}{r_0} N_n(\sqrt{S_2}r_0) - \frac{\mu}{\gamma K}\sqrt{S_2}(S_2 - a)N_n'(\sqrt{S_2}r_0)\right] \end{array} \right\}}$$

$$m_4 \equiv \frac{\left\{ \begin{array}{l} [S_1 N_n(\sqrt{S_1}r_0)]\left[\frac{n\gamma}{r_0} J_n(\sqrt{S_2}r_0) - \frac{\mu}{\gamma K}\sqrt{S_2}(S_2 - a)J_n'(\sqrt{S_2}r_0)\right] \\ - [S_2 J_n(\sqrt{S_2}r_0)]\left[\frac{n\gamma}{r_0} N_n(\sqrt{S_1}r_0) - \frac{\mu}{\gamma K}\sqrt{S_1}(S_1 - a)N_n'(\sqrt{S_1}r_0)\right] \end{array} \right\}}{\left\{ \begin{array}{l} [S_2 N_n(\sqrt{S_2}r_0)]\left[\frac{n\gamma}{r_0} N_n(\sqrt{S_1}r_0) - \frac{\mu}{\gamma K}\sqrt{S_1}(S_1 - a)N_n'(\sqrt{S_1}r_0)\right] \\ - [S_1 N_n(\sqrt{S_1}r_0)]\left[\frac{n\gamma}{r_0} N_n(\sqrt{S_2}r_0) - \frac{\mu}{\gamma K}\sqrt{S_2}(S_2 - a)N_n'(\sqrt{S_2}r_0)\right] \end{array} \right\}}.$$

r_1 = inside radius of the ferrite cylinder,

$r_0 \equiv$ radius of the circular waveguide.

Solving (6) and (7) for $n = \pm 1$ yields the circularly polarized propagation constants for the modified TE_{11} mode. Then by use of (1), the saturation rotation can be obtained for the composite ferrite and dielectric structures shown in Fig. 1.

Some of these theoretical results are given in Fig. 2 and Fig. 3.

ACKNOWLEDGMENT

The author wishes to express his sincere appreciation to Prof. F. J. Beck for his valuable advice during the course of this investigation. He also wishes to acknowledge his indebtedness to various members of the Microwave Group, Missile Systems Division, Raytheon Manufacturing Company, for their valuable help.

Spectral Distribution of Thermal Noise in a Gas Discharge*

SAUL M. BERGMANN†

Summary—**By means of thermodynamic considerations it is shown under which conditions microwave noise power generated by a gas discharge can be considered thermal. A critical analysis of Mumford's hypothesis is made.**

INTRODUCTION

MUMFORD [1] has pointed out that a fluorescent lamp filled with argon at 2-mm pressure and a drop of mercury having a saturated pressure of 6–8 microns, can be used as a standard microwave noise source having an equivalent temperature of 11,400°K. By considering the case of a black body radiating at a temperature of 11,400°K, and calculating from Wien's displacement law the wavelength of maximum radiation at this temperature, Mumford found $\lambda_m = 2535$Å. The fact that an intensive mercury line lies at 2537Å led Mumford to postulate that in a gaseous discharge, radiating light energy substantially at one particular wavelength λ, the microwave noise power available is the same as that available from a black body radiating maximum power at that wavelength. In this paper, it is shown under which conditions the noise power generated by a gas discharge can be considered thermal. To this end a critical analysis of Mumford's hypothesis is made. Three broad lines of attack are open.

1) A general quantitative formulation of the frequency spectrum distribution of the gas discharge from the far ultraviolet region down to the microwave range, on a kinetic theory basis. A theoretical treatment has been made by Parzen and Goldstein [2], but by invoking some critical arguments put forth by van der Ziel [3] it can be shown that their results hold only for microwave frequencies and would not hold for higher ones. The general treatment however is very difficult.
2) An experimental investigation.
3) An approach based on thermodynamical considerations which can be dealt with semiquantitatively. This course will be followed in this treatment.

* Manuscript received by the PGMTT, December 19, 1956; revised manuscript received, June 3, 1957.
† Raytheon Mfg. Co., Waltham, Mass.

THERMODYNAMIC THEORY OF THERMAL NOISE IN A GAS DISCHARGE

Mumford's hypothesis can be reformulated by dividing it into two parts.

1) In a gaseous discharge the microwave noise power available is the same as that available from a black body at a particular temperature, T.

2) That particular temperature, T, is of such magnitude as to correspond to a maximum power radiation at a wavelength λ_m at which light energy is radiated substantially monochromatically.

Consider a cavity with walls perfectly reflecting at all frequencies.

Let the cavity contain particles with Maxwellian distribution of velocities and in thermal equilibrium with radiation present in it. It has been shown by Einstein [4] that the radiation energy density in the cavity will then follow Planck's radiation law

$$U_\nu d\nu = (8\pi h\nu^3/c^3)[\exp(h\nu/\kappa T) - 1]^{-1} \cdot d\nu \qquad (1)$$

where T corresponds to the temperature of the particles.

Planck has shown [5], that if some carbon dust or any other material, capable of reaching high temperatures without absorbing too much heat, is brought into a perfectly reflecting cavity containing radiation, the radiation will redistribute itself and follow (1) after thermal equilibrium has been established. The temperature T will then be that of the material agent. Thus, if the cavity originally contained sharp mercury lines those would be absorbed, and partially re-emitted, and the radiation energy density would eventually obey (1).

Consider a gas discharge tube in a waveguide in a

plane parallel to the electric vector and let both ends of the waveguide be terminated by a perfect short circuit. Let it be assumed that the cavity thus formed has perfectly reflecting walls at all frequencies in the spectrum under consideration. In this case, the material medium consists of the particles in the gas discharge. The electrons owing to the applied external field and their small mass have by far higher velocities than the other particles in the gas discharge. Since, on the other hand, the interaction energy between radiation and a charged particle is proportional to the velocity of the particle, the contribution of the electrons to the radiation energy will be much more important than that of any other particles in the gas discharge. If, in addition, the electron distribution is Maxwellian—and only Maxwellian, neglecting quantum effects—the concept of electron temperature T_e is meaningful and the radiation energy density in the cavity will follow (1) with

$$T = T_e. \tag{2}$$

It can be shown that the noise power available from a black body is given by the quantum theory form of Nyquist's theorem

$$dP = h\nu[\exp(h\nu/\kappa T) - 1]^{-1} \cdot d\nu. \tag{3}$$

In our case the power available using (2) is

$$dP = h\nu[\exp(h\nu/\kappa T_e) - 1]^{-1} \cdot d\nu. \tag{4}$$

So far it has been assumed that the walls were reflecting perfectly at all frequencies. In fact, perfect reflection obtains in the microwave region and therefore (4) holds in that frequency range.

For microwave frequencies one has

$$h\nu/\kappa T_e \ll 1 \tag{5}$$

so that (4) reduces to

$$dP = \kappa \cdot T_e \cdot d\nu. \tag{6}$$

The first part of Mumford's hypothesis is then valid.

It is seen from (4) that the frequency corresponding to maximum power radiation is a function of the electron temperature T_e. On the other hand (4) holds irrespective of the particular properties associated with a given material in the cavity. This is a direct result of the second law of thermodynamics. It therefore follows that part two of Mumford's hypothesis is not valid.

Acknowledgment

Thanks are extended to Professor J. C. Slater, Professor Ladislas Goldstein, and Dr. E. Schloemann for stimulating discussions.

Bibliography

[1] W. W. Mumford. "A Broad-Band Microwave Noise Source," *Bell System Technical Journal*, Vol. 38 (October, 1949), p. 608.
[2] P. Parzen and L. Goldstein, "Current Fluctuations in the Direct-Current Gas Discharge Plasma," *Physical Review*, Vol. 79 (June 1, 1951), pp. 190–191.
[3] A. van der Ziel. "Thermal Noise at High Frequencies," *Journal of Applied Physics*, Vol. 21 (May, 1950), pp. 399–401.
[4] A. Einstein, "Zur Quantentheorie der Strahlung," *Physikalische Gesellschaft*, Zurich, Switzerland, Mitt. No. 18; 1916.
[5] M. Planck. "Waermestrahlung," 4th ed., p. 49; J. A. Barth, Leipzig (1921).
[6] K. S. Knol. "Determination of the Electron Temperature in Gas Discharges by Noise Measurements," *Philips Research Reports*, Vol. 6 (August, 1951), p. 288.
[7] W. Klein and W. Friz, Jr. "Gaseous Discharge Tubes as Standards in Noise Measurement in the CM Waveguide Range," *Journal of Electronics*, Vol. 1 (May, 1956), pp. 589–600.

Design of Aperture-Coupled Filters*

FLORIAN SHNURER†

Summary—**A procedure for the design of aperture-coupled filters is presented, based on the theory of conventional coupled circuits. This design procedure accounts for the relatively low insertion loss of aperture-coupled filters as compared with other known designs of microwave filters. The factors which contribute to this low value of insertion loss are the following:**

1) Use of a high Q-mode configuration such as a cylindrical cavity in the TE_{011} mode.

2) Aperture coupling of elements eliminating the losses of impedance transforming sections of transmission line.

3) A mechanical design which eliminates joints at critical points and also provides control over interior surface finishes.

* Manuscript received by the PGMTT, February 18, 1957; revised manuscript received, June 17, 1957.
† Gen. Elec. Co., Advanced Electronics Center, Ithaca, N. Y.

I. Introduction

MANY system applications require band-pass filters at microwave frequencies having a low insertion loss. While band-pass filters can be built by cascading resonant cavities formed by irises in rectangular waveguide such as described by Mumford,[1] the insertion loss of this filter structure becomes prohibitively large for many applications at X band and higher frequencies.

[1] W. W. Mumford, "Maximally flat filters in waveguide," *Bell Sys. Tech. J.*, vol. 27, pp. 684–713; October, 1948.

To achieve a lower insertion loss, a filter structure was developed which involves the coupling of cylindrical cavities operating in the TE_{011} mode through coupling apertures in the thin wall separating two adjacent cavities. By holding the thickness of this wall to 0.025 inch, it was possible to reduce materially the insertion loss through this filter structure, which will be called an aperture-coupled filter. For example, a four-section aperture-coupled filter was built at K band which had an insertion loss of 0.3 db, while the comparable iris-in-waveguide structure had an insertion loss of approximately 2.5 db.

The purpose of this paper is to describe the procedure for the design of aperture-coupled filters and to give experimental results on their performance.

II. Coupling to a TE_{011}-Mode Cylindrical Cavity

The basic element used in the design of aperture-coupled filters is a resonant cavity. A photograph of the cylindrical cavity used in the TE_{011}-mode configuration is shown in Fig. 1 with requisite coupling holes. The wall thickness at the coupling holes is 0.020 inch, while the accompanying plunger allows the cavity to be tuned ± 10 per cent of center frequency.

The TE_{011} mode was selected because of its very high unloaded Q, but any other normal mode can be chosen. The resonant wavelength of a TE_{011}-mode cavity is given by the expression[2]

$$\lambda = \frac{2}{\sqrt{\left[\frac{7.664}{\pi D}\right]^2 + \left[\frac{1}{L}\right]^2}} \tag{1}$$

where D is the diameter of the cavity and L, its length. However, for optimum Q, it is desirable to have D equal to L, so that if the resonant wavelength is known, the diameter of the cavity is given by the following:

$$D = 1.318\lambda. \tag{2}$$

Since the cavity dimensions are known, only the dimensions of the apertures which couple the cavities to the waveguide, or which couple adjacent cavities together, need to be determined. It should be clear that it is the dimensioning of these coupling apertures which finally determines the band-pass filter characteristic.

An analysis of the loaded Q, Q_L, of a cylindrical cavity oscillating in the TE_{011} mode, coupled to a rectangular waveguide, is given in Appendix I. The basic relation finally stated in (21) for an infinitesimally thin circular coupling aperture centrally located on the curved wall of the cavity is

$$\frac{1}{Q_L} = \frac{1.32\lambda^2 d^6}{ab\lambda_g D^4 L} \tag{3}$$

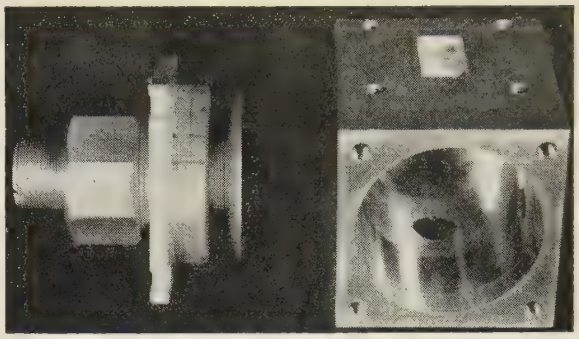

Fig. 1—Prototype TE_{011}-mode filter section.

where d is the diameter of the coupling hole, a and b the width and height of the waveguide, and λ_g the guide wavelength in the rectangular waveguide. This equation is the result of applying Bethe's theory of diffraction by small holes.[3] Consequently, the result is valid only for the case in which $d \ll \lambda$. This result also neglects heat losses in the cavity walls, so that it will yield a value of Q_L slightly higher than observed.

The coefficient of coupling γ between two adjacent TE_{011}-mode cavities coupled together by a common hole of diameter d may be expressed approximately by

$$\gamma = \frac{d_1^3}{2\pi D^2 L}. \tag{4}$$

This approximate relation is given by Bethe,[3] and allows filter theory as developed for circuits which are usually expressed in terms of parameters Q_L and γ (*i.e.*, the loaded Q of the resonant circuit and the coupling coefficient between adjacent resonant circuits) to be applied to the design of a microwave filter in a quantitative manner.

III. Specific Cases and Experimental Data

A. A Single Resonant Cavity

Eq. (3) can be applied directly to the design of a band-pass filter. If the filter is to consist of a single cavity with two equal but diametrically opposite coupling holes, the loaded Q of the structure will then be halved so that

$$\frac{1}{Q_l} = \frac{2.64\lambda^2 d^6}{ab\lambda_g D^4 L}. \tag{5}$$

Measurements were made on the structure shown in Fig. 1 for various values of coupling hole diameter. The experimental points and the theoretical curve, as obtained from (5), are given in Fig. 2 for the case in which

$\lambda = 0.875$ inch
$a = 0.622$ inch
$b = 0.311$ inch
$D = 1.250$ inches
$L = 0.860$ inch.

[2] T. Moreno, "Microwave Transmission Design Data," McGraw-Hill Book Co., Inc., New York, N. Y., p. 219; 1948.

[3] H. A. Bethe, "Theory of diffraction by small holes," *Phys. Rev.*, vol. 66, pp. 163–181; October, 1944.

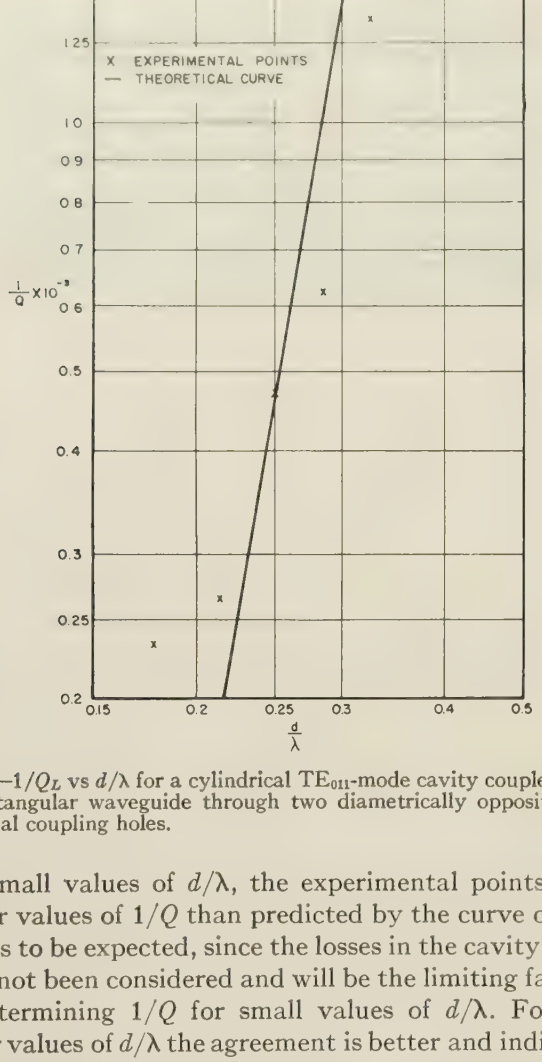

Fig. 2—$1/Q_L$ vs d/λ for a cylindrical TE_{011}-mode cavity coupled to a rectangular waveguide through two diametrically opposite and equal coupling holes.

For small values of d/λ, the experimental points give higher values of $1/Q$ than predicted by the curve of (5). This is to be expected, since the losses in the cavity walls have not been considered and will be the limiting factors in determining $1/Q$ for small values of d/λ. For the larger values of d/λ the agreement is better and indicates that Bethe's small-hole theory is a satisfactory approximation for holes of the order of $\lambda/4$ in diameter.

B. Two Resonant Cavities Coupled Together

The structure that is visualized, is the coupling of two TE_{011}-mode cavities, as shown in Fig. 3, by a common-coupling hole.

This circuit can be treated in terms of the equivalent circuit of a double-tuned coupled circuit treated by Terman.[4] The equivalent circuit is illustrated in Fig. 4.

The loaded Q of the primary and secondary is determined by the usual relations

$$Q_p = \frac{\omega_0 L_p}{R_p} \qquad Q_s = \frac{\omega_0 L_s}{R_s}. \tag{6}$$

For the case of the microwave structure, the loaded Q of the primary and secondary is determined from (3) by substituting the dimension of the particular cavity, waveguide, and coupling hole. The only other variable determining the filter characteristic, is the diameter of the coupling hole which couples two adjacent cavities.

[4] F. E. Terman, "Radio Engineering," McGraw-Hill Book Co., Inc., New York, N. Y., pp. 58–66; 1947.

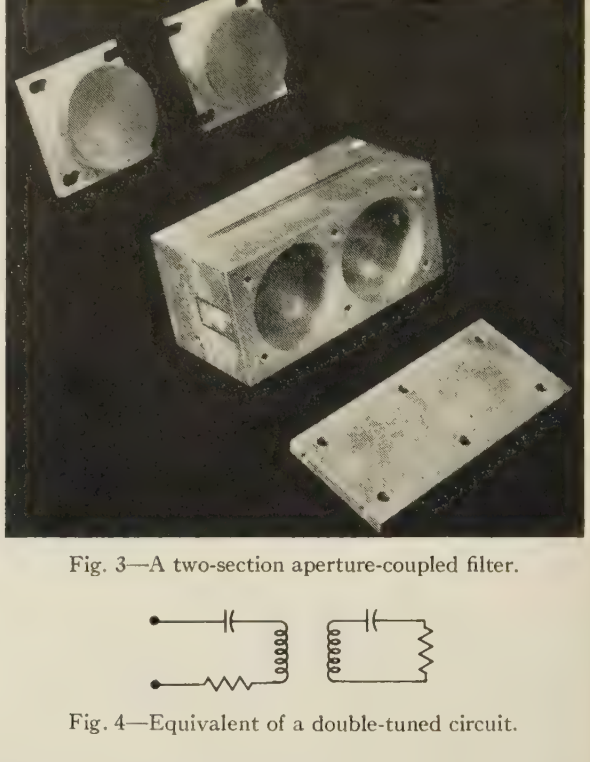

Fig. 3—A two-section aperture-coupled filter.

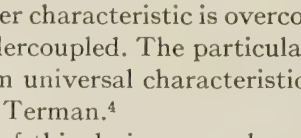

Fig. 4—Equivalent of a double-tuned circuit.

This diameter can be determined from (4) once the value of coupling coefficient γ is known. γ determines whether the filter characteristic is overcoupled, critically coupled, or undercoupled. The particular value of γ can be selected from universal characteristic curves such as those given by Terman.[4]

An example of this design procedure is given for the following case of a two-cavity band-pass filter at X band. A filter having a half-power bandwidth of 3.0 mc centered at 9000 mc was desired. Two TE_{011}-mode cavities, 1.94 inches in diameter and 1.15 inches in length, were used. A curve of the half-power bandwidth vs coupling hole diameter for a single cavity coupled to waveguide, is given in Fig. 5. The cavities were coupled to RG-52/U waveguide at the input and output of the filter and were coupled together by a common coupling hole. From universal resonance curves it was established that the single cavity coupled to a waveguide must have a half-power bandwidth of 2.0 mc. Fig. 5 indicates that a hole diameter of 0.323 inch is required to couple the cavities to the input and output waveguides. The only remaining quantity to be determined was the diameter of the hole coupling the two cavities together. Substituting in (4), the coefficient of coupling for critical coupling, $\gamma = 1/Q_L = 2/9000$, and solving for the hole diameter yielded a value of 0.176 inch. Experimental tests showed that this value was somewhat too small, so that the filter had an undercoupled characteristic. A direct method of determining the coupling coefficient of a given coupling hole is given in Appendix II. This experimental method led to a coupling hole of 0.182 inch in diameter and a filter characteristic corresponding to a critically coupled double-resonant circuit.

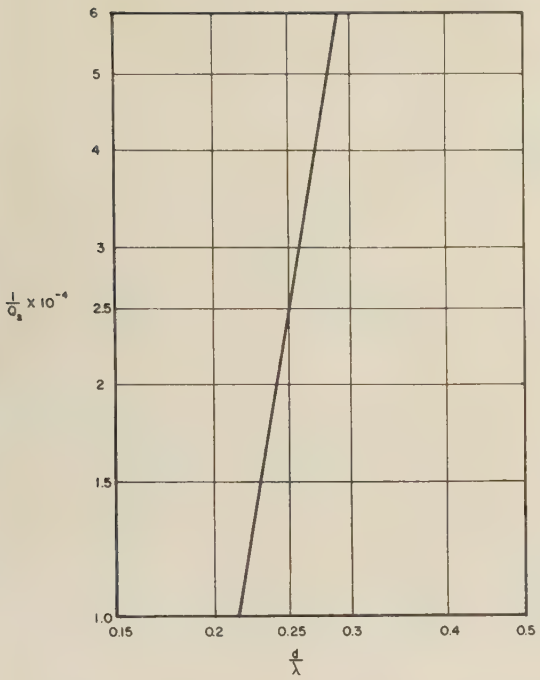

Fig. 5—$1/Q_L$ vs d/λ for a cylindrical TE_{011}-mode cavity coupled to a rectangular waveguide through a single coupling hole.

IV. Insertion Loss in Aperture-Coupled Filters

The insertion loss in any microwave component usually can be attributed to a copper loss in the conducting walls or to an absorption of energy by some additional dissipative element within the device. As no dissipative element is introduced into the resonant cavities of the filters in question, the remaining cause of loss is simply the heat loss on the cavity walls and in the coupling irises. Therefore, the problem is that of deducing a simple expression for this insertion loss.

Let us examine the basic definition of Q as given in (13) of Appendix I.

$$Q = \frac{\omega \text{ (energy stored in the circuit)}}{\text{average power loss}} \cdot \tag{7}$$

For a given cavity, the energy storage should be a function of the mode of oscillation and, therefore, independent of loading. Average power loss, however, can be ascribed to losses within the cavity, and to losses caused by a transfer of power out of a cavity. Consider the ratio Q_L/Q_u, where Q_u is the cavity Q with no power coupled to an outside circuit, and Q_L is as defined in Appendix I.

$$\frac{Q_L}{Q_u} = \frac{\omega W_s}{P_t} \cdot \frac{P_h}{\omega W_s} = \frac{P_h}{P_t} \tag{8}$$

where P_h is the average power lost by rf heating in the walls and P_t is the average power transferred to an external circuit. If Q_L is taken as the quantity defined by (21), then the ratio $Q_L/2Q_u$ represents the ratio of power lost in rf heating to the power transferred through a cavity having two symmetrically placed coupling holes. The power loss though the cavity L in decibels is given by

$$L = 10 \log_{10} \left[\frac{1}{1 - \frac{Q_L}{2Q_u}} \right]. \tag{9}$$

Since $Q_L/2Q_u \ll 1$,

$$L \cong 10 \log_{10} \left[1 + \frac{Q_L}{2Q_u} \right]. \tag{10}$$

This expression represents the power loss in just one cavity. In order to calculate the total power loss it is necessary to sum over the total number of cavities, N.

$$L_T \cong \sum_{i=1}^{N} 10 \log_{10} \left[1 + \frac{Q_{Li}}{2Q_{ui}} \right]. \tag{11}$$

In calculating the above power loss, Q_L is obtained by substituting physical dimensions of the cavity in (21), while values Q_u can be calculated or obtained from universal curves as given by Moreno.[2] Eq. (11) can be applied to the X-band filter described in Section III-B. The unloaded Q for the single cavity is about 20,000, while the loaded Q should be about 2100. Substituting into (11), one obtains

$$L_t = \sum_{i=1}^{2} 10 \log_{10} \left[1 + \frac{2100}{40{,}000} \right] = 0.44 \text{ db}. \tag{12}$$

The measured insertion loss was 0.5 db, which is in good agreement with the computed value. Eq. (11) is an approximation in which Q_L is considered to be the value of Q obtained when a cavity is loaded by coupling it to an external waveguide circuit. In general, this is not the case because the cavity in question may be coupled to two adjacent cavities. In spite of this approximation, the results obtained using (11) agree quite well with measured values of insertion loss, indicating that the losses in the coupling holes or irises are essentially negligible in comparison with the rf losses over the cavity walls.

Appendix I

Derivation of Loaded Q of a TE_{011}-Mode Cylindrical Cavity Coupled to a Rectangular Waveguide

The basic relation for the Q of any circuit can be expressed as follows:[5]

$$\frac{1}{Q} = \frac{\text{average power loss}}{\omega \text{ (energy stored in the circuit)}} = \frac{S}{\omega W_s} \cdot \tag{13}$$

[5] S. Ramo and J. R. Whinnery, "Fields and Waves in Modern Radio," John Wiley & Sons, Inc., New York, N. Y., p. 9; 1944.

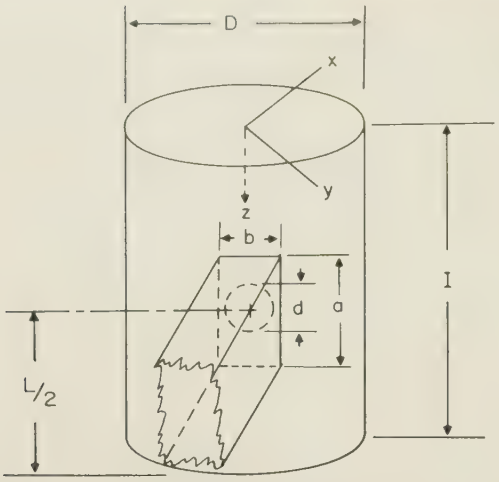

Fig. 6—Cavity and waveguide configuration with cavity system of coordinates.

Assume that a cylindrical cavity of diameter D and length L is coupled to a rectangular waveguide of width a and height b by a hole of diameter d. The configuration is shown in Fig. 6.

Assume that the TE_{011} mode is excited in the cylindrical cavity with the following field components:

$$\begin{aligned} E_\theta &= J_1(k_1 r)\sin\frac{\pi z}{L} \\ E_p &= E_Z = H_\theta = 0 \\ H_p &= \frac{\pi}{j\omega\mu L} J_1(k_1 r)\cos\frac{\pi z}{L} \\ H_Z &= \frac{-k_1}{j\omega\mu} J_0(k_1 r)\sin\frac{\pi z}{L} \end{aligned} \tag{14}$$

where $k_1 = 7.664/D$, and a time variation of exp $(j\omega t)$ is assumed. The energy stored in the cavity W_s is given by

$$W_s = \frac{\epsilon}{2}\int_v E_\theta^2 dV \tag{15}$$

where V is the volume of the cavity. Substituting (14) into (15) the expression for the stored energy can be evaluated as

$$W_s = \frac{\pi\epsilon D^2 L}{16} J_0^2(3.832) \tag{16}$$

where J_0 is the Bessel function of the first kind of order zero.

According to Bethe,[3] the average power lost through a window can be expressed as

$$S = \frac{k^2}{2S_a}\left| PE_{on}E_{an} + jM_1 H_{ol}H_{al} + jM_2 H_{om}H_{am}\right|^2 \tag{17}$$

where P, M_1, and M_2 are the polarizabilities of the window which depend on the geometrical configuration of the window. S_a is a normalizing constant. The fields with subscript 0 are the cavity fields, while the fields with subscript a are waveguide fields. The subscripts n, l, m refer to the principal axes of the window. The geometrical orientation is shown in Fig. 7. The waveguide fields for the dominant TE_{10} mode are given as

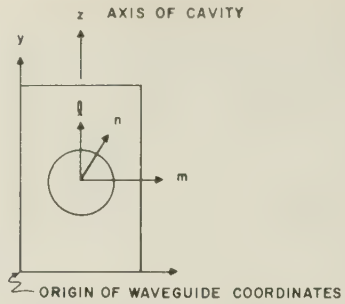

Fig. 7—System of coordinates in the window.

$$\begin{aligned} H_z &= H_1\cos\frac{\pi x}{a} \\ H_x &= \frac{j2aH_1}{\lambda_g}\sin\frac{\pi x}{a} \\ E_y &= \frac{-jn2aH_1}{\lambda}\sin\frac{\pi x}{a}. \end{aligned} \tag{18}$$

The average power transmitted down the waveguide is given by

$$S_a = \frac{2a^3 b\eta}{2\lambda\lambda_g} H_1^2. \tag{19}$$

For a circular window, the polarizabilities are $M_1 = M_2 = d^3/6\eta$, and $P = d^3/3\eta$.[6]

The expression for the average power lost through the window can now be obtained by substituting the values for the polarizabilities, (18), (19), and (14) into (17) to obtain

$$S = \frac{1.63\lambda d^6}{ab\,D^2\lambda_g\eta} J_0^2(3.832). \tag{20}$$

The final form of the expression for $1/Q$ can now be obtained by substitution (15) and (20) into (13).

$$\frac{1}{Q_L} = \frac{1.32\lambda^2 d^6}{ab\lambda_g D^4 L}. \tag{21}$$

This equation expresses the loaded Q of the cavity in terms of the waveguide and cavity and coupling hole dimensions. A correction can be made to account for heat losses, but it is usually not warranted because of the high unloaded Q of the cavity.

[6] A. T. Starr, "Radio and Radar Technique," Pitman Publ. Corp., New York, N. Y.; 1953. See p. 157 for the polarizabilities in mks units.

Appendix II

Experimental Method of Determining Coupling Coefficient

Consider two identical structures consisting of a waveguide coupled to a cavity, as shown in Fig. 6, to be coupled together through a common coupling hole. The diameter of this coupling hole can be approximated using (4), but an experimental check of the value is highly desirable.

The equivalent circuit under consideration is illustrated in Fig. 8.

The impedance looking into the input waveguide is

$$Z_1 = \frac{(\omega M_1)^2}{Z + \dfrac{(\omega M)^2}{Z}} \tag{22}$$

where

$$Z = R + j\left(\omega L - \frac{1}{\omega C}\right).$$

At resonance

$$Z_1 = \frac{(\omega M_1)^2}{R[1 + (\gamma Q_L)^2]} \tag{23}$$

where γ is the coupling coefficient, and $Q_L = \omega_0 L/R$ can be obtained from (21).

The reflection coefficient is given by the following relation:

$$\Gamma = \frac{Z_1 - Z_0}{Z_1 + Z_0} \tag{24}$$

where Z_0 is the characteristic impedance of the input waveguide. Substituting (23) into (24) yields

$$\Gamma = \frac{(\omega M_1)^2 - RZ_0[1 + (\gamma Q_L)^2]}{(\omega M_1)^2 + RZ_0[1 + (\gamma Q_L)^2]}. \tag{25}$$

If the first cavity in the circuit is tuned to resonance and the second is detuned, then $k = 0$ and

$$\Gamma = \frac{(\omega M_1)^2 - RZ_0}{(\omega M_1)^2 + RZ_0}. \tag{26}$$

If critical coupling is attained, $\gamma_c = 1/Q_L$ and it follows that

$$\Gamma_c = \frac{(\omega M_1)^2 - 2RZ_0}{(\omega M_1)^2 + 2RZ_0}. \tag{27}$$

Solving (26) for $(\omega M_1)^2$ yields

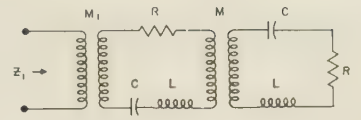

Fig. 8—Equivalent circuit of a two-cavity filter.

$$(\omega M_1)^2 = RZ_0 \frac{[1 + \Gamma_0]}{[1 - \Gamma_0]} = RZ_0 S_0 \tag{28}$$

where S_0 is the input vswr that is measured with the second resonator detuned. Substituting this result into (25) yields

$$\Gamma = \frac{S_0 - [1 + (\gamma Q_L)^2]}{S_0 + [1 + (\gamma Q_L)^2]}. \tag{29}$$

Eq. (29) can now be solved for the γQ_L to give

$$\gamma Q_L = \frac{\gamma}{\gamma_c} = \sqrt{\frac{S_0 - 1 - \Gamma(S_0 + 1)}{+1}}. \tag{30}$$

Using the fact that Γ is real, it is possible to express (30) in terms of S_0, the vswr measured with the second cavity detuned, and S, the vswr measured with both cavities tuned to resonance.

$$\frac{\gamma}{\gamma_c} = \sqrt{\frac{S_0 - S}{S}}. \tag{31}$$

Knowing the ratio γ/γ_c, and that the coupling coefficient varies as the cube of the hole diameter, it is possible to compute the hole diameter for critical coupling and hence for any value of coupling coefficient desired.

Besides obtaining the value of coupling coefficient experimentally, the conditions for a matched input looking to the filter can be derived. If (26) and (27) are solved simultaneously with the variables $(\omega M_1)^2$ and RZ_0, then the condition for the existence of a solution requires that

$$\Gamma_c = \frac{1 - 3\Gamma_0}{\Gamma_0 - 3}. \tag{32}$$

Therefore, a good match with critical coupling requires that $\Gamma_0 = 1/3$. The more general case follows from setting $\Gamma = 0$ in (29) and solving for γ/γ_c.

$$\gamma/\gamma_c = \sqrt{S_0 - 1}. \tag{33}$$

This equation determines the coupling coefficient for $S = 1$ at the filter resonant frequency.

Optimum Impedance and Dimensions for Strip Transmission Line*

KARLE S. PACKARD†

Summary—This paper makes use of the higher mode limitations on the dimensions of symmetrical strip transmission line to derive the permissible dimensions at any given frequency and characteristic impedance. In conjunction with Cohn's results for the attenuation in strip transmission line these are used to obtain the maximum achievable Q at any frequency and the optimum characteristic impedance; that is, the impedance providing the lowest attenuation. This provides the basis for selecting the characteristic impedance for resonant elements in strip line filters and other applications wherein the lowest possible attenuation is desired. Conclusions are also reached regarding the best form factor (ratio of strip thickness to ground-plane spacing) for a given characteristic impedance.

Introduction

IN MANY microwave applications it is desirable to use a section of transmission line having the lowest possible attenuation. This is particularly true in the case of narrow band microwave filters where lengths of transmission line are used as resonant elements. In such an application, the characteristic impedance and the line dimensions may usually be chosen arbitrarily. It is necessary, therefore, to know how the attenuation varies with these parameters and what limitations are imposed upon them. Although this information is well known for coaxial line and uniconductor waveguides, it is not generally known for strip transmission lines. It is the purpose of this paper to present this information for symmetrical strip line comprising a flat strip center conductor centrally located between, and parallel to, two parallel ground planes.

As has been shown by Cohn,[1] the attenuation of symmetrical strip line decreases as the characteristic impedance is decreased for a constant ground-plane spacing, and decreases as the ground-plane spacing is increased for a constant characteristic impedance. Therefore, strip transmission line does not have an optimum impedance for fixed outer conductor size analogous to the case of coaxial line. However, if the outer conductor size of coaxial line is not limited, the optimum impedance is limited by the first circumferential mode; it is 92.6 ohms, and produces the absolute minimum attenuation.[2] Similarly, by considering the size limitations due to higher modes in symmetrical strip lines, we may deduce the optimum impedance for these lines.

Higher Mode Limitations on Line Dimensions

One limit on the line dimensions is imposed by the TM modes, the lowest of which has a cut-off wavelength equal to twice the ground-plane spacing. This gives an absolute upper limit to the ground-plane spacing. For spacings less than this, a possible circumferential TE mode can also impose a limit. The cut-off frequency of this TE mode depends on the strip width and the ground-plane spacing. The TE cut-off wavelength may be calculated[3] from the analogous E-plane bifurcation in rectangular waveguide, and for the lowest mode is given by

$$\lambda_c = 2w + 4d \tag{1}$$

where d is the distance from the edge of the strip to the open-circuit point, and is given for infinitesimally thin strips by,[4]

$$d = \frac{D}{\pi} \ln 2 + \frac{\lambda}{2\pi}\left[S_1\left(\frac{2D}{\lambda}\right) - 2S_1\left(\frac{D}{\lambda}\right)\right] \tag{2}$$

with

$$S_1(x) = \sum_{n=1}^{\infty}\left(\arcsin\frac{x}{n} - \frac{x}{n}\right).$$

(See Marcuvitz[4] for tabulation of arcsine sum functions.)

The meaning of w and D are as shown in Fig. 1, where the field configuration for this mode is shown and Fig. 1(b) shows the "uniform field" equivalent of Fig. 1(a); that is, a line having the same propagation constant and characteristic impedance, but no fringing capacitance. Although (2) holds only for an infinitesimally thin strip, the results may be put in a form which takes account of the strip thickness, t. Consider the "uniform field" equivalent for a thick strip as shown in Fig. 2(a). For the line in Fig. 2(a) to have the same characteristic impedance and cut-off wavelength as that in Fig. 1(b), we must have,

$$w' = w + 2d, \qquad D' = D + t.$$

Now the line in Fig. 2(a) is the equivalent of some actual line shown in Fig. 2(b). Therefore, a line with a strip of thickness, t, has the same cut-off wavelength as

* Manuscript received by the PGMTT, February 25, 1957; revised manuscript received, June 14, 1957.

† Airborne Instruments Lab., Inc., Mineola, N. Y.

[1] S. Cohn, "Problems in strip transmission lines," IRE TRANS., vol. MTT-3, pp. 119–126; March, 1955.

[2] G. L. Ragan, "Microwave Transmission Circuits," McGraw-Hill Book Co., Inc., New York, N. Y., p. 146; 1948.

[3] A. A. Oliner, "Theoretical Developments in Symmetrical Strip Transmission Line," presented at Symposium on Modern Advances in Microwave Techniques, Polytechnic Inst. of Brooklyn, Brooklyn, N. Y.; November, 1954.

[4] N. Marcuvitz, "Waveguide Handbook," McGraw-Hill Book Co., Inc., New York, N. Y., p. 353; 1951.

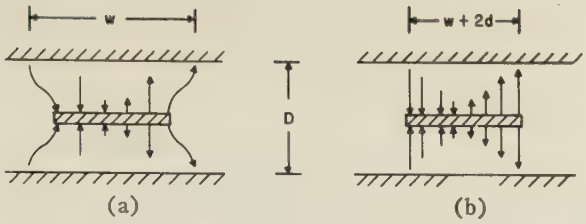

Fig. 1—Zero-thickness strip line. (a) Actual line; (b) uniform field equivalent.

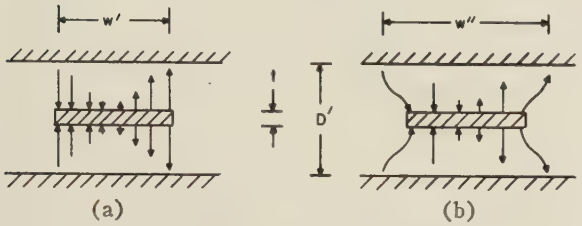

Fig. 2—Thick-strip line. (a) Uniform field equivalent; (b) actual line.

a line of the same characteristic impedance but with a zero-thickness strip and a ground-plane spacing less than that of the former by the amount, t.

We may combine (1) and (2) and write

$$\frac{w}{D} = \frac{v}{2}\frac{1}{Df_c} - \frac{2\ln 2}{\pi} - \frac{v}{\pi}\frac{1}{Df_c}\left[S_1\left(\frac{2}{v}Df_c\right) - 2S_1\left(\frac{1}{v}Df_c\right)\right] \qquad (3)$$

where v is the phase velocity and f_c is the cut-off frequency. Eq. (3) gives the maximum value of w/D at the cut-off frequency from which the minimum permissible characteristic impedance may be calculated.[5,6] If now this characteristic impedance is plotted as a function of $\sqrt{\epsilon}Df_c$, the curves of Fig. 3 result, where those for thick strips are obtained by multiplying the abscissas of the $t=0$ curve by $D'/(D'-t)$. Therefore, as used in Fig. 3, D refers to any line regardless of strip thickness. These curves are useful in determining the operating frequency limit for a line of given dimensions. We will make further use of them, however, in deriving the optimum characteristic impedance.

It should be noted that the assumption made in using an analysis based on the waveguide E-plane bifurcation and the "uniform field" equivalents is that there is no higher mode interaction between the two edges of the strip. This assumption is true providing that the strip is not too narrow. For the ranges of characteristic impedance and t/D used in Fig. 3, the value of w/D is not less than 0.35 for values of $\sqrt{\epsilon}Df_c$ up to 5.75. Furthermore, this minimum value of w/D holds for thin strips, whereas the minimum value of w/D is even larger for thicker strips. It can be expected, therefore, that for practical strip line geometries higher mode interaction will not be a serious factor and the results based on this assumption will be valid.

[5] S. Cohn, "Characteristic impedance of the shielded-strip transmission line," IRE Trans., vol. MTT-2, pp. 52–57; July, 1954.

[6] R. H. T. Bates, "The characteristic impedance of the shielded slab line," IRE Trans., vol. MTT-4, pp. 28–33; January, 1956.

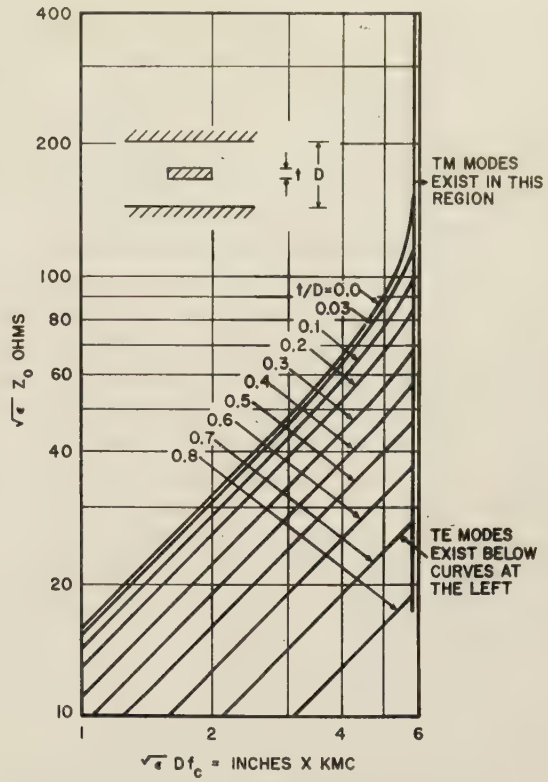

Fig. 3—Minimum characteristic impedance vs higher mode cut-off frequency.

Optimum Characteristic Impedance

From Cohn's calculations of losses in symmetrical strip line[1] the ground-plane spacing should be as great as possible for low loss, but from the curves in Fig. 3 it is seen that a high impedance must then be used which in itself implies high loss. Due to the nonlinear relations involved, however, it appears that there should be a minimum loss. That is, over the range of characteristic impedance to be considered, inspection of the curves used by Cohn[1] show that the unloaded Q of a resonant line as a function of the frequency, ground-plane spacing and impedance can be approximated by a linear function,

$$Q\sqrt{f} = Df(A - B\sqrt{\epsilon}Z_0)$$

where $A \gg B$ and both are constants. The lower asymptote of each of the curves in Fig. 3 is

$$\sqrt{\epsilon}Z_0 = 15.95\sqrt{\epsilon}(D - t)f$$

so that in this region the maximum Q is given by

$$Q\sqrt{f} = Df[A - C(D - t)f]$$

where C is a constant and the second term on the right is much smaller than the first over the range of Df to be considered. Therefore, $Q\sqrt{f}$ is an increasing function of Df in this range. As the curve in Fig. 3 departs from this

asymptote, however, the minimum impedance rapidly approaches a very large value and therefore $Q\sqrt{f}$ must decrease as Df increases. Due to the unwieldy functions involved, this maximum is most easily found by graphical methods. The results of these calculations for copper conductors are shown in Fig. 4, for several values of t/D from which it is seen that the minimum loss for very thin strips is obtained for a characteristic impedance of about 95 ohms at a ground-plane spacing of $t+0.44\lambda/\sqrt{\epsilon}$ inches. This has been verified experimentally for thin strips and is true for values of t/D up to 0.14 at which point the limit for the TM mode is reached. For t/D greater than 0.14 the maximum achievable Q is limited only by the ground-plane spacing, the optimum impedance being indicated by the intersection of the parametric curves in Fig. 3 with the line $\sqrt{\epsilon}Df_c=5.9$, which is the cut-off condition for the lowest TM mode.

The curves in Fig. 4 also show that there is an optimum set of dimensions for minimum loss. That is, the ratio $t/D=0.25$ and a characteristic impedance of 76 ohms, with a ground-plane spacing of one-half wavelength at the operating frequency, produces the absolute minimum attenuation. The maximum obtainable resonator Q for this case is $2.25\times10^4/\sqrt{f}$ which is comparable to the $2.1\times10^4/\sqrt{f}$ obtainable for coaxial line using copper conductors. It should also be mentioned that, although the approximations used in calculating the attenuation as a function of characteristic impedance do not permit the full range of values of t/D to be included, Cohn's calculations have been extended by the writer to higher values of t/D. Although the limits imposed do not permit a positive statement, it does appear that the minimum attenuation for a *fixed-ground-plane spacing* will also be obtained for $t/D=0.25$ over the impedance range 80 to 130 ohms. The improvement over the case $t/D=0.1$ is not great, however, and for all practical purposes the latter may be used for fixed ground-plane spacing throughout the range of impedances most used.

The accuracy of these calculations is limited by the accuracy of Cohn's formulas for attenuation. These are admittedly approximate, but are accurate to ±4 per cent which is certainly sufficient for most all applications.

Practical Applications of Results

It should be pointed out that the optimum impedance and ground-plane spacing arrived at by this procedure dictate operation at the cut-off frequency of one or more higher modes. In actual engineering practice it would be necessary to provide some margin of safety by operating below these cut-off frequencies, particularly in the case of the TM modes which will radiate.[3] In some applications it may be permissible to operate under conditions where the TE modes can exist, and, in fact, what might be called super-Q resonators have been made at this Laboratory under these conditions.

To provide sufficient reactive attenuation of the higher modes of the strip line, an analysis can be made

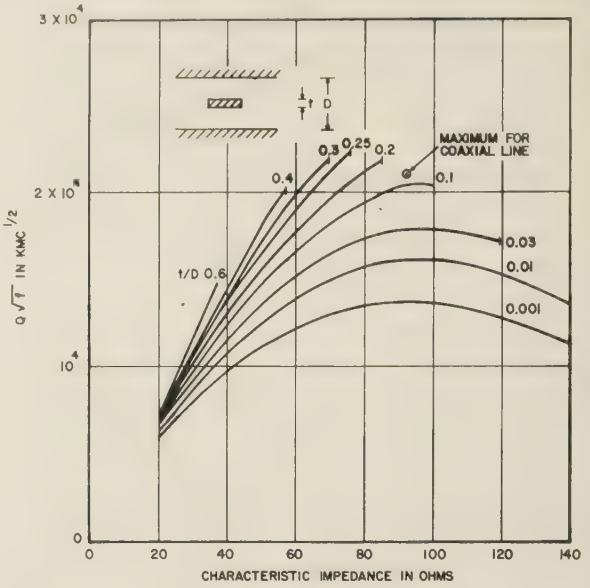

Fig. 4—Maximum obtainable Q vs characteristic impedance.

using the expression for the attenuating effect of a waveguide below cut-off,

$$L = 54.5\frac{d}{\lambda_c}\sqrt{1-(\lambda_c/\lambda)^2} \text{ db per length, } d.$$

This may be put in a form more useful for the present purpose giving the following equation for the new operating conditions in terms of the desired higher mode attenuation,

$$Df = Df_c\sqrt{1-(L/27.3)^2},$$

where L is the desired attenuation in db per ground-plane spacing. L has a maximum value of 27.3, as may be seen from the equation for L by letting $\lambda\rightarrow\infty$ and $d=D$, since D/λ_c has a maximum of $\frac{1}{2}$. If the same reactive attenuation is required for both TE and TM modes, then the optimum characteristic impedance will remain unchanged since the whole operating curve in Fig. 3 is shifted to the left. If the attenuation is only required for the TM modes, then the optimum characteristic impedance will be given by the intersection of the parametric curves in Fig. 3 with the new constant Df line. The maximum Q may be found by transferring these limiting values of impedance to the curves in Fig. 4. For arbitrary amounts of reactive attenuation for the two types of higher mode the user can readily find the optimum characteristic impedance from the principles used above. Particular care in these matters must be taken in designing filters as the unwanted modes can seriously affect the coupling between the filter elements.

Conclusion

To summarize the results obtained, several points may be brought out. The first of these is that caution must be exercised in regard to TE modes in low imped-

ance circuits. For example, it is not generally appreciated that, for typical values such as $D=\lambda/4$ and $t/D=0.1$, the TE mode cut-off corresponds to a characteristic impedance of 43 ohms. Whereas the existence of this mode does not necessarily cause serious trouble, it may often explain discrepancies between experimental results and those calculated on the basis of a pure TEM mode. As is obvious from Fig. 3, this may be avoided by using a thicker strip.

The second point is the existence of an optimum characteristic impedance for obtaining the lowest attenuation. The value of this optimum will depend on the desired higher mode attenuation. Because the conditions will vary widely for different applications, the data presented cover the case of operation at the cut-off frequency of both the lowest TE and TM modes. This condition produces the lowest possible loss. For practical applications, however, the method for obtaining the optimum in other cases has been outlined.

A few final words should be said in regard to an interesting point shown by the curves in Fig. 3 and 4. It is assumed that one usually wishes to operate with the lowest possible line losses and this generally imples a high value of D, and therefore, of Df. As to the strip dimensions for lowest line loss an examination of the curves in Figs. 3 and 4 shows that for low values of characteristic impedance, it is desirable (see Fig. 4) and often necessary (see Fig. 3) to use high values of t/D. From the curves for characteristic impedance given by Bates[6] it is seen that high values of t/D imply small values of w/D. On the other hand, Bates also shows that a high characteristic impedance can *only* be obtained with small values of t/D. Therefore, it may be concluded that, in addition to the preceding considerations of the optimum characteristic impedance, one may make the generalization that a high impedance line with lowest loss should be in the familiar strip line from ($t \ll w$) whereas low impedance lines with lowest loss should be made with much thicker strips, in some cases with the strip thickness exceeding the strip width ($t > w$).

Deflection of Waveguide Subjected to Internal Pressure*

LUCIEN G. VIRGILE†

Summary—**The pressure carrying capacity of a large range of standard waveguide sizes can be readily determined by the use of formulas presented in this paper. The derivation of these formulas is obtained by a continuous beam analogy and comparable test results are shown which substantiate the validity of the theoretical analysis.**

Where high pressure conditions prevent the use of standard waveguide, these same formulas are utilized in the development of special high-strength lightweight guide. Techniques for designing such waveguide, including the use of a honeycomb sandwich construction, are discussed.

THE DEVELOPMENT of radar systems of increasing range has been brought about largely by the use of greater and greater power. In order to increase the power handling capacity of the microwave packages, pressurization is utilized to prevent electrical breakdown. It is, therefore, extremely desirable to be able to determine quickly the pressure carrying capacity of a given waveguide and, when standard waveguide cannot safely carry the required pressure, to be able to design special guide of minimum weight and/or cost.

The derivation of formulas that express the relationship of wall thickness to pressurization capacity is presented for a considerable range of waveguide sizes. The criteria for this relationship are 1) that the waveguide should not permanently distort, and 2) that the elastic deflection should not exceed the amount permissible for satisfactory microwave use. The problem is approached both analytically and empirically with good correlation between the two methods.

Fig. 1(a) depicts a typical cross section of unpressurized guide. The application of internal pressure results in distortion as shown in Fig. 1(b). The question frequently arises, "How can the short wall bend inward when the pressure should be forcing it outward?" A simplified explanation of this phenomenon is that the corner moment, due to the relatively greater length of the long wall, is sufficient to more than overcome the internal pressure on the short wall, resulting in an inward deflection. This is borne out by both the derived formulas and actual test results.

The pressurized waveguide cross section is considered to be similar to a uniformly loaded continuous beam of an infinite number of spans (or a simple beam with end moments[1]) as shown in Fig. 2. The analysis that follows pertains to unsupported waveguide which, as a practical consideration, means that it is applicable to sections that

* Manuscript received by the PGMTT, March 13, 1957; revised manuscript received, May 13, 1957.

† Microwave Electronics Div., Sperry Gyroscope Co., Great Neck, N. Y.

[1] T. N. Anderson, "Rectangular and ridge waveguide," IRE TRANS., vol. MTT-4, pp. 201–209; October, 1956.

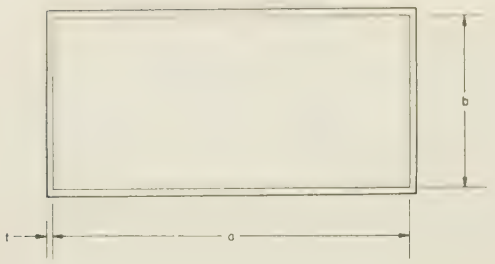

(a)

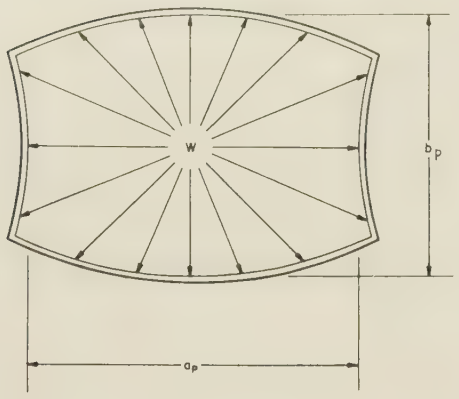

(b)

Fig. 1—(a) Unpressurized waveguide; (b) waveguide under pressure.

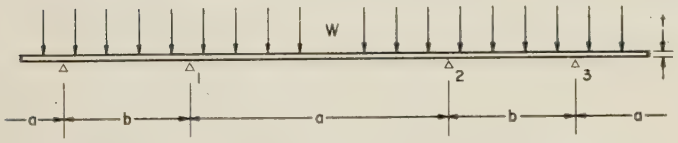

Fig. 2—Waveguide shown as infinite continuous beam.

are distant from flanges (or other supports) by a length of more than the broad wall dimension. Symbols used in the derivations are defined in Table I.

The three-moment equation is applied to the first three spans of the continuous beam resulting in:

$$\frac{M_1 a}{I_1} + 2M_2\frac{(a+b)}{I_2} + \frac{M_3 b}{I_3} = \frac{w(a^3+b^3)}{4I} .$$

The beam (for standard waveguide) is of constant cross section, allowing the I term to drop out. Since the waveguide is symmetrical at each corner,

$$M_1 = M_2 = M_3 = M \text{ and}$$

$$3M(a+b) = \frac{w}{4}(a^3+b^3)$$

$$M = \frac{w(a^3+b^3)}{12(a+b)} . \tag{1}$$

It may be noted that (1) is consistent with the common structural practice of considering the maximum bending moment on any span of a continuous beam of many equal spans to be equal to $wL^2/12$.

TABLE I

Symbols and Elementary Equations

a = inside long dimension in inches
b = inside short dimension in inches
t = thickness in inches
w = pressure in pounds per square inch*
$I = t^3/12$ = moment of inertia*
M = bending moment at any corner or point of support (since $M_1 = M_2 = M_3 = M_4$, etc.)
E = modulus of elasticity in pounds per square inch
s = stress at yield point** in pounds per square inch
k_1, k_2, k_3 = constants for given values of a, b, and t
y_a = deflection of a at $a/2$ in inches
y_b = deflection of b at $b/2$ in inches
$a_p = a + 2y_b$ = dimension a when presssurized
$b_p = b + 2y_a$ = dimension b when pressurized
$c = t/2$ = distance to most remote fiber
X = an unknown arbitrary length
L = a known arbitrary length

* Based on unit length to permit simplified analysis.
** The limit to which the analysis is valid since beyond this point strain and stress are no longer proportional.

Using the basic relationship between stress and strain, and substituting (1), the formula for pressure becomes:

$$S = \frac{Mc}{I} = \frac{\dfrac{w(a^3+b^3)}{12(a+b)}\ \dfrac{t}{2}}{\dfrac{t^3}{12}} = \frac{w(a^3+b^3)}{2t^2(a+b)}$$

$$w = \frac{2st^2(a+b)}{(a^3+b^3)} . \tag{2}$$

Thus, by substituting the known dimensions a, b, and t for a given size waveguide and the allowable stress s for a given material, the maximum allowable pressure is easily obtained from (2). Conversely, the same formula can be utilized to solve for s or t for a given pressure.

To determine the waveguide deflection under pressure, it is necessary to combine the deflections due to load and moment.[2] Deflection due to load is expressed as

$$y = \frac{5}{384}\frac{wL^4}{EI},$$

and deflection due to moment as

$$y = 2\left\{\frac{1}{6}\frac{M}{EI}\left(3x^2 - \frac{x^3}{L} - 2Lx\right)\right\} .$$

The direction of the moment is such that it opposes the effect of the load. Thus,

$$y_a = \frac{5}{384}\frac{wa^4}{EI} - \frac{Ma^2}{8EI}$$

$$y_a = \frac{5}{384}\frac{wa^4}{EI} - \frac{wa^2(a^3+b^3)}{96EI(a+b)}$$

$$y_a = \frac{w}{E}\left\{\frac{5}{32}\frac{a^4}{t^3} - \frac{a^2(a^3+b^3)}{8(a+b)t^3}\right\} \tag{3}$$

[2] R. J. Roark, "Formulas for Stress and Strain," McGraw-Hill Book Co., Inc., New York, N. Y., p. 109; 1954.

TABLE II
WAVEGUIDE CONSTANTS

a	b	t	k_1	k_2	k_3	w^*
6.500	3.250	0.080	0.000404	215,000	−48,000	2.0
4.300	2.150	0.080	0.000920	43,400	−9,200	4.6
3.400	1.700	0.080	0.00148	16,400	−3,570	7.4
2.840	1.340	0.080	0.00211	7,880	−1,650	10.6
1.872	0.872	0.064	0.00309	2,940	−619	15.5
1.372	0.622	0.064	0.00579	836	−171	29
1.122	0.497	0.064	0.00864	379	−76	43
0.900	0.400	0.050	0.00820	585	−66	41
0.622	0.311	0.040	0.01103	149	−32	55
0.420	0.170	0.040	0.02388	30	−5	119

* Maximum pressure (in pounds per square inch gauge) that may be utilized without permanent deformation in annealed standard aluminum waveguide.

TABLE III
S AND E VALUES

Waveguide Material	S—As received	S Annealed	E
2S Aluminum	13,000 psi	5000 psi	10^6 psi
61S Aluminum	35,000 psi		10^6 psi
Brass	40,000 psi	12,000 psi	1.2×10^6 psi

and similarly,

$$y_b = \frac{w}{E}\left\{\frac{5}{32}\frac{b^4}{t^3} - \frac{b^2(a^3+b^3)}{8(a+b)t^3}\right\}. \tag{4}$$

Thus, the deflections are expressed in simple known terms. These deflections are then added to the original inside measurements to find the inside dimensions under pressure as follows:

$$a_p = a + 2y_b$$
$$b_p = b + 2y_a.$$

Eqs. (2)–(4) can also be expressed as

$$w = k_1 s \tag{5}$$

$$y_a = k_2\frac{w}{E} \tag{6}$$

$$y_b = k_3\frac{w}{E} \tag{7}$$

where k_1, k_2, and k_3, are functions of a, b, and t. To avoid future repetitious calculations, Table II has been prepared showing these constants for various sizes of standard waveguide.

Values of E and s are required to complete the solutions and may be obtained from a number of standard reference sources. A caution to be observed lies in the selection of suitable s values, since the waveguide material may be annealed in the making of the microwave component (for example, in attaching flanges by oven brazing). Table III shows values for E and s that have proved to be satisfactory.

A substantial number of tests have been performed at the Sperry Gyroscope Company that show close agreement between experimental results and values calculated from the above formulas. Typical comparisons are shown in Fig. 3 and Fig. 4. These curves represent a specimen of 2S aluminum L-band waveguide with heliarc welded (no annealing) flanges. Tests on other sizes of guide have yielded similarly good correlation to the theory. The slight discrepancies that exist between calculated and test values are probably due to variations in waveguide dimensions (calculated values are based on nominal waveguide size) and/or inhomogeneous modulus of elasticity as well as test inaccuracies.

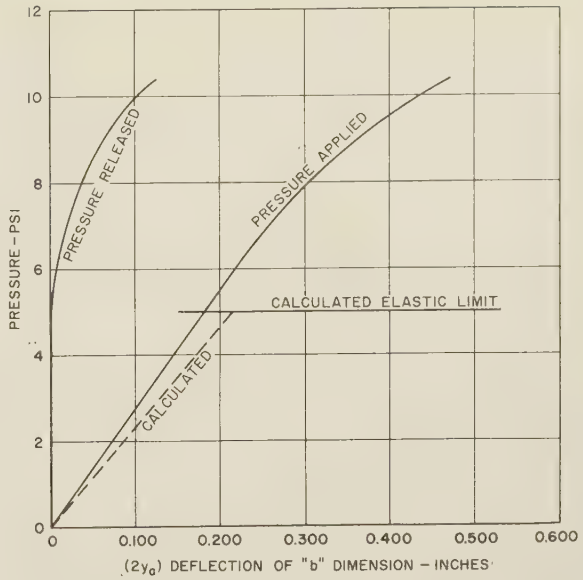

Fig. 3—Effect of pressurization on 2S aluminum L-band waveguide (WR 650).

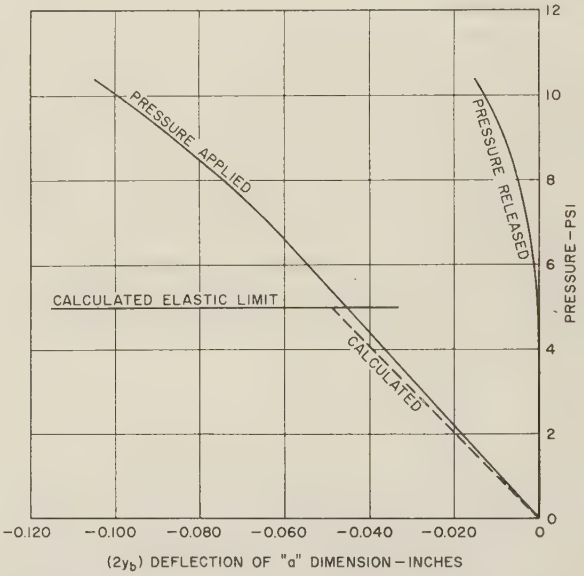

Fig. 4—Effect of pressurization on 2S aluminum L-band waveguide (WR 650).

It should be borne in mind that it is generally unsatisfactory to determine pressure carrying capacity solely from the stress point of view. In most cases it is necessary also to calculate the deflection with consideration of the specific application. For example, the waveguide

deflection in an impedance transformer would be limited to a few thousandths of an inch to prevent power leakage past the shorts and the stress in the guide walls would, consequently, be very small. On the other hand, a piece of interconnecting waveguide might be permitted to deflect to 5 per cent or more over its original dimensions, in which case the yield stress could well become the limiting factor. In passing, it should be noted that it is seldom necessary to calculate the change in the broad dimension as this will be less than one-quarter of the narrow dimension change.

Where pressures are involved that are in excess of the capacity of the standard waveguide under question, a number of strengthening procedures can be employed. Most of the reinforcement methods can be expressed as an increase of the average wall thickness or section modulus, thus making possible the use of (1)–(4) to determine the required increase in section. Simplified formulas (5)–(7) can also be employed for many such cases by recalling that pressure-carrying capacity varies directly as the square of wall thickness and that deflection varies inversely as the cube of wall thickness.

Perhaps the most common means of strengthening waveguide is the addition of brazed, welded, or bolted braces, the design of which at minimum weight and cost involves considerable ingenuity. A second method is that of simply increasing the over-all waveguide wall thickness, utilizing such processes as precision cored sand casting or by welding plate together to form a waveguide; under such conditions, a useful but generally overlooked weight advantage can be obtained by making the narrow wall thinner than the broad wall, since, as noted in a previous paragraph, the change of the broad dimension under pressure is less than one-quarter that of the narrow dimension change. It is also possible to construct waveguide that is both stronger and lighter than standard guide. Successful means of accomplishing this end are 1) reinforced plastic guide coated with conductive metallic resin, and 2) a waveguide wall construction composed of two thin sheets of aluminum sandwiched over an aluminum honeycomb core. This latter method has resulted in construction of L-band honeycomb waveguide weighing 60 per cent of standard aluminum guide and increasing strength by a factor of four; it also appears likely that if the weight of the honeycomb guide is made equal to standard waveguide, the strength ratio would be approximately twenty to one. Both the reinforced plastic and honeycomb waveguide have been built and the former has already been utilized in radar systems by the Microwave Electronics Division of the Sperry Gyroscope Company.

It is apparent that the wall thicknesses of standard waveguide were not established with regard to pressure carrying capacity. As shown in the last column of Table II, a wide variation exists in this respect for the different waveguide sizes. Specially drawn material is available[1] to carry high pressure in large size guide. It would seem worthwhile to carry this approach a step further and provide reduced wall thicknesses in the smaller sizes to obtain lighter weight, particularly for airborne applications wherein pressures are not too great. With reasoning of this type as a basis, it appears that an investigation of a revised standardization for waveguide wall thicknesses would be justified.

The Calibration of Microwave Attenuators by an Absolute Method*

ELIZABETH LAVERICK†

Summary—**A bridge method by means of which microwave attenuators can be calibrated absolutely is described, with a consideration of the main possible sources of error. A bridge was set up at $\lambda_0 = 3.2$ cm to test the principle of the method. It was shown that, using nonspecialized equipment, a high degree of accuracy was obtainable. An attenuator was calibrated over a range of 20 db, with an accuracy of the order of ± 0.02 db. This accuracy is within the accuracy of other methods of calibration in current use, and there seems no reason why, with suitable precautions, the order of accuracy should not be improved still further, if required.**

* Manuscript received by the PGMTT, March 26, 1957; revised manuscript received, June 26, 1957.

† Microwave Division, Elliott Brothers (London) Ltd., Borehamwood, Herts., Eng.

Introduction

THE MAIN method in current use of calibrating microwave attenuators involves calibration in terms of a standard attenuator, usually the piston attenuator,[1–3] whose law of attenuation is accurately

[1] C. G. Montgomery (ed.), "Technique of Microwave Measurements," M.I.T. Rad. Lab. Ser. No. 11, McGraw-Hill Book Co., Inc., New York, N. Y., Ch. 11 and 13; 1947.

[2] L. G. H. Huxley, "A Survey of the Principles and Practice of Waveguides," Cambridge University Press, Cambridge, Eng., pp. 57–61; 1947.

[3] G. F. Gainsborough, "A method of calibrating standard signal generators and radio-frequency attenuators," *J. IEE*, pt. III, vol. 94, pp. 203–210; May, 1947.

calculable. As the frequency band is extended, manufacturing tolerances on the standard attenuator become tighter and the accuracy of the standard decreases rapidly. To overcome this, the usual technique is to compare the microwave attenuator with a standard attenuator which is operating at an intermediate frequency. By this means, the accuracy of that standard is maintained, and calibrations correct to ± 0.02 db are obtained. However, the auxiliary electronic equipment required is extensive and complex, and the method is neither direct nor absolute.

The following text describes a method whereby microwave attenuators may be calibrated absolutely and directly, at the frequency of operation. The accuracy obtainable is at least comparable with that of the standard attenuators in current use, and the method has the advantages that it is comparatively simple, and uses microwave and electronic apparatus which is generally available in most microwave laboratories.

Method of Calibration

The circuit consists essentially of a three-arm waveguide bridge or network as shown in Fig. 1, fed by a single oscillator. The bridge output is fed to a detector. Arm S contains the attenuator to be calibrated (X), a level-setting attenuator (L), and a phase shifter. Arm P contains a variable uncalibrated attenuator and a phase shifter. Arm Q contains a fixed attenuator such that it permits a signal of some suitable amplitude a and arbitrary phase to appear at the detector. Arms P and Q also contain waveguide switches. The procedure for calibration is as follows:

1) With arm P out of circuit and the unknown attenuator X at maximum attenuation, the level-setting attenuator L and phase shifter in arm S are adjusted for zero reading at the detector. When this occurs, the signal at the detector from arm S must be equal in amplitude and of opposite phase to that from arm Q; *i.e.*, the signal from S is $-a$.
2) With arm Q switched out and arm P switched in, the attenuator and phase shifter in arm P are adjusted for zero reading at the detector, the signal from P being $+a$.
3) With all three arms switched in, we have $+2a$ from P and Q and $-a$ from S. To obtain zero output, the unknown attenuator X in arm S must be adjusted to give $-2a$ at the detector; *i.e.*, four times the original power. X is consequently changed by -6.02 db. Unless the attenuator in arm S is phase shiftless it will be necessary to readjust the phase shifter in arm S for zero output. Repeating steps 2 and 3, S is repeatedly adjusted to give amplitudes $-3a$, $-4a$, $\cdots$, $-na$, the corresponding attenuation steps being -3.52 db, -2.50 db, etc.

The magnitude of the fixed attenuator and the number of steps $(n-1)$ are chosen according to the range of attenuation over which calibration is required. For example, if it is required to cover a range of 20 db, 9 steps are used ($n=10$) and the fixed attenuator is chosen to be slightly greater than 20 db. It is not necessary, however, to know the exact magnitude of the fixed attenuator.

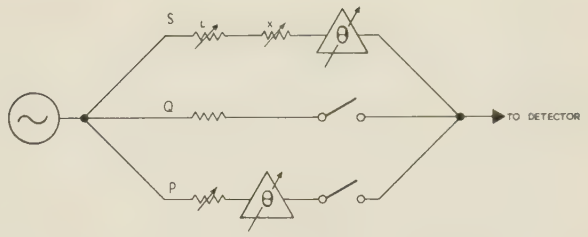

Fig. 1—Bridge network for the absolute calibration of attenuators.

It will be observed that the calibration is carried out in a direction of increasing amplitude or decreasing attenuation; *i.e.*, the starting point of the calibration is at the maximum attenuation end of the range, whereas it is usually required to calibrate an attenuator from the "zero" or minimum attenuation point. For instance, in the example quoted above, at the tenth step the attenuator is adjusted to -20 db with respect to the starting point. In general, however, X will not then be exactly at the "zero." In order to adjust for this, the attenuator is set at the "zero" and the balance condition reobtained by adjusting the level-setting attenuator in arm S. The calibrating procedure is then completely repeated, step 1 giving the point 20 db up on the zero and step 9 giving "zero," or minimum attenuation.

Apparatus

The Microwave System

The microwave bridge is shown in Fig. 2. The power is divided in a known ratio between the three arms of the bridge network by means of two hybrid-T junctions. Arm S contains a level-setting attenuator, a phase shifter, and the attenuator to be calibrated, X; Arm Q contains a switch (consisting of a highly attenuating vane which can be switched in or out of the waveguide as required) and the fixed attenuator; and Arm P contains a switch, phase shifter, and variable attenuator. The signals from the three arms are recombined by means of two further hybrid T's, and the bridge output taken to some form of detector.

The Detecting System

The source (a reflex-klystron) is square-wave modulated at 1 kc. In order to achieve the necessary sensitivity, a superheterodyne detecting system is employed and to this end a hybrid-T balanced mixer with reverse polarity crystals is used. The square-wave modulated IF signal from the mixer is amplified and passed to an audio-frequency amplifier, the output from which is indicated by a meter.

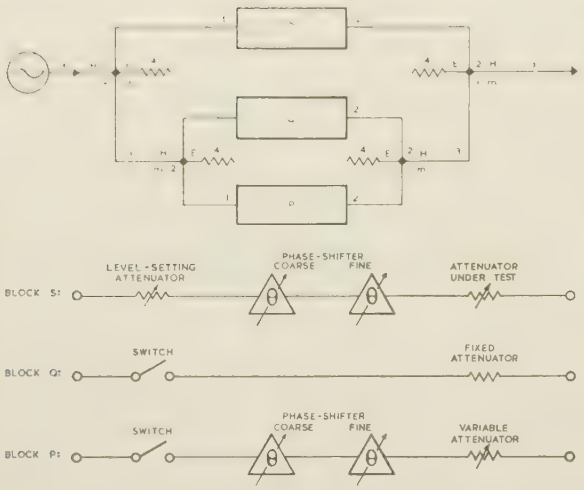

Fig. 2—Circuit for studying the effects of multiple reflections within the bridge network.

Sources of Error

Multiple Reflections Within the Bridge Network

Because of multiple reflections, cross coupling will occur between the arms of the bridge network and this will result in an error of measurement. An estimate of the magnitude of this error can be made from a knowledge of the reflection and transmission coefficients of the bridge arms. For example, it can be shown that for a calibration over a 20-db range the total error δ is given by

$$\delta = 20 \log \left(\frac{10 + \Delta}{10} \right) \text{db}$$

where, in terms of the moduli of the scattering coefficients,

$$\Delta \leq 10\Delta s_{11}(m_{11} + m_{12}) + 10\Delta s_{22}(m_{12} + m_{22}) + \frac{m_{22} + 3m_{12}}{2}\left[45(q_{11} + q_{11}^{x}) + 9(p_{11} + p_{11}^{x})\right] + \frac{m_{11} + 3m_{12}}{2}\left[45(q_{22} + q_{22}^{x}) + 9(p_{22} + p_{22}^{x})\right]. \quad (1)$$

In this equation

m = hybrid T's,
s = arm S,
q = arm Q in circuit,
q^x = arm Q when switched out of circuit,
p = arm P in circuit,
p^x = arm P when switched out of circuit (see Fig. 2),
Δs_{11} and Δs_{22} = change in S_{11} and S_{22}, respectively, during the measurement procedure.

This result is based on the following assumptions:

1) Equal power-split in the hybrid T's.
2) Reflections are small, therefore terms involving more than two reflections can be neglected.
3) The attenuation in each of the three arms in always such that terms in p_{12}^3, q_{12}^3, s_{12}^3 can be neglected.

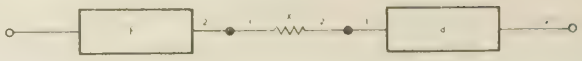

Fig. 3—Block S in Fig. 2. Circuit for studying the effects of multiple reflections within the arm of the bridge network containing the unknown attenuator, X.

4) Measurements are made only when the bridge is balanced, and effectively zero signal is incident on the detector. Under these circumstances the mismatch of the detector can be neglected.
5) Since s, p, and p^x vary during the course of the calibration, maximum values have been assumed in order to estimate the maximum possible error.

By placing suitable attenuating pads at both ends of each arm, and thereby reducing the effect of reflections, the error in calibration can be decreased accordingly.

It is clear from the form of (1) that this error increases with the range of attenuation.

Multiple Reflections Within the Arm of the Bridge Network Containing the Unknown Attenuator X

It is essential that multiple reflections within the arm of the bridge network containing the attenuator under test should be kept to within certain limits depending on the accuracy required.[4] This is achieved by placing attenuating pads on both sides of the attenuator under test, which is the normal condition of operation for any attenuator when high accuracy is required.

It can be shown that the error in calibration arising from multiple reflections within the arm containing the attenuator is given by

δ, in db where

$$\delta = 20 \log_{10} \left(\frac{10 + \Delta}{10} \right),$$

$$\Delta \leq 2f_{22}X_{11} + 2d_{11}X_{22} + 2f_{22}d_{11}X_{12}^2, \text{ and} \quad (2)$$

X, f and d are moduli of the scattering coefficients. X refers to the attenuator under test, and f and d refer to the match on either side of the attenuator under test (see Fig. 2 and Fig. 3).

Leakage through Switches

A third source of error arises from the finite transmission coefficient of the open-circuited bridge arms. In the case of a 20-db calibration range it can be shown that the error arising from this is

$$\delta = 20 \log \left(\frac{10 + \Delta}{10} \right) \text{db}$$

where

$$\Delta \leq \frac{18\delta_{q^x}}{q_{12}} = 180\delta_{q^x} \quad (3)$$

[4] R. W. Beatty, "Mismatch errors in the measurement of μ.h.f. and microwave variable attenuators," *J. Res. NBS*, vol. 52, pp. 7–9; January, 1954.

and $\delta_q{}^x$ = modulus of transmission coefficient through the switch in arm Q (see Fig. 2).

It is assumed above that the switches in arms P and Q are identical.

Experimental Results

In order to test this method of calibrating attenuators, a bridge was set up at a wavelength of 3.2 cm, and a rotary attenuator was calibrated over a 20-db range. A detailed circuit of the bridge network is shown in Fig 4.

Performance of the Individual Components of the Bridge Network Hybrid T's

At $\lambda_0 = 3.2$ cm the moduli of the scattering coefficients are as follows:

$$|m_{11}| = 0.033$$
$$|m_{22}| = 0.028$$
$$|m_{12}| = 0.040.$$

Attenuators

Rotary attenuators were used as the fixed and variable attenuators in arms P and Q. Their reflection coefficients were ≤ 0.05. The level-setting attenuator L, in arm S, was of the guillotine type using a resistive vane. Its reflection coefficient was ≤ 0.02.

Switches

Each switch consisted of a length of waveguide into which a highly attenuating vane could be inserted through a slot in the broad face. The mechanism was completely shielded to eliminate radiation. The switches had a reflection coefficient of 0.026 and a transmission coefficient < 0.0001 with the vane fully in; and effectively zero reflection coefficient and unity transmission coefficient with the vane fully out.

Phase Shifters

The coarse phase shifters which were used to roughly equalize the path lengths of the bridge arms were of the "trombone" type having a reflection coefficient of 0.06, which is constant with change of phase. The fine phase shifters, used to obtain the final phase balance, were shielded slotted squeeze sections with a reflection coefficient of 0.006.

Attenuating Pads

The attenuating pads used to minimize the effects of multiple reflections were made up of tapered resistive vanes, of reflection coefficient ≤ 0.005.

Estimate of Padding Necessary to Attain Required Accuracy. Multiple Reflections Within the Bridge Network

Referring to (1) and Fig. 2, and substituting the practical values given above for the various components,

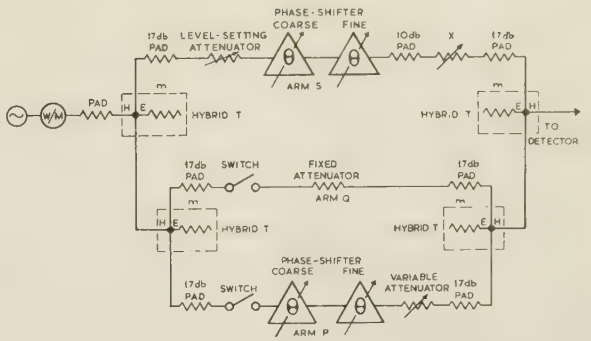

Fig. 4—Detailed circuit of the bridge network.

$$\Delta s_{22} = \Delta s_{11} \leq 2s_{11} \leq 2(0.02 + 0.066 + 0.05) = 0.272$$
$$q_{11} = 0.052 \qquad q_{22} = 0.052$$
$$q_{11}{}^x = 0.026 \qquad q_{22}{}^x = 0.052$$

assuming 20 db in the fixed attenuator; *i.e.*, $q_{12} = 0.1$.

$$p_{11} = (0.066 + 0.05) = 0.116$$
$$p_{11}{}^x = 0.026$$
$$p_{22}{}^x = (0.05 + 0.001) = 0.051$$
$$p_{22}{}^x = (0.05 + 0.001) = 0.051;$$
$$\therefore \Delta \leq 2\ 72(0.033 + 0.08 + 0.028) + 0.074(3.51 + 1.278) + 0.077(4\ 68 + 0.918)$$
$$= 1.169.$$

Using 17-db pads at both ends of P, Q, and S, Δ is reduced to ≤ 0.025, or the error over 20 db is ≤ 0.021.

Multiple Reflections Within the Arm Containing the Unknown Attenuator X

Referring to (2) and Fig. 2 and Fig. 3, it can be seen that

$$f_{22} = 0.062 + 0.02 + 0.033 = 0.115$$
$$d_{11} = 0.028$$
$$X_{11} = X_{22} = 0\ 05;$$
$$\therefore \Delta \leq (0.23 \times 0.05) + (0.056 \times 0.05) + (0.23 \times 0.028)$$
$$= 0.021 \text{ or } \delta \leq 0.02 \text{ db.}$$

In practice a 17-db pad is inserted between the unknown attenuator X and the hybrid T, as a result of the consideration of multiple reflections in the bridge network. By inserting a 10-db pad between X and the phase shifters, the error calculated above is reduced to a negligible amount.

Leakage through Switches

Referring to (3) and substituting $\delta_q{}^x = 0.0001$,

$$\Delta \leq 0.018$$

and

$$\delta \leq 0.009 \text{ db.}$$

Result of Calibration

It is reasonable to suppose, on the basis of the above estimates, that the calibration of the rotary attenuator by this method should be accurate to ± 0.02 db over a 20-db range, the accuracy being greatest over the first part of the range.

The results obtained are shown in Fig. 5, where the error or deviation in db is plotted for various settings of the rotary attenuator, which is in itself an absolute instrument. For comparison, the same attenuator was calibrated against an IF piston attenuator, the results being shown in the same illustration. The deviations are, in both cases, of the order expected.

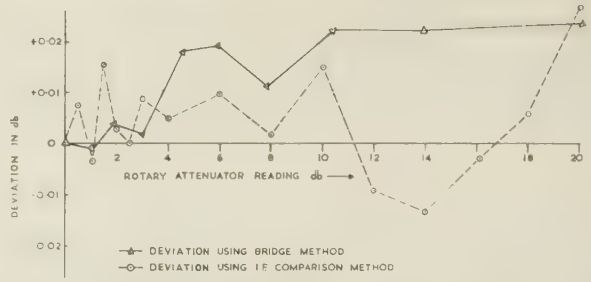

Fig. 5—Deviations of attenuation from rotary attenuator reading using the bridge method and IF comparison method of calibration. The rotary attenuator is an absolute instrument.

Conclusion

The method described above for the absolute calibration of microwave attenuators has been tested experimentally at a wavelength of 3.2 cm. Estimates were made of the padding required to attain an accuracy of the order of ± 0.02 db over a 20-db range. It was shown that the results obtained are accurate to within the design limits of the apparatus, and to within the accuracy of other methods in current use. By further reducing the effects of multiple reflections in the microwave circuit it should be possible to attain even greater accuracy, if required. The method is insensitive to power fluctuations and used comparatively simple and readily available microwave and electronic apparatus.

Acknowledgment

The author wishes to thank E. A. N. Whitehead for the basic idea, and her other associates of the Microwave Division of Elliott Brothers (London) Limited who helped to put the idea into practice. The comparison with a piston attenuator was carried out at the Radar Research Establishment at Malvern, Worcestershire, and the author would like to acknowledge their cooperation.

Pulse Waveform Degradation Due to Dispersion in Waveguide*

ROBERT S. ELLIOTT†

Summary—**Phase velocity in a waveguide is a nonlinear function of frequency and thus causes dispersion of the spectral components in a pulse waveform. For most practical cases, it is a good assumption to consider the phase constant to be a quadratic function of frequency. An expression can then be derived for the exit waveform shape as a function of guide length, dispersion, and width of the input rectangular pulse. The derived expression is given in terms of tabulated error functions and Fresnel integrals. It is universal in form and applicable to a wide range of practical problems. A family of degraded wave shapes has been computed from this expression and is presented graphically. The results apply for any mode in a straight waveguide of arbitrary but constant cross section.**

Introduction

AS THE usable range of microwave frequencies has been pushed higher and higher, a run of waveguide whose physical length is L has assumed an electrical length great enough to affect transmission of pulsed energy, even when loss is ignored. The reason for this lies in the frequency behavior of the phase constant. If $\beta(\omega)$ is the phase constant, then

$$\beta(\omega) = \frac{2\pi}{\lambda_g} = \frac{\sqrt{\omega^2 - \omega_c^2}}{v} \tag{1}$$

in which λ_g is the guide wavelength at the angular frequency ω, and $v = (\mu\epsilon)^{-1/2}$, with μ and ϵ the permeability and permittivity, respectively, of the medium filling the guide. Eq. (1) applies for any mode in a straight section of waveguide of any constant cross section. ω_c is the cutoff angular frequency of the particular mode being considered.

Eq. (1) can be expanded in a Taylor's series about the angular frequency ω_0, giving

$$\beta(\omega) = \beta_0 + \frac{\omega_0}{v^2\beta_0}[\omega - \omega_0] - \frac{1}{2}\frac{\omega_c^2}{v^4\beta_0^3}[\omega - \omega_0]^2 + \frac{1}{2}\frac{\omega_0\omega_c^2}{v^6\beta_0^5}[\omega - \omega_0]^3 - \cdots \tag{2}$$

* Manuscript received by the PGMTT, April 4, 1957; revised manuscript received, June 14, 1957. The research reported in this paper was performed for the Allan B. DuMont Labs. under contract with the Naval Bur. of Aeronautics.

† RANTEC Corp., Calabasas, Calif.

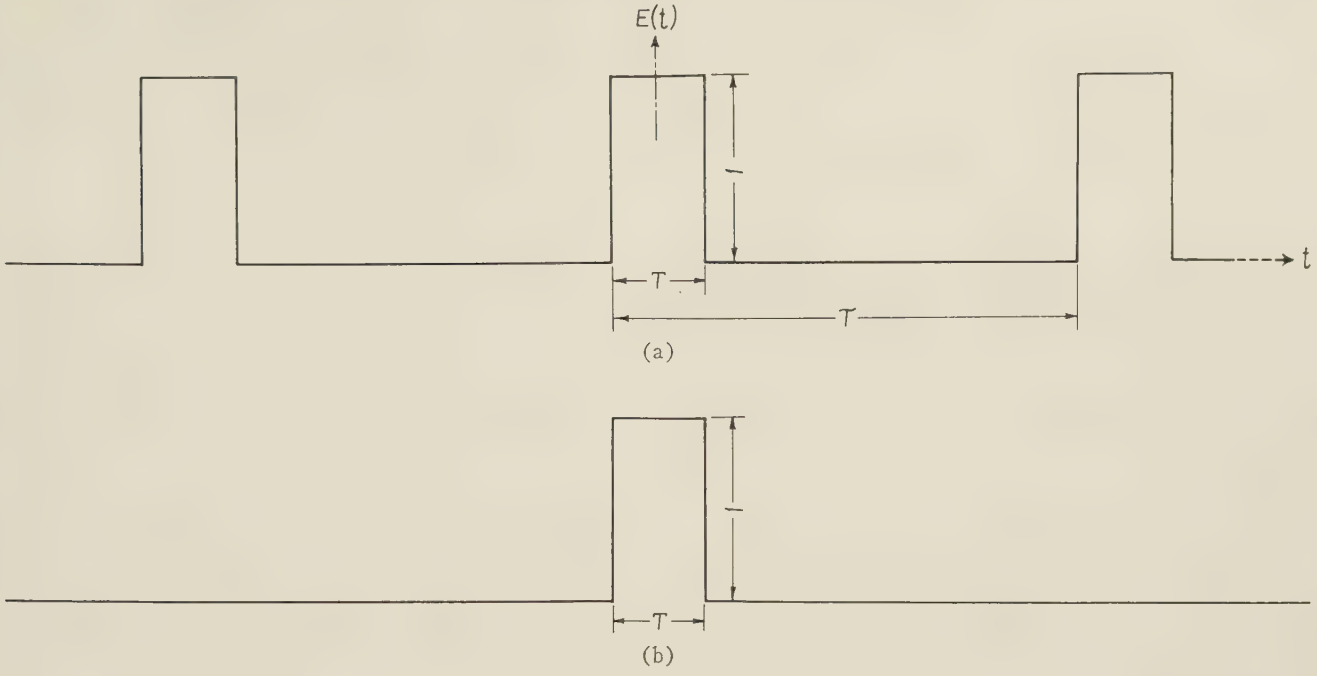

Fig. 1—Rectangular pulse waveforms.

It is apparent from (1) and (2) that $\beta(\omega)$ is not a linear function of ω. Thus, the Fourier components of a pulse traveling down the waveguide are dispersed, and the exit waveform is degraded. The amount of degradation depends on the Fourier composition of the pulse, the length L of the run of waveguide, and the rapidity of convergence of the series (2). This convergence depends on ω_0, ω_c, and the bandwidth $\omega_0-\omega_1\leq\omega\leq\omega_0+\omega_1$ needed to adequately represent the pulse.

This problem of pulse degradation has received both theoretical and experimental attention in the literature, An interesting display of the effect of delay distortion on a rectangular pulse has been provided by the experimental equipment of Beck.[1,2] A series of analytical papers[3–6] has considered the effect of dispersion on a Heaviside unit step function and on a Dirac function, in lossy as well as lossless waveguides. However, in all cases, the analysis was based on the exact relation (1). A precise expression for the exit waveform can be derived in this manner, but, unfortunately, the expression is unwieldy and not given in terms of tabulated functions. Thus, calculated waveshapes which can be compared to Beck's observations have not been readily available.

For most cases of practical interest, an approximation of (1) can be made which yields useful results in a greatly simplified form. This approximation consists of taking only the first three terms of the expansion (2), thus treating $\beta(\omega)$ as a quadratic function of ω. An analysis can be based on this approximation, culminating in an expression for the exit waveform containing only error functions and Fresnel integrals, for both of which adequate tables are available. Sample computations yield a family of graphs of exit waveforms of various degrees of degradation.

Analysis

Let a microwave carrier signal at the angular frequency ω_0 be modulated by a train of rectangular pulses of width T and separation τ. [See Fig. 1(a).] In most practical applications τ/T is so large that the Fourier series spectrum differs negligibly from the Fourier integral spectrum found by considering only one pulse in the train.

Thus, if

$$e(t) = E(t)\cos\omega_0 t \tag{3}$$

is the waveform being injected into a run of waveguide, with $E(t)$ given by Fig. 1(a), it is assumed that a satisfactory model results from saying that (3) is the waveform being injected into the run of waveguide, with $E(t)$ given instead by Fig. 1(b). Then

$$E(t) = \int_{-\infty}^{\infty} g(\omega)e^{i\omega t}d\omega \tag{4}$$

and

$$g(\omega) = \frac{T}{2\pi}\,\frac{\sin\dfrac{\omega T}{2}}{\dfrac{\omega T}{2}}. \tag{5}$$

[1] A. C. Beck, "Microwave testing with millimicrosecond pulses," IRE Trans., vol. MTT-2, pp. 93–100; April, 1954.
[2] A. C. Beck, "Measurement techniques for multimode waveguides," IRE Trans., vol. MTT-3, pp. 35–42; April, 1955.
[3] M. Cotte, "Propagation d'une perturbation dans une guide electrique," *Ann. Télécommun.*, vol. 1, pp. 49–52; March–April, 1946.
[4] M. Namiki and K. Horiuchi, "On the transient phenomena in the waveguide," *J. Phys. Soc. Japan*, vol. 7, pp. 190–193; March–April, 1952.
[5] P. Poincelot, "Propagation of a signal along a waveguide," *Ann. Télécommun.*, vol. 9, pp. 315–317; November, 1954.
[6] M. Cotte, "Propagation of a pulse in a waveguide," *Ondé Elec.*, vol. 34, pp. 143–146; February, 1954.

Substitution and symmetry considerations yield

$$e(t) = \frac{T}{2\pi}\int_{-\infty}^{\infty} \frac{\sin\frac{\omega T}{2}}{\frac{\omega T}{2}} \cos(\omega + \omega_0)t \cdot d\omega \qquad (6)$$

as the Fourier equivalent of the input waveform (3).

Referring to the discussion about phase constant in the preceding section, it is assumed that

$$\beta(\omega') = \beta_0 + A[\omega' - \omega_0] - B[\omega' - \omega_0]^2 \qquad (7)$$

in which

$$A = \frac{\omega_0}{v^2\beta_0}$$

$$B = \frac{1}{2}\frac{\omega_c^2}{v^4\beta_0^3}. \qquad (8)$$

In a waveguide run of length L, the Fourier component at angular frequency ω' is shifted in phase an amount βL.

Assuming that the attenuation is frequency insensitive,[7] the output waveform is proportional to

$$f(t) = \frac{T}{2\pi}\int_{-\infty}^{\infty} \frac{\sin\frac{\omega T}{2}}{\frac{\omega T}{2}} \cos[(\omega + \omega_0)t - \beta_0 L - AL\omega + BL\omega^2]d\omega. \qquad (9)$$

From (9) it follows that

$$f(t + AL) = \frac{T}{2\pi}\cos[\omega_0(t + AL) - \beta_0 L] \int_{-\infty}^{\infty} \frac{\sin\frac{\omega T}{2}}{\frac{\omega T}{2}} \cos[\omega t + BL\omega^2]d\omega - \frac{T}{2\pi}\sin[\omega_0(t + AL) - \beta_0 L] \int_{-\infty}^{\infty} \frac{\sin\frac{\omega T}{2}}{\frac{\omega T}{2}} \sin[\omega t + BL\omega^2]d\omega. \qquad (10)$$

The output modulation envelope is therefore given by

$$F(t) = \frac{T}{2\pi}\sqrt{\{F_1(t)\}^2 + \{F_2(t)\}^2} \qquad (11)$$

with

$$F_1(t) = \int_{-\infty}^{\infty} \frac{\sin\frac{\omega T}{2}}{\frac{\omega T}{2}} \cos[\omega t + BL\omega^2]d\omega \qquad (12)$$

$$F_2(t) = \int_{-\infty}^{\infty} \frac{\sin\frac{\omega T}{2}}{\frac{\omega T}{2}} \sin[\omega t + BL\omega^2]d\omega. \qquad (13)$$

If the trigonometric functions occurring in the integrands of (12) and (13) are replaced by their equivalent exponential forms, the Fourier transforms of (12) and (13) can be deduced with the repeated use of formula 731.1 of Campbell and Foster.[8] One concludes that

$$F(t) = \frac{1}{2}\sqrt{\left\{\operatorname{erf}\left[\frac{x+1}{a}\right] - \operatorname{erf}\left[\frac{x-1}{a}\right]\right\}^2 + \left\{C\left[\left(\frac{x+1}{a}\right)^2\right] - S\left[\left(\frac{x+1}{a}\right)^2\right] - C\left[\left(\frac{x-1}{a}\right)^2\right] + S\left[\left(\frac{x-1}{a}\right)^2\right]\right\}^2} \qquad (14)$$

with

$$x = \frac{2t}{T} \qquad (15)$$

$$a = \frac{4}{T}\sqrt{BL} \qquad (16)$$

and

$$\operatorname{erf}[z] = \frac{2}{\sqrt{\pi}}\int_0^z e^{-u^2}du \qquad (17)$$

$$C[z] = \sqrt{\frac{2}{\pi}}\int_0^{\sqrt{z}} \cos u^2 du \qquad (18)$$

$$S[z] = \sqrt{\frac{2}{\pi}}\int_0^{\sqrt{z}} \sin u^2 du. \qquad (19)$$

$Erf[z]$ is the error function and $C[z]$, $S[z]$ are the Fresnel integrals. Adequate tables of the error function are available for all values of z of interest in this analysis. Tables of $C[z]$, $S[z]$ are available for $0 \leq z \leq 50$. For $z > 50$, the asymptotic expressions, due to Cauchy,[9] may be used. The first two terms are sufficient, giving

$$C[z] - S[z] \cong \sqrt{\frac{2z}{\pi}}\left\{\left[\frac{1}{2z} + \frac{1}{(2z)^2}\right]\cos z + \left[\frac{1}{2z} - \frac{1}{(2z)^2}\right]\sin z\right\}. \qquad (20)$$

[7] This is obviously not true in the entire range $-\infty < \omega' < \infty$. However in the restricted range $\omega_0 - \Omega \leq \omega' \leq \omega_0 + \Omega$ needed to adequately represent the pulse, it is a reasonable assumption.

[8] G. A. Campbell and R. M. Foster, "Fourier Integrals for Practical Applications," D. Van Nostrand Co., Inc., New York, N. Y.; 1948.

[9] A. L. Cauchy, "Asymptotic expansions for Fresnel integrals," *C.R. Acad. Sci., Paris*, vol. 15, pp. 554, 573; 1842. See also, G. N. Watson, "Bessel Functions," Cambridge University Press, Cambridge, Eng., 2nd ed., p. 545; 1952.

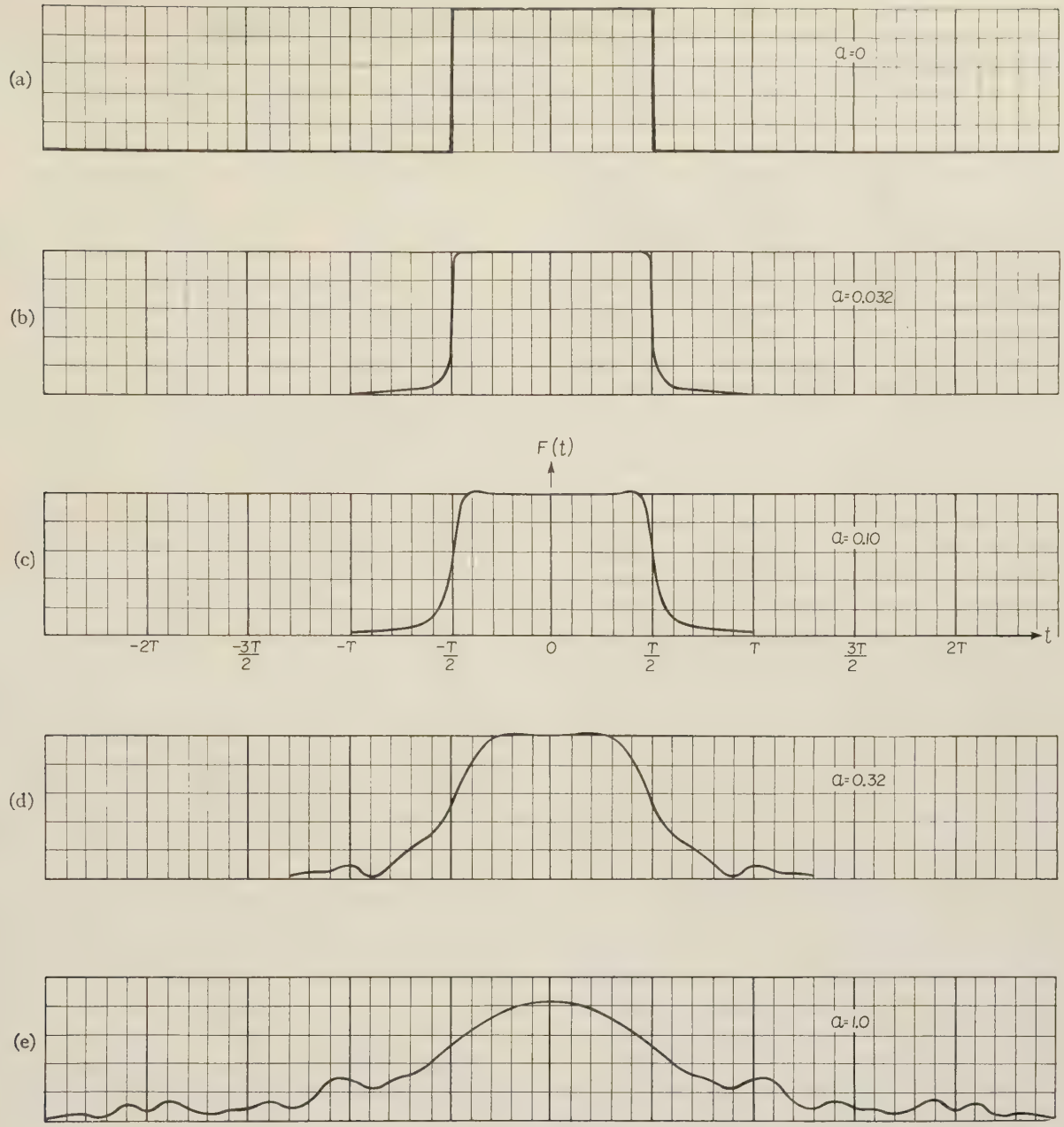

Fig. 2—Degraded waveforms.

Output waveforms have been computed from (14) for the parameter values $a=0$, 0.032, 0.1, 0.32, 1.0. These are shown in Fig. 2 and comprise a universal family of degraded waveforms. For any particular application, one need only compute B from (8) and a from (16). A rough estimate of the output waveform can be obtained from Fig. 2 by examining the curve for the appropriate value of a. A more exact estimate can be obtained by inserting the precise value of a in (14) and computing $F(t)$ with the aid of the tables of error function and Fresnel integrals.

A study of Fig. 2 reveals that the degradation increases with a. Thus, the narrower the pulse, the longer the waveguide run, the closer one operates to cutoff, the greater the pulse degradation. These are all reasonable results and (14) establishes the degree to which these factors have an influence.

As an example, consider a K_a band delay line consisting of circular waveguide 0.500 inch in outside diameter with a 0.032-inch wall, and carrying a TE_{01} mode. If the carrier frequency is 34,200 mc and the pulse width is 0.125 μsec, the round trip delay in a length of forty feet is only 0.3 μsec, and the exit waveform is approximately Fig. 2(c). By increasing the length to four hundred feet, the delay can be raised to 3 μsec, but the pulse is further degraded, being given approximately by Fig. 2(d).

Conclusion

By assuming that phase velocity in a waveguide is a quadratic function of frequency, it is possible to derive a compact formula for pulse degradation due to dispersion. From the formula, a family of universal curves can be computed, showing the effect of guide length, pulse width, and dispersion on the pulse shape.

Broad-Band Quarter-Wave Plates*

WESLEY P. AYRES†

Summary—Analytical expressions are given for the propagation constant for the two orthogonal dominant modes in a square waveguide loaded with a centered slab of dielectric. These are combined to find the differential phase shift in a loaded section. Solutions of these equations are given for polystyrene which enables one to design broad-band quarter wave plates. The problem of transforming from unloaded to loaded guide is discussed and two solutions are given and another suggested. Experimental results are given and it is found that the work in square guide carries over to circular guide almost intact. It is shown that quarter-wave plates may easily be designed to cover a normal waveguide bandwidth.

Introduction

CIRCULARLY-polarized waves are being used to a great extent to exploit the possibilities of microwave techniques. To convert the microwave energy from linear to circular polarization or vice versa, some form of quarter-wave plate is necessary. A quarter-wave plate creates a relative phase delay, or differential phase shift, of 90° between two spatially orthogonal modes. A detailed description of the operation and the uses of quarter-wave plates as well as some of the early work is described elsewhere.[1,2] Among the various forms there is good reason to believe that the dielectric slab in a waveguide is one of the more suitable constructions for broadbanding. The reasoning behind this belief comes from the nature of the dispersiveness of a waveguide loaded as in Fig. 1 with a slab of dielectric. It will be seen later that the differential phase shift which is the difference in dispersiveness for the two orthogonal modes is not a monotonically increasing function of frequency as one might expect, but is actually a second or third-order curve in the frequency range of interest.

Although a quarter-wave plate can always be constructed by trial and error, this procedure gives a bandwidth which cannot be predicted in advance or be systematically improved. Thus, a method of calculating the differential phase shift for two orthogonal linearly-polarized waves in a partially dielectric-loaded square waveguide is presented. The results for square waveguide should carry over to circular waveguide quite well and this is verified experimentally.

The normal modes of a rectangular waveguide, with a longitudinal slab of dielectric in it, are longitudinal section electric and magnetic modes, or for brevity LSE and LSM modes, respectively. A detailed mathematical treatment of these modes, starting with Maxwell's equations and the boundary conditions, was carried out

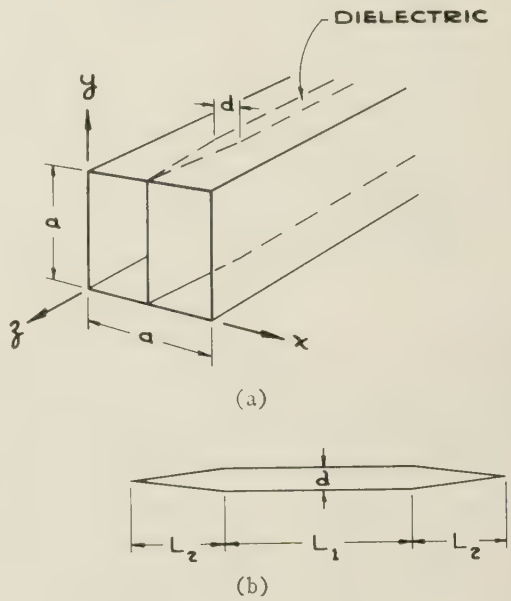

Fig. 1—(a) Dielectric loaded square waveguide; (b) top view of tapered quarter-wave plate.

and follows the method of Pincherle.[3] The results of the mathematics for the two modes of interest in quarter-wave plate design are given. These are the modes that become TE_{10} and TE_{01} modes when the dielectric slab is reduced to zero thickness. Method of solution of the characteristic equations is graphical. Using these graphical solutions, design of quarter-wave plates and experimental results for one of the designs are discussed.

Theory

For the purpose of constructing a quarter-wave plate, one is interested in the differential phase shift in wavelengths,

$$\Phi = L\left(\frac{1}{\lambda_{g1}} - \frac{1}{\lambda_{g2}}\right) \tag{1}$$

where L is the length of the plate and λ_{g1}, λ_{g2} are the guide wavelengths for two orthogonal linear polarizations. This differential phase shift must be maintained at a constant value, 0.250, over a given frequency range. For this purpose, a dielectric loaded square waveguide, as shown in Fig. 1(a), propagating the two lowest modes is now considered. For each mode, one must solve an equation which is due to the boundary conditions at the dielectric-air interfaces to obtain a quantity which is called the transverse eigenvalue. This quantity can then be substituted into an equation relating the propagation constants, or, as written here, relating the various wavelengths. For the LSE mode corresponding to the empty

* Manuscript received by the PGMTT, May 6, 1957; revised manuscript received, June 25, 1957. Work performed at Sylvania's Electronic Defense Laboratory, Mountain View, Calif., under Signal Corps contract No. DA 36-039-sc-31435.

† Microwave Eng. Labs., Inc., Palo Alto, Calif.

[1] A. G. Fox, "An adjustable waveguide phase changer," PROC. IRE, vol. 35, pp. 1489–1498; December, 1947.

[2] G. C. Southworth, "Principles and Applications of Waveguide Transmission," D. Van Nostrand Co., Inc., New York, N. Y., p. 325; 1950.

[3] L. Pincherle, "Electromagnetic waves in metal tubes filled longitudinally with two dielectrics," *Phys. Rev.*, vol. 66, pp. 118–130; September, 1944.

waveguide TE_{10} mode ($E_x=0$), the boundary condition relation to be solved is[4]

$$\frac{\tan x_1}{x_1} = K\frac{\operatorname{ctn}\sqrt{K^2x_1^2+C^2}}{\sqrt{K^2x_1^2+C^2}} \tag{2}$$

where

$K=d/(a-d)$,
$C=\pi d(\epsilon-1)^{1/2}/\lambda$,
d = thickness of the dielectric,
ϵ = relative dielectric constant of the slab,
λ = free space wavelength, and
x_1 = variable related to the transverse eigenvalue.

The lengths have been normalized to the guide width a to make the solutions easily adaptable to any waveguide size. The method of solution of (2) is graphical and, as one can see, there is an infinity of solutions due to the periodic functions involved. The solution for the desired mode is that for which $|x_1|$ is smallest. This result is then substituted into the propagation constant equation

$$\nu_1^2 = \nu_0^2 - \eta_1^2 \tag{3}$$

where

$\eta_1 = x_1 a/\pi(a-d)$
$\nu_0 = a/\lambda$
$\nu_1 = a/\lambda_g$ = phase shift per unit length in units of wavelengths/guide widths.

For the LSM mode corresponding to the empty waveguide $TE_{01}(E_y=0)$ mode, the boundary condition relation to be solved is

$$x_2\tan x_2 = -\frac{1}{K\epsilon}\sqrt{K^2x_2^2+C^2}\tan\sqrt{K^2x_2^2+C^2}. \tag{4}$$

The method of solution is again graphical and, as before, the desired solution is that for which $|x_2|$ is smallest. In solving (2) and (4) it must be kept in mind that x_1 and x_2 may be either real or imaginary. The solution for x_2 is then substituted into the propagation constant

$$\nu_2^2 = \nu_0^2 - \eta_2^2 - \tfrac{1}{4} \tag{5}$$

in order to find ν_2. All quantities here are defined the same as for (2) and (3) except the subscripts are changed to 2.

The relations given above are exact, no approximations have been made. All of the numerical results to be described are for polystyrene, $\epsilon=2.55$, and were obtained by graphical means. The propagation constants were found to three or four significant figures to obtain their difference to three significant figures. The solutions of (3) and (5) are used to find the differential phase shift per unit length a

$$\phi = \nu_1 - \nu_2. \tag{6}$$

The differential phase shift is found for a number of frequencies and plotted in Fig. 2 as a function of $f/f_c = 2\nu_0$. Here f is the frequency parameter and f_c is the cutoff frequency of the empty waveguide. From this information, quarter-wave plates may be designed.

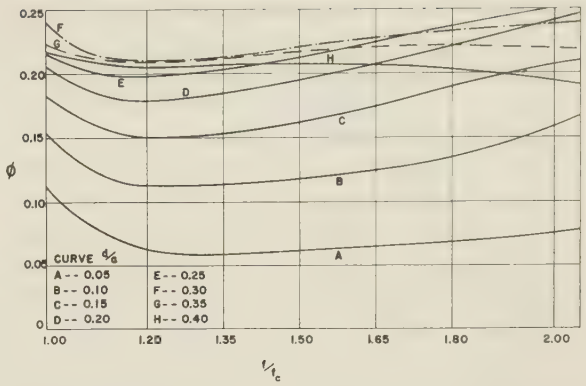

Fig. 2—Differential phase shift as a function of frequency for polystyrene plates, $\epsilon=2.55$, of various thicknesses, d.

In actual practice one must match the ends of the plate to the empty waveguide. This is most easily done in a predictable manner by tapering the thickness d at both ends as shown in Fig. 1(b). In order to predict the effect of these tapers, many curves are needed for different plate thicknesses. A family of these are shown in Fig. 2 with d as a parameter. These are cross-plotted in Fig. 3 with d as the variable and f/f_c as the parameter for the family. From Fig. 3 the effect of tapers can be estimated. These curves are integrated and the results plotted in Fig. 4 so that the effect of linear tapers up to any thickness d can be found immediately. In using these curves, the normalization of all quantities must be remembered and, in particular, it must be noticed that the differential phase shift is in units of 2π radians per unit width a of the waveguide.

Design of Quarter-Wave Plates

To design a complete plate, the sum of the differential phase shifts due to the two tapers and the flat midsection must add up to 0.250 over frequency band of interest. This is done by using Figs. 3 and 4 to pick a value of d that gives a reasonably flat differential phase shift for a combination of the tapers and flat midsection. Then the sum of the differential phase shifts are multiplied by an appropriate constant to make the total shift

$$\Phi = 2L_{\text{taper}}\,\theta + L_{\text{midsection}}\phi = 0.250 + \Delta\Phi$$

where $\Delta\Phi$ is the error in wavelengths. The error $\Delta\Phi$ in differential phase shift gives rise to elliptical polarization instead of circular when the plate is used. Axial voltage ratio defined as the ratio of the electric field along the major axis of the ellipse to that along the minor axis is

$$A = \tan\left(|\Delta\Phi| + \tfrac{1}{4}\right)\pi \tag{7}$$

[4] C. G. Montgomery, R. H. Dicke, and E. M. Purcell, "Principles of Microwave Circuits," M.I.T. Rad. Lab. Ser., McGraw-Hill Book Co., Inc., vol. 8, pp. 386–387; 1948. Eq. (49), p. 387, appears to be a typographical error. It should have *-ctn* replaced by *tan*. As (49) is written together with (50) it would give the propagation constant for the next higher order LSE mode which is the one that evolves from the empty waveguide TE_{20} mode as dielecrtic is introduced into the waveguide. The curves on p. 386 are essentially correct except for small irregularities which are not shown. These irregularities are not important for most work. However, they are extremely important for quarter-wave plate work where the small differences between these curves and another similar set are the differential phase shifts.

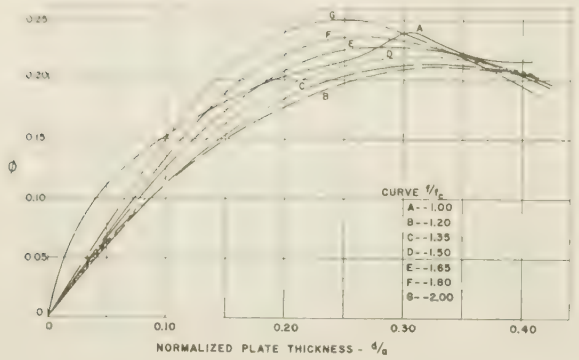

Fig. 3—Differential phase shift as a function of plate thickness for a polystyrene dielectric, $\epsilon = 2.55$, for various frequencies.

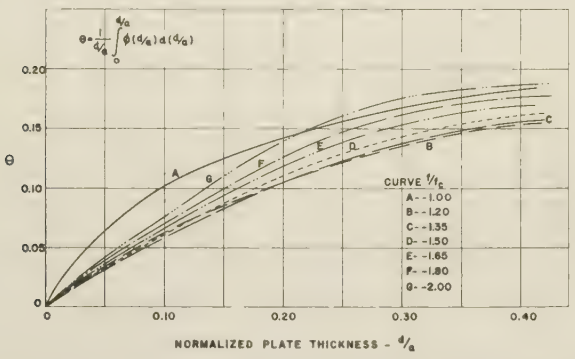

Fig. 4—Differential phase shift for a tapered plate of polystyrene as a function of the final thickness d of the taper for various frequencies.

and is plotted in Fig. 5. In practice the power going into the undesired circular polarization manifests itself as a transmission loss given by

$$P_{\text{loss}}/P_0 = \sin^2 \pi\Delta\Phi. \tag{8}$$

This loss is expressed as an insertion loss in decibels on the right-hand ordinate scale of Fig. 5.

To illustrate the design procedure, an example will be carried out. Fig. 2 indicates that $d/a = 0.40$ (curve H) gives a frequency response for a flat slab of dielectric which is nearly constant with the differential phase shift dropping slightly at higher frequencies. This is a good choice since Fig. 4 shows that the differential phase shift for tapered slabs of dielectric increases with increasing frequency for all thicknesses for f/f_c between 1.2 and 2.0. Choosing several values of L_1/L_2, the ratio of the flat length to the tapered length, and using $d/a = 0.40$, the following results are obtained for the usual bandwidth $1.2 < f/f_c < 2.0$.

$$L_1 / L_2 = 4, \qquad L_1 = 0.874a, \qquad L_2 = 0.219a,$$
$$\Delta\Phi = \pm\, 0.003.$$

Loss due to incorrect circular polarization ≤ 0.0005 db.

$$L_1/L_2 = 0, \qquad L_1 = 0, \qquad L_2 = 0.731a,$$
$$\Delta\Phi = \pm\, 0.024.$$

Loss due to incorrect circular polarization ≤ 0.025 db.

A practical aspect of the problem now arises; namely, the reflections from the ends of the dielectric. For the

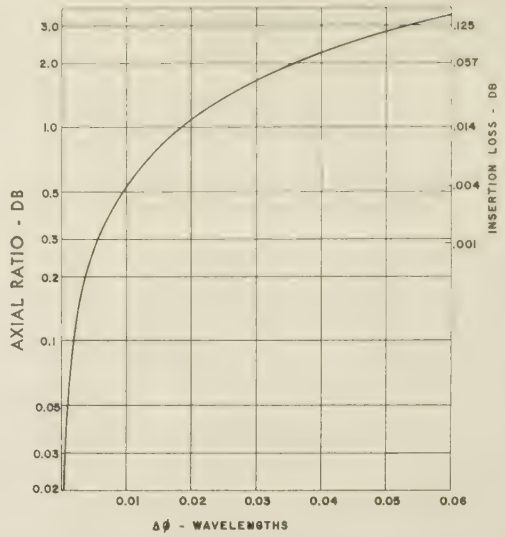

Fig. 5—Axial ratio of output from quarter-wave plate and insertion loss due to incorrect circular polarization as a function of the error in differential phase shift.

case of $L_1/L_2 = 4$, L_2 is so small that the tapers present an angle of almost 45° to the incident wave and will produce so much reflection that the device would be useless as a quarter-wave plate. On the other hand, the taper angle for $L_1 = 0$ is about 15° and the loss due to the incorrect circular polarization is still very small. Thus, from a practical standpoint, the choice $L_1 = 0$ would be much better than $L_1/L_2 = 4$ for this thickness. A quarter-wave plate was made with $L_1 = 0$, and the results will be discussed later.

In light of the reflection problem, perhaps it is better to choose a smaller value of d. Taking $d/a = 0.2$, $L_1 = 0$ then $L_2 = 1.042a$, $\Delta\Phi = \pm 0.031$, and loss due to incorrect circular polarization ≤ 0.04 db. Taper angle for this is about $5\frac{1}{2}°$ which should produce negligible reflections.

Experimental Results

A quarter-wave plate was built of polystyrene, $\epsilon = 2.55$ with $d/a = 0.40$ and $L_1 = 0$ to cover the range $1.0 < f/f_c < 2.0$. The theoretical prediction and the experimental results are shown in Fig. 6 for comparison. The experimental points were found by measuring the phase of the two orthogonal waves separately and subtracting them to obtain the differential phase shift. The experimental points represent a frequency range of 7.6 to 12.5 kmc. The only substantial disagreement with the theoretical curve is seen to be at the extremes of the curve. At these points the frequency is outside the recommended operating range of the waveguide components used. The departure of the remaining points from the theoretical curve may be attributed to internal reflections in the quarter-wave plate. These are not calculable by any simple analysis, but do not seem to be too bothersome for the tapers used.

In using such a plate, it must be made certain that equal incident amplitudes are obtained in each of the two orthogonal directions. First, the plate must be oriented at exactly 45° to the polarization of the incident linearly-polarized wave. Then, the reflections from one of the

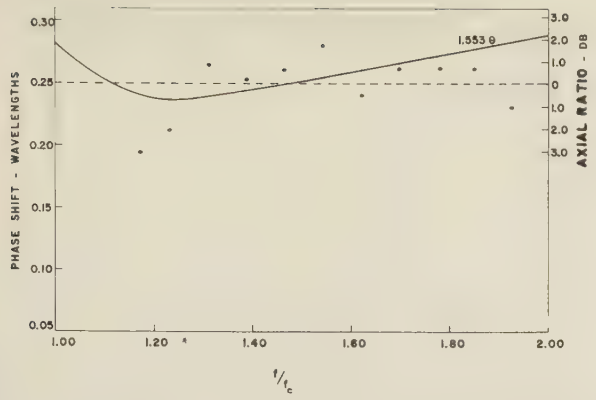

Fig. 6—Theoretical curve and experimental points for a polystyrene taper 1.553 guide widths long and 0.40 guide width thick at its thickest point.

two orthogonal directions of polarization must not be stronger than from the other. Effectively this destroys the condition of equal amplitude through the plate for the two polarizations. In measurements on circularity of the transmitted wave, this effect has been very confusing at times. In general, the only solution to this problem is to make the tapers gradual enough so that these reflections are not detrimental to the operation of the quarter-wave plate. From this standpoint, a better practical solution may well be the design given at the end of the last section for which the taper angle is only $5\frac{1}{2}°$ and the loss is less than 0.04 db. The same problems can be caused also by dielectric loss. However, polystyrene does not have enough loss to be significant in this regard. A quarter-wave plate designed for square waveguide was experimentally checked in square guide and then rechecked in a circular guide of diameter just slightly larger than the width of the square guide. Its performance in circular guide over the frequency band 8.0 to 12.5 kmc was slightly better than in square guide. This confirmed the opinion that there should be very little difference between the performance of a quarter-wave plate in square guide and in circular guide.

Another design which departs from the tapers and uses step transitions is shown in Fig. 7. The transformers on each end were arrived at by considering the match for the TE_{10} mode only since this mode is much more perturbed by the dielectric plate than the TE_{01} mode. The impedances of the steps were calculated on a power-voltage basis by considering the wave guide to be filled with some effective dielectric constant. The effective dielectric constant is found from the relation

$$\lambda_g = \lambda[\epsilon_{\text{eff}} - (\lambda/2a)^2]^{-1/2},$$

and used in the power-voltage impedance equation

$$Z_{P,v} = 2(Z_0/\sqrt{\epsilon_{\text{eff}}})b\lambda_g/a\lambda$$

which gives the impedance relation that was used,

$$Z_{P,v} = 2Z_0(\lambda_g/\lambda)^2[1 + (\lambda_g/2a)^2]^{-1/2}$$

where the guide wavelengths were found from existing curves.[4] The appropriate quarter wavelengths were also found from these curves. It is seen in Fig. 7 that this quarter-wave plate turned out quite well having an axial

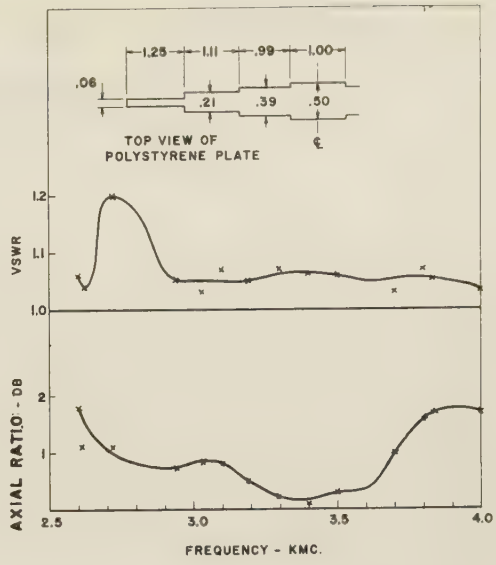

Fig. 7—Top view of step tapered polystyrene quarter-wave plate. VSWR and axial ratio of output circular polarization are given as functions of frequency. Waveguide was circular with an inside diameter of 3.125 inches.

ratio under 2 db and a vswr under 1.2 to 1 over *S* band. A study that will facilitate the design of step transitions is now being carried out by the author and others. A study that should be undertaken is that of the differential phase shift for the two orthogonal modes for a dielectric plate that is tapered in the opposite plane to the taper of Fig. 1(b). For the same taper length this type of taper gives much smaller reflections than the tapers described here. Unfortunately, calculations for this taper seem impractical to carry out. Furthermore, this taper will not carry high peak powers since, unlike the previous two tapers described, it has a region where a small air gap separates the dielectric and the waveguide. From experience, these small air gaps break down quite easily.

Conclusion

By using slabs of dielectric in a square waveguide, quarter-wave plates may be built to operate over a wide frequency band. It is shown theoretically that they can be made to operate over a 2 to 1 frequency band and there is no reason that this could not be expanded considerably. In practice, one has to consider the higher order modes that this plate would generate over such bandwidths. Experimentally, quarter-wave plates were made to operate over a standard waveguide bandwidth.

Complete design information is given for quarter-wave plates made of polystyrene. The matching problem is solved by tapering the ends for which calculations are given. The experimental results closely follow the calculated values. Experimental results also show that the quarter-wave plate action is very closely the same in circular as in square waveguide.

Acknowledgment

The author would like to acknowledge the generosity of G. Guthrie in allowing the use of his data on the step tapered plate.

Coherent Spontaneous Microwave Emission by Pulsed Resonance Excitation*

L. E. NORTON†

Summary—This paper describes an investigation of the coherent microwave emission from pulse-excited ammonia molecules. Coherent and periodic pulses of near resonance frequency and 1-μsec duration excited the gas from its initial thermal equilibrium condition. Self-induced coherent emission (molecular ringing) continued after the excitation field was removed. This radiation was observed during a period of 10 μsec. In an actual experiment performed, a new Doppler bandwidth reduction method was used in the gas cell. The observed spectral width of the ammonia 7,7 line was about 5 kc. The emission was used to stabilize the excitation signal source to a short-term frequency stability of 2×10^{-10}.

DURING the period 1952–1955, the author was concerned with an investigation of a new way to reduce the Doppler contribution to total microwave spectral line bandwidth.[1] The basic concept on which the Doppler reduction aspect hinged was due to a proposal by Dicke. In one of the Doppler reduction experiments which were performed, the signal was obtained as a small, nonsustained self-induced coherent microwave emission (frequently termed spontaneous coherent emission, or molecular ringing) from the ammonia gas. This emission was induced by coherently pulsed resonance excitation of the gas molecules. In view of the present interest in spontaneous emission and its relation to molecular and atomic oscillators and amplifiers, it appears desirable to describe these early experiments and results which have not hitherto been published. The difference between the described resonance-radiation excited nonthermal equilibrium condition and the beam deflection state separation utilized by Townes and Gordon[2] in the now well-known Maser is quite apparent. A different but related system has also been reported by Hahn,[3] and Hahn and Maxwell,[4] who used pulse-induced spin flipping in their pulse echo work. While this paper was in final stages of preparation still another publication,[5] with a vastly different point of view, made its appearance.

One of the experimental arrangements is shown in Fig. 1. The Doppler bandwidth reduction details[1] are omitted in this figure. Detailed operation of Fig. 1 is described later. For the moment, the important detail is that one of the repetitively pulsed sidebands provided microwave resonance excitation for the two quantum levels involved. Additionally, the excitation frequency was swept slowly and cyclically to record either the envelope or the dispersion of the line.

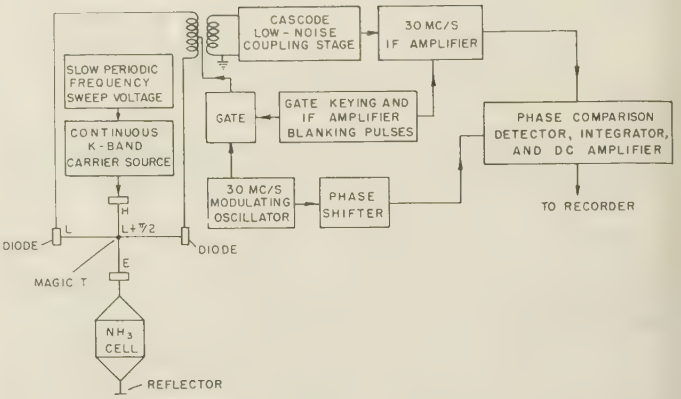

Fig. 1—Block diagram of simplified system for obtaining envelope and dispersion of spectral lines by spontaneous coherent emission.

The basic operation of Fig. 1 is shown in Fig. 2. The primary excitation field E_D was applied at $t=0$ and removed at $t=t_0$. The receiver was actuated from $t=t_0$ to $t=t_1$ so that the signal, emitted from the ringing molecules, could be obtained during this interval. The excitation was applied again and the receiver disabled at $t=t_1$ to initiate a new cycle. Solutions to this problem are contained implicitly in a paper by Dicke[6] and more specifically in a forthcoming theoretical paper by Bloom.[7] However, for the microwave region of the spectrum, and under experimental conditions which permit omission of all collision effects, it is possible to go directly, and with good approximation, to expressions for self-induced coherent emission after removal of primary drive.

A particle with unperturbed normal Hamiltonian H_0 is subjected suddenly to an excitation field which adds perturbation energy

$$V(x, t) = -eE_D x \sin \omega t. \tag{1}$$

The electric excitation field E_D is at frequency ω and its electric vector is directed along x.

Considering only two nondegenerate states at energy levels W_1, W_2, the time-dependent probability amplitudes may be put in the form

* Manuscript received by the PGMTT, May 13, 1957.
† RCA Labs., Princeton, N. J.

[1] "Investigation and Study of Practical Utilization of Molecular Absorption for Frequency Control," Contract No. DA 36-039-sc-15525, Dept. of the Army Project No. 3-99-11-021, Signal Corps Project No. 33-142B. Reps. No. 1–No. 10 for period May 1, 1952 to April 22, 1955.

[2] J. P. Gordon, H. J. Zeiger, and C. H. Townes, *Phys. Rev.*, vol. 99, pp. 1264–1274; August 15, 1955.

[3] E. L. Hahn, *Phys. Rev.*, vol. 80, pp. 580–594; November 15, 1950.

[4] E. L. Hahn and Maxwell, *Phys. Rev.*, vol. 88, pp. 1070–1084; December 1, 1952.

[5] R. H. Dicke and R. H. Romer, "Pulse techniques in microwave spectroscopy," *Rev. Sci. Inst.*, vol. 26, pp. 915–928; October, 1955.

[6] R. H. Dicke, *Phys. Rev.*, vol. 93, pp. 99–110; January 1, 1954.

[7] S. Bloom, *J. Appl. Phys.*, vol. 27, pp. 785–788; July, 1956.

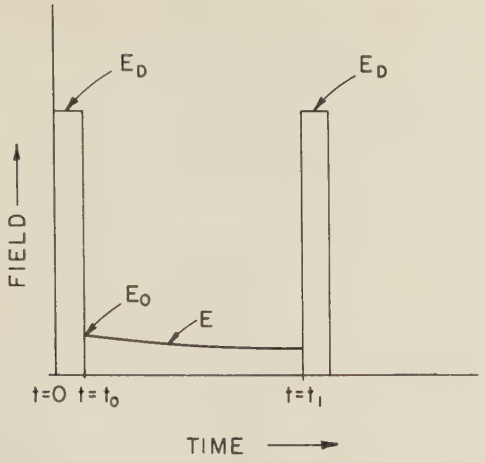

Fig. 2—Time application of coherently pulsed excitation to molecular system, and received spontaneous coherent emission. E_D is primary drive field, and E is time dependent spontaneous coherent emission field with initial value $E_0 \cdot dE/dt$ does not change sign in the particular illustration plotted.

$$\left.\begin{aligned} i\dot{a}_1 &= -\sin \omega t \quad (p_{11}a_1 + p_{12}a_2\epsilon^{-i\omega_0 t}) \\ i\dot{a}_2 &= -\sin \omega t \quad (p_{12}^{*}a_1\epsilon^{i\omega_0 t} + p_{22}a_2) \end{aligned}\right\} \tag{2}$$

where

$$p_{ij} = E_D\mu_{ij}/\hbar, \quad \text{and} \quad \omega_0 = (W_2 - W_1)\hbar.$$

The probabilities of state occupancy under initial thermal equilibrium conditions (before application of excitation) for $\hbar\omega_0/kT \ll 1$, are

$$\left.\begin{aligned} N_1(0)/N &= 1/2 + \hbar\omega_0/4kT \\ N_2(0)/N &= 1/2 - \hbar\omega_0/4kT \end{aligned}\right\} \tag{3}$$

where $N_1(0)$, $N_2(0)$ are the thermal equilibrium numbers of particles in states 1 and 2 in a system of N particles.

First, consider the case where, to the time scale of interest, particle density is chosen sufficiently small and particle container dimensions sufficiently large so that collision processes are relatively unimportant. Upon application of resonance excitation at frequency $\omega = \omega_0$ at time $t = 0$, neglecting incoherent spontaneous drop-downs in this microwave region of the spectrum, from (3) and a solution of (2), the probability of occupancy of the upper state after $t = 0$ is

$$N_2(t)/N = 1/2 - \hbar\omega_0/4kT \cdot \cos\left[(\mu E_D/\hbar)t\right] \tag{4}$$

where μ is the effective dipole moment for the transition involved.

The power input to the system of N particles just before excitation shutoff at $t = t_0$ is

$$\begin{aligned} P_{\text{in}} &= \hbar\omega_0 N \cdot d/dt[N_2(t)/N] \\ &= m\omega_0^2\mu E_D N/4kT \cdot \sin\left[(\mu E_D/\hbar)t_0\right]. \end{aligned} \tag{5}$$

Similarly, the initial power emission from the system just after excitation removal at $t = t_0$ is

$$P_0 = \hbar\omega_0^2\mu E_0 N/4kT \cdot \sin\left[(\mu E_D/\hbar)t_0\right] \tag{6}$$

where E_0 is the field initially emitted.

The value of E_0 may be obtained by noting that, after excitation shutoff, E_0 is the field in the transmission path containing the particles undergoing transitions. Hence, neglecting any field dependence as a function of position in the transmission path,

$$cE_0^2 A/4\pi = \hbar\omega_0^2\mu E_0 N/4kT \cdot \sin\left[(\mu E_D/\hbar)t_0\right]$$

and

$$E_0 = \pi\hbar\omega_0^2\mu N/ckTA \cdot \sin\left[(\mu E_D/\hbar)t_0\right] \tag{7}$$

where A is the cross sectional area of the transmission path containing the molecules.

Finally, from (6) and (7), the initial coherent power radiated by the particles at excitation shut-off is

$$P_0 = \pi(\hbar\omega_0^2\mu/2kT)^2 \cdot N^2/cA \cdot \sin^2\left[(\mu E_D/\hbar)t_0\right]. \tag{8}$$

Excitation periods given by

$$\mu E_D/\hbar \cdot t_0 = (2n + 1)\pi/2 \tag{9}$$

provide state saturation conditions (equality of state populations) and produce maximum initial coherent emission; those given by

$$\mu E_D/\hbar \cdot t_0 = (2n + 1)\pi \tag{10}$$

define "inverted" states in which the sense of population inequality is appropriate for a negative interpretation of T in the Boltzmann factor exponential.

Under conditions where collision processes may be neglected, the same simple model may be used to evaluate with good accuracy the change of coherent emission P with time from its initial value P_0. During primary excitation, transitions are induced by drive of constant amplitude; after removal of primary drive the situation is similar except that the self-induced driving field intensity changes with time. In practical cases the change is very slow on the time scale of interest, for the following interrelated reasons:

1) Available coherently pulsed microwave driving ing power is small.
2) To keep the effect of competing collision processes small, especially for electric dipole transitions, pressures must be low; even so, corresponding reasonable drive intervals are of the order of a microsecond, with following observation intervals about ten times longer.
3) Since coherent emission intensity after primary excitation removal goes as N^2, increase in A is desirable but this in turn reduces the field due to the small driving power. Without accompanying increase in the excitation power, the improvement factor is only slightly greater than unity.
4) At microwave frequencies $\hbar\omega_0/kT < 1$. Under these circumstances, the ratio of self-induced driving field to primary field is ordinarily very small. As a result, intensity changes in the self-induced driving field during the limited observation period (usually 10^{-5} seconds, or less) are very small. For this case, from (6) and by extending (6) to time after primary drive removal, we write immediately

$$P/P_0 = (E/E_0)^2$$

$$= E/E_0 \sin [(\mu E_D/\hbar \cdot t_0) - \mu E/\hbar \cdot t]/\sin [(\mu E_D/\hbar)t_0]$$

or

$$E/E_0 = \sin (\alpha - E/E_0 \cdot \mu E_0/\hbar \cdot t)/\sin \alpha \qquad (11)$$

where $\alpha = \mu E_D/\hbar \cdot t_0$, E is the self-emissive field after $t = t_0$, and P is the corresponding power.

Because E_0/E_D is so small, the departure and eventual decay with time of E from E_0, in any reasonable experimental circumstances, inevitably requires a much longer time than the primary excitation interval. Hence, eventually other competing processes (collisions, for example), which are not a part of this simple model, must be taken into account. The same slow decay also indicates that when the next coherent pulse is applied at $t = t_1$, there may still be appreciable energy storage in the particles. Results, taking into account thermal collisions, are included in the solution of Bloom.[7] In general, the effect of thermal collisions is to superpose an exponential time decay on the coherent emission.

Since reduction of Doppler contribution to spectral line bandwidth was the objective of the experiment as performed, the spectral envelopes and dispersion characteristics were displayed as functions of slowly varying excitation frequency near resonance. Hence, the time decay characteristics of the initial spontaneous coherent emission (P_0, E_0) were never observed directly.

However, the foregoing results are still directly applicable to the slowly-varying excitation frequency case. Specifically, when the excitation and resonance frequencies are identical, the initial coherent emissive power is P_0. The situation for small departures from the resonance frequency is interpreted as follows. The product terms $\epsilon^{-i\omega_0 t} \sin \omega t$, and similarly $\epsilon^{i\omega_0 t} \sin \omega t$, appear in the probability amplitude espressions of (2). Expansion of the product terms lead to sum and difference frequencies $(\omega + \omega_0)$ and $(\omega - \omega_0)$. Upon integration, the corresponding terms are $\sin (\omega + \omega_0)t \cdot 1/(\omega + \omega_0)$ and $\sin (\omega - \omega_0)t \cdot 1/(\omega - \omega_0)$. The sum frequency term may be neglected since it has little influence on the magnitudes of the time dependent probability amplitudes. The difference term $\sin (\omega - \omega_0)t \cdot 1/(\omega - \omega_0)$ in the probability amplitudes produces maxima at resonance, $\omega = \omega_0$.

Typical experimental recordings show that the results predicted by the foregoing, indeed, do have physical reality. The dispersion characteristic of the NH_3 7,7 line as a function of slowly varying excitation frequency is shown in Fig. 3. Itwas obtained as a spontaneous coherent emission in the periods $t = t_0$ to $t = t_1$ by the use of the coherently pulsed resonance excitation system of Fig. 1. The corresponding envelope appears in Fig. 4. Time intervals $t = 0$ to $t = t_0$, and $t = t_0$, to $t = t_1$ in Fig. 2 were 10^{-6} and 10^{-5} seconds, respectively, in the experiment as performed. The Doppler reduction system was designed for a spectral line bandwidth of 5 kc and was achieved by reduction of Doppler bandwidth from its normal value

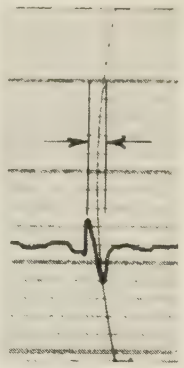

Fig. 3—5-kc bandwidth dispersion of NH_3 7,7 spectral line.

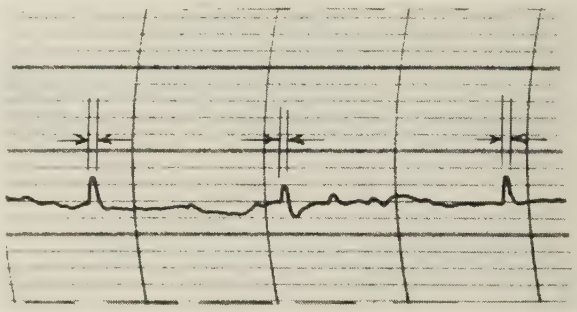

Fig. 4—5-kc bandwidth envelope of NH_3 7,7 spectral line.

of about 70 kc for ammonia at 25,000 mc and room temperature. For observation of a 5-kc-bandwidth line, bandwidth contributions due to particle-particle thermal collisions, and particle-cell wall thermal collisions, must be of the order of 5 kc or less. To achieve this condition, the ammonia pressure was about 1.85×10^{-4} mm Hg; the required 10-cm minimum cell dimension was obtained by using a cube 10 cm on a side. The corresponding total number of ammonia molecules, N', was 7.5×10^{15}. However, because of the Doppler bandwidth reduction in the experiment as performed,[1] the "molecular effectiveness" was only about 6 per cent. That is, the intensity of the reduced bandwidth signal was as if only 6 per cent of the actual total number of molecules were contributing to it.

Because of the requirement for narrow spectral distribution, and coherence in its pulsing, the K-band excitation source (Fig. 1) became rather complex. It consisted of a periodically frequency-swept 13.2+mc crystal controlled oscillator, followed by many stages of frequency multiplication with an over-all multiplication factor of 1944. The output frequency was smaller by 30 mc than 25,715+mc, the resonance frequency of the $N^{14}H_3$ 7,7 line. One simplified form of several arrangements used is shown as a block diagram in Fig. 1. The gate-keying and IF-blanking pulser opens the gate in the 30-mc oscillator output circuit, and simultaneously disables the IF amplifier during intervals $t = 0$ to $t = t_0$. Hence, continuously supplied K-band carrier and gated 30-mc output are applied to the magic-T and associated diodes, which functions as a balanced modulator during this time. The upper sideband produced by the balanced

modulator served as cell excitation. In this arrangement, application of the gated 30-mc output to the center of the transformer winding avoids (by phase balancing) overloading and delayed blocking of the cascode low-noise coupling stage in the receiving channel.

The same gate-keying and IF-blanking pulser closes the 30-mc gate, and actuates the IF amplifier during receiving intervals $t=t_0$ to $t=t_1$. Hence, the sideband intensity (excitation field E_D) becomes zero and spontaneous coherent emission from the cell and continuously applied K-band carrier output impinge on the diodes attached to the magic-T. During these intervals this unit operates as a superheterodyne mixer, supplying output to the input transformer preceding the cascode low-noise coupling stage. The push-pull to single-ended connection of the transformer in conjunction with the $\pi/2$ differential path length in the similar arms of the magic-T, insures complete uncoupling of the cascode-input circuit and gate-input circuit; hence none of the small intensity signal output is wasted in the gate-output circuit. Reference phase from the 30-mc modulating oscillator and 30-mc signal phase are compared in the phase sensitive detector, yielding output signals of the types shown in Figs. 3 and 4. To attain a favorable signal-to-noise ratio with the small signal intensity available, the signal bandwidth imposed by the integration circuit following the phase sensitive detector was made about 0.1 cycle. This required that the frequency sweep rate of the cell excitation unit be very slow; it was usually made about 1/40 cps.

Because of the nature of the primary-excitation unit and of the components available when the experiment was performed, available peak drive in the 10^{-6} second excitation periods was small. It was in the range from 10^{-4} to 10^{-5} watts, and usually was nearer the latter. Neglecting field position dependency in the cell, by assuming the mean field to prevail throughout the cube, the corresponding E_D was about 2×10^{-2} volts/cm and $\mu E_D/\hbar\cdot t_0$ was only 8.6×10^{-2}. From (4), the departure from thermal equilibrium conditions and the energy storage in the molecular system by the small perturbing resonance excitation, were slight. Unavoidably, and due only to the inadequacy of the primary excitation intensity, the initial spontaneous coherent emission, P_0, as given in (8) was small. For $E_D=2\times10^{-2}$ volts/cm, P_0 was 4.4×10^{-18} watts. Taking into account the "molecular effectiveness" in the reduced Doppler bandwidth signal,[1] even if the initial emission were completely monochromatic, and neglecting collisions, the time required for the self-induced emissive power to fall to half its initial value would be about 2.8×10^{-2} seconds. This is about 2800 ties the 10^{-5} second listening period, and therefore the change in P from P_0 was insignificant in the listening period for E_D as indicated. For a receiver noise figure of 10 and the previously mentioned 0.1-cycle signal bandwidth due to the integration circuit following the phase sensitive detector, the room temperature signal-to-noise ratio was calculated to be about 1×10^3, at best. For a variety of reasons, including the space dependency of the field in the cell, and utilization of only some of the discrete Stark components, the actual signal-to-noise ratio was always less. Assuming a worsening of the ratio, due to these causes, of somewhat less than an order of magitude, the actual signal-to-noise values as observed in Figs. 3 and 4 appear quite reasonable.

By using the received signal as a reference frequency, and assuming that the primary excitation source is servocontrolled to 1/1000 of the 5-kc spectral bandwidth (a fairly severe but reasonable assumption), by long time-averaging servoaction, the frequency stability of the excitation source is 2×10^{-10}.

Acknowledgment

The author wishes to express appreciation to Dr. D. O. North of RCA Laboratories for many helpful and stimulating discussions relating to the theoretical aspects of this problem, and to G. W. Leck, also of RCA who built much of the required specialized equipment.

Corrections

Karle S. Packard, author of "Planar Transmission Lines—Part III," a correspondence which appeared on page 163 of the April, 1957 issue of these TRANSACTIONS, wishes to make the following correction to his paper.

The quantity $\sqrt{k}$ should be replaced by $\sqrt{K}$, where K is the relative dielectric constant.

Leonard Sweet, co-author with M. Sucher of the correspondence, "The Available Power of a Matched Generator from the Measured Load Power in the Presence of Small Dissipation and Mismatch of the Connecting Network," which appeared on pages 167–168 of the April, 1957 issue of these TRANSACTIONS, has brought the following correction to the attention of the editors.

Eq. (6) on page 168 should be

$$(1-|S_{22}|^2)^2-|S_{22}|^2-|S_{11}|^2+|S_{11}S_{22}|^2 \geq 2\ \mathrm{Re}\ S_{12}{}^{*2}S_{11}S_{22}.$$

Correspondence

Determination of Equivalent Circuit Parameters*

At a given frequency, a lossless discontinuity on a transmission line may be represented by an equivalent circuit consisting of an ideal transformer and two lengths of transmission line.[1] With reference to Fig. 1, let

n = turns ratio of ideal transformer.
θ_1, θ_2 = electrical lengths of transmission lines.
ϕ_1 = electrical distance of electric field null from reference plane T_1.
ϕ_2 = electrical distance of short circuit from reference plane T_2.
Z_1 = normalized characteristic impedance of output transmission line.

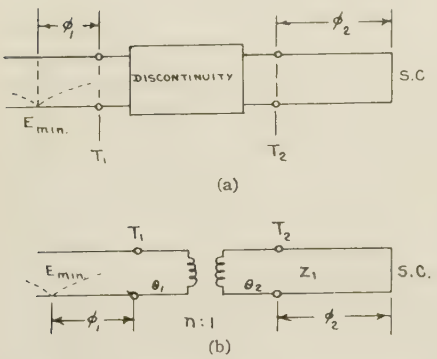

Fig. 1—A lossless discontinuity and equivalent circuit.

The field minimum position ϕ_1 is related to the short-circuit position ϕ_2 by a bilinear transformation of the form

$$\tan \phi_1 = \frac{A + B \tan \phi_2}{C + D \tan \phi_2}. \quad (1)$$

An analysis of the equivalent circuit of Fig. 1(b), shows that the field minimum position is given by

$$\tan (\phi_1 + \theta_1) = - N^2 \tan (\phi_2 + \theta_2) \quad (2)$$

where $N^2 = n^2 Z_1$.

This expression can be cast into the form of (1).

The analysis to follow will derive relations between θ_1, θ_2, N, and A, B, C, D. A plot of ϕ_1 vs ϕ_2 from (2) yields a curve of the form illustrated in Fig. 2. The curve is symmetrical about a line of slope -1 and periodic with a period π. If $N<1$, the slope of the curve at P_1 is $-N^2$ and at P_2 is $-(1/N^2)$. Also at P_2,

$$\phi_1 + \theta_1 = + n\pi + \frac{\pi}{2}$$

and

$$\phi_2 + \theta_2 = s\pi + \frac{\pi}{2}$$

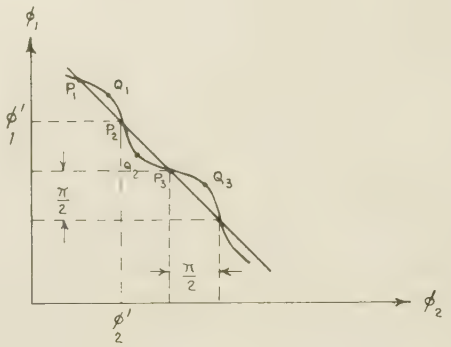

Fig. 2—Typical curve of ϕ_1 vs ϕ_2.

where n, s are suitable integers. If $N>1$, the slope at P_2 is $-N^2$ and $\phi_1+\theta_1=n\pi$, $\phi_2+\theta_2=s\pi$ at P_2. These results will be used later in the analysis.

If (1) is differentiated and the derivative $d\phi_1/d\phi_2$ equated to -1, one gets

$$1 + \tan^2 \phi_1 = \frac{(AD - BC)(1 + \tan^2 \phi_2)}{(C + D \tan \phi_2)^2}. \quad (3)$$

Eliminating ϕ_1 by means of (1) gives

$$(D^2 + B^2 - AD + BC) \tan^2 \phi_2 + (2CD + 2AB) \tan \phi_2 + (C^2 + A^2 + BC - AD) = 0. \quad (4)$$

This equation may be solved for ϕ_2 and determines the points Q_1, Q_2, Q_3 in Fig. 2. The solution is of the form

$$\tan \phi_2 = \alpha \pm \beta. \quad (5)$$

Let ϕ_{21} and ϕ_{22} be the two values of ϕ_2 obtained from (5). If these two values of ϕ_2 are averaged, either the point P_2 or P_3 is determined. One has

$$\tan (\phi_{21} + \phi_{22}) = \frac{\tan \phi_{21} + \tan \phi_{22}}{1 - \tan \phi_{21} \tan \phi_{22}} = \frac{2\alpha}{1 - \alpha^2 + \beta^2}. \quad (6)$$

When α and β are determined from (4), one gets

$$\phi_2' = \frac{\phi_{21} + \phi_{22}}{2} = \frac{1}{2} \tan^{-1} \frac{2(AB + CD)}{A^2 + C^2 - B^2 - D^2}. \quad (7)$$

As yet it is not known whether ϕ_2' corresponds to the point P_2 or P_3. However, if one takes arbitrarily, $\theta_2 = -\phi_2' + s\pi$, then from (1)

$$\phi_1' = \tan^{-1} \frac{A + B \tan \phi_2'}{C + D \tan \phi_2'} \quad (8)$$

and

$$\theta_1 = - \phi_1' + n\pi.$$

From the results presented earlier, it is noted that at the point where $\phi_1+\theta_1=n\pi$ and $\phi_2+\theta_2=s\pi$, the slope of the curve is always $-N^2$. Thus, equating the derivative $d\phi_1/d\phi_2$ to $-N^2$ at the point ϕ_1', ϕ_2' gives

$$n^2 Z_1 = N^2 = \frac{(AD - BC)(1 + \tan^2 \phi_2')}{(C + D \tan \phi_2')^2 (1 + \tan^2 \phi_1')}. \quad (9)$$

If the value of N from (9) is greater than unity, then ϕ_2' corresponds to the point P_2; if it is less than unity, ϕ_2' corresponds to the point P_1 or P_3. In either case, it is not necessary to know which point ϕ_2' corresponds to in order to determine N. Having determined one equivalent circuit from (1) by means of (7)–(9), another one may be obtained by adding transmission lines of length $\pm(\pi/2)$ to θ_1 and θ_2 and choosing a new turns ratio $n^1 = 1/nZ_1$.

Other equivalent circuits also are readily found from a knowledge of the coefficients in the bilinear transformation given in (1). Two alternatives are illustrated in Fig. 3(a) and 3(b) and their parmaeters are given by

$$X_1 = - \frac{A}{C} \quad (10a)$$

$$X_2 = \frac{A}{C} - \frac{B}{D} \quad (10b)$$

$$n^2 Z_1 = \frac{DA}{C^2} - \frac{B}{C} \quad (10c)$$

for Fig. 3(a) and by

$$X_{11} = - \frac{B}{D} \quad (11a)$$

$$X_{22} = \frac{CZ_1}{D} \quad (11b)$$

$$X_{12} = \pm \sqrt{\frac{AZ_1}{D} - \frac{BCZ_1}{D^2}} \quad (11c)$$

for Fig. 3(b).

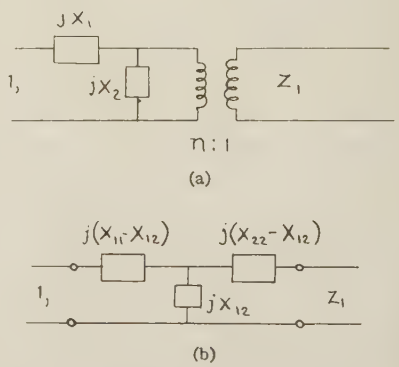

Fig. 3—Alternative equivalent circuits.

In the analysis of the equivalent circuit for slotted dielectric interfaces in free space,[2] as well as for dielectric steps in waveguides,[3] one obtains a bilinear transformation of the

* Received by the PGMTT, June 26, 1957.

[1] A. Weissflock, "Anwendung des transformersatzes über verlustlose vierpolen auf die hinter einander schaltung, von vierpolen," *Hochfreq. Tech. Elec. Akust.*, vol. 61, pp. 19–28; January, 1943.

[2] Paper in preparation by author.

[3] R. E. Collin and J. Brown, "Calculation of Equivalent Circuit of an Axially Unsymmetrical Waveguide Junction," IEE (London), Monograph No. 145R; August, 1955.

form given by (1). The above results are useful for determining the equivalent circuit parameters without the necessity of plotting the curve of ϕ_1 vs ϕ_2 and analyzing this curve by the standard procedures.

R. E. Collin,
Canad. Armament Res. and
Dev. Establ.
Valcartier, Quebec, Canada

Effect of a Mismatched Ring in a Traveling-Wave Resonant Circuit*

In traveling-wave resonant ring circuits wave amplitude "amplification" has been predicted and shown experimentally.[1-5] In the present note, the input reflection coefficient (input vswr) and wave amplification are considered when the resonant ring circuit contains a mismatch. Qualitatively a small mismatch (low vswr) can produce under resonant conditions a greatly "magnified" input vswr and reduces the maximum attainable amplification in the ring.

In Fig. 1 are shown resonant circuits consisting of ideal lossless directional couplers and a voltage mismatch Γ in each of the lossless waveguide rings. It should be noted that the designation of the output terminals of the directional couplers differ in the two circuits relative to the input terminals. Using scattering matrix notation,[6] the fundamental equations are:

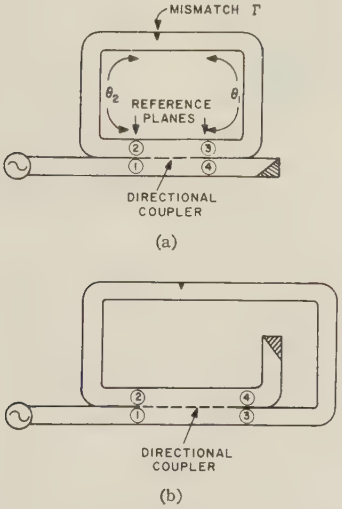

Fig. 1—Resonant ring circuits.

$$\begin{aligned} b_1 &= a_3 S_c \\ b_2 &= a_3 S_T \\ b_3 &= a_1 S_c + a_2 S_T \\ a_2 &= b_3 \tau e^{-j(\theta_1+\theta_2)} + b_2 \Gamma e^{-j2\theta_2} \\ a_3 &= b_3 \Gamma e^{-j2\theta_1} + b_2 \tau e^{-j(\theta_1+\theta_2)} \end{aligned} \tag{1}$$

where

$$\begin{aligned} S_T &\equiv S_{13} = S_{31} = S_{24} = S_{42} \\ S_c &\equiv S_{14} = S_{41} = S_{23} = S_{32} \\ |\tau| &= \sqrt{1 - |\Gamma|^2}. \end{aligned}$$

The input reflection coefficient, which exhibits a resonance phenomena when ϕ is varied, is given by:

$$\frac{b_1}{a_1} = \frac{S_c^2 \Gamma e^{-j2\theta_1}}{1 + |S_T|^2 e^{-j2\varphi} - 2|\tau S_T| e^{-j\phi}} \tag{2}$$

where

$$\phi \equiv \theta_1 + \theta_2 + \angle S_T + \angle \tau$$

$$\theta_\Gamma - \theta_\tau = \pm \frac{\pi}{2}.$$

If

$$|\Gamma| \leq \frac{|S_c|^2}{2 - |S_c|^2},$$

a single-peak resonance occurs when $\phi = 2\pi n$ radians, $n = 1, 2, 3, 4$, etc. and

$$\left|\frac{b_1}{a_1}\right| = \frac{|S_c^2 \Gamma|}{1 + |S_T|^2 - 2|\tau S_T|}. \tag{3}$$

If

$$|\Gamma| \geq \frac{|S_c|^2}{2 - |S_c|^2} \quad \text{then} \quad \left|\frac{b_1}{a_1}\right| = 1$$

when:

$$\phi = \pm \cos^{-1}\left|\frac{\tau(1 + S_T|^2)}{2S_T}\right|. \tag{4}$$

The two values of ϕ in (4) indicate double-peak resonance behavior.

Eq. (3) is plotted in Fig. 2 and shows that for small values of $|\Gamma|$, there is a reflection coefficient "magnification" of 37.9 and 5.8 for the 10- and 3-db couplers, respectively. For large values of $|\Gamma|$, the input vswr can become infinite at ring resonance, *i.e.*, when (4) is satisfied.

The wave amplification in the ring circuit is given by the following equation and is equivalent to that given by Tischer:[7]

$$\frac{b_3}{a_1} = S_c \frac{1 - |\tau S_T| e^{-j\phi}}{1 + |S_T|^2 e^{-j2\varphi} - 2|\tau S_T| e^{-j\phi}}. \tag{5}$$

Eq. (5) exhibits a single-peak maximum when $\sin \phi = 0$ and a double-peak maxima when

$$\phi = \pm \cos^{-1} \frac{|\tau S_T| + \frac{1}{|\tau S_T|} - |\Gamma| \sqrt{\frac{1}{|\tau S_T|^2} + |S_T|^2 - 2}}{2}. \tag{6}$$

It should be pointed out that for very small values of $|\Gamma|$, only a single-peak resonance exists since $\cos \phi$ of (6) exceeds unity. The maximum values of $|\Gamma|$ which will yield single-peak resonance for 10-db and 3-db couplers are 0.026 and 0.177 respectively. To a very rough approximation these values of $|\Gamma|$ are about one-half of $|S_c|^2/(2 - |S_c^2|)$. Operating under single-peak resonance conditions, the wave amplification $|b_3/a_1|$ as a function of $|\Gamma|$ is plotted in Fig. 3.

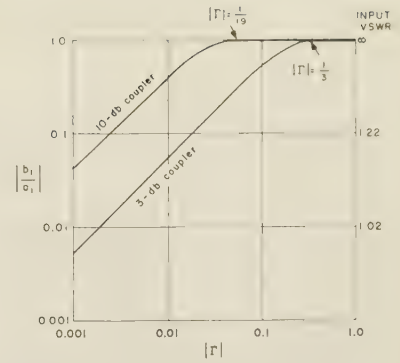

Fig. 2—Input reflection coefficient.

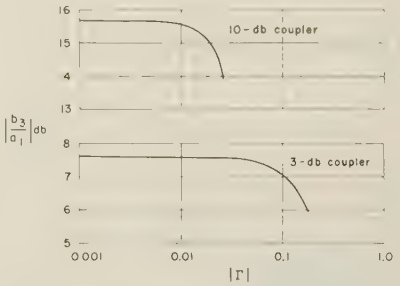

Fig. 3—Wave "amplification."

Another effect within the resonant ring due to the mismatch is on the ratio of incoming to outgoing waves at terminal 3 in Fig. 1. The analysis shows that with a 3-db coupler and when $\sin \phi = 0$,

$$\left|\frac{a_3}{b_3}\right| = \frac{\sqrt{2}|\Gamma|}{\sqrt{2 - |\tau|}} \doteq 3.42\,|\Gamma| \text{ for small values of } |\Gamma|. \tag{7}$$

Thus the vswr within the ring circuit is also "magnified." For a 10-db coupler the corresponding quantity is $19.5|\Gamma|$.

Referring to the annular-waveguide rotary joint,[2] the input vswr had a maximum value of about 3 (diagonal-arm condition) when the coupler "A" was about half open or approximately at 3-db coupling. These data would imply, referring to Fig. 2 above, that the mismatch vswr in the ring would be about 1.2 and this value appears entirely plausible.

In summary, a traveling-wave resonator requires very careful matching in the ring circuit if the input vswr is to be low and if maximum wave amplification is desired.

Kiyo Tomiyasu
GE Microwave Lab.
Palo Alto, Calif.

* Received by the PGMTT, May 31, 1957.

[1] P. J. Sferrazza, "Traveling-wave resonator," *Tele-Tech.*, vol. 14, pp. 84–85, 142–143; November, 1955.

[2] K. Tomiyasu, "A new annular waveguide rotary Joint," Proc. IRE, vol. 44, pp. 548–553; April, 1956.

[3] S. B. Cohn and F. S. Coale, "Directional channel-separation filters," Proc. IRE, vol. 44, pp. 1018–1024; August, 1956.

[4] F. S. Coale, "A traveling-wave directional filter," IRE Trans., vol. MTT-4, pp. 256–260; October, 1956.

[5] F. J. Tischer, "Resonance properties of ring circuits," IRE Trans., vol. MTT-5, pp. 51–56; January, 1957.

[6] E. W. Matthews, Jr., "The use of scattering matrices in microwave circuits," IRE Trans., vol. MTT-4, pp. 21–26; April, 1956.

[7] Tischer, *op. cit.*, (22).

Application of Rayleigh-Ritz Method to Dielectric Steps in Waveguides*

Collin and Vaillancourt[1] write that in a previous paper of mine[2]: "the coupling of the LSE modes by the step when a LSM mode is incident is neglected."

This remark is true, only in reference to the approximate numerical results obtained in my paper, but does not apply to the variational expressions. All derivations and results about the four-terminal network equivalent to the discontinuity, are perfectly general and include *Hy* as well as *Ey* modes. The summations in all the expressions in my paper extend to both types of modes.

The particular trial field chosen for the numerical computation of the admittance is such that the contribution of the *Hy* modes is zero. It is with this thought in mind that I asked the reader, at the beginning of the paper, to ignore the *Hy* modes. I did not mean to say that they are not excited. In fact, if another trial field is inserted into the expressions given for the admittances in my paper, they will yield contributions from the *Hy* modes.

It is actually very easy to show that *Hy* modes are excited at the discontinuity, simply by matching all the fields at that plane.

In my thesis at the Polytechnic Institute of Brooklyn, I discussed both types of modes. My intention in the paper, was to reduce its length to a minimum by not including the *Hy* mode functions.

This opportunity to point out the generality of the theory and the limitations of the numerical results, I owe to Dr. Collin who, before the publication of his paper, called my attention to the possibility of misinterpreting the statement in mine.

CARLOS M. ANGULO
Brown University
Providence, R. I

* Received by the PGMMT, June 21, 1957.

[1] R. E. Collin and R. Vaillancourt, IRE TRANS., vol. MTT-5, pp. 177–184; July, 1957.

[2] C. M. Angulo, "Discontinuities in a rectangular waveguide partially filled with dielectric," IRE TRANS., vol. MTT-5, pp. 68–74; January, 1957.

Contributors

Wesley P. Ayres (M'56) was born on September 26, 1924, at Los Angeles, Calif. He served as an electronic technician aboard a destroyer during World War II. He returned to college in 1948 and received the B.S. degree in physics from Fresno State College in 1951. He then entered Stanford University where he received the M.S. degree in 1953, and the Ph.D. degree in physics in 1954. In 1954, he joined the Electronic Defense Laboratory of Sylvania Electric Products, Inc., Mountain View, Calif., where he engaged in ferrite research at Microwave frequencies. In 1956, Dr. Ayres helped to found Microwave Engineering Laboratories, Inc., Palo Alto, Calif., where he is presently doing research on microwave components.

W. P. AYRES

Dr. Ayres is a member of RESA and the American Physical Society.

❖

Saul M. Bergmann (M'56) was born in Antwerp, Belgium, on September 7, 1927. He graduated in electrical engineering from the Institute of Technology, Haifa, Israel, in 1951. He then joined the Societe Belge-Radio-Electrique in Brussels.

S. M. BERGMANN

From 1953 to 1956 he did postgraduate work in physics at the University of London under R. Furth. He then joined the Microwave Research Institute in Brooklyn as Research Associate. He is currently employed by the Raytheon Manufacturing Company doing work on microwave ferrite devices with the Special Microwave Device Group.

❖

Kenneth R. Bushore was born in San Diego, Calif. on April 27, 1915. After graduating from the Navy's Radio Materiel Schools at Chicago, Ill., Del Monte, Calif., and Treasure Island, Calif., he served as an electronic technician with the Pacific fleet during World War II.

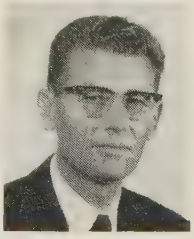

K. R. BUSHORE

In 1949, Mr. Bushore was employed by the Navy Electronics Laboratory, San Diego, Calif., where he engaged in microwave research and development as a member of the Microwave Components Group of the Radar Branch from 1950 until early 1957. He is currently a member of a newly organized group at N.E.L. which is investigating optical system applications for radar use.

❖

Robert S. Elliott (A'51–SM'53) was born in Brooklyn, N. Y., on March 9, 1921. He was a Pulitzer Scholar at Columbia University, New York, N. Y., where he received the A.B. degree in 1942 and the B.S. degree in 1943.

From 1943 to 1946, he was employed by the Applied Physics Laboratory of Johns Hopkins University, serving as a junior engineer on problems in radar, guided missiles, and the proximity fuse. In 1946, he became a member of the electrical engineering staff at the University of Illinois, where his duties included undergraduate and graduate teaching and research in antennas and microwave tubes. While at Illinois he received the M.S. degree in 1947, and the Ph.D. degree in 1952.

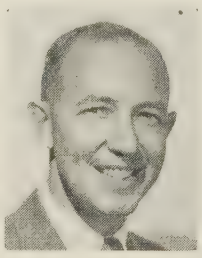

R. S. ELLIOTT

Summer employment in the antenna groups at Sperry Gyroscope Co. in 1949, and North American Aviation, in 1950, supplemented his Illinois employment. Upon leaving Illinois in 1952, Dr. Elliott served one year of active duty in the U. S. Navy and then joined the technical staff of the Hughes Aircraft Company, where he was in charge of the antenna research section of the Microwave Laboratory. At Hughes, Dr. Elliott specialized in surface wave antennas and uhf arrays. He is presently technical director and vice-president of the RANTEC Corporation.

He is a member of Tau Beta Pi and Sigma Xi.

❖

Elizabeth Laverick (SM'55) was born in Amersham, Buckinghamshire, England in November, 1925. She received the B.S. degree in physics from Durham University in 1946, and the Ph.D. degree in 1950. From 1950 to 1953, she worked at the Research Laboratories of the General Electric Company, Ltd., at Stanmore, Middlesex, in charge of a section on microwave antennas. In Decem-

E. LAVERICK

ber, 1953; she joined Elliott Brothers (London), Ltd., where she is head of the research group in the Microwave Division of that company. This group is currently engaged on investigation into microstrip, ferrite devices, antenna design and millimeter wave techniques.

Miss Laverick is an associate member of the IEE and Institute of Physics.

❖

Lowell E. Norton was born on August 12, 1909, in Arlington, Minn. He received the B.S. degree in electrical engineering in 1932, and the M.S. degree in communications in 1935, both from the University of Minnesota.

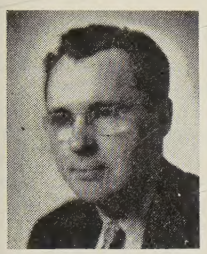

L. E. Norton

He entered the services of the Research Division of the RCA Manufacturing Company at Camden, N. J., in 1935, and since 1942, has been at RCA Laboratories, Princeton, N. J.

Mr. Norton is a member of Sigma Xi.

❖

Karle S. Packard (M'50–SM'56) was born in Boston, Mass., on July 15, 1921. He received the A.B. degree in physics in 1943 from Columbia University and the M.S. degree in physics in 1951 from New York University. During 1943–1944, he worked on the development of the magnetic airborne detector at Columbia University's Division of War Research. From 1944 to 1946, he was employed by the National Carbon Company where he worked on the proximity fuze and later on dielectric heating.

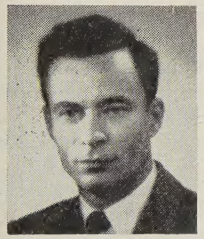

K. S. Packard

In 1946, Mr. Packard joined Airborne Instruments Laboratory, Mineola, N. Y., as a project engineer. He has been responsible for the development of equipment for magnetic surveying, automatic swr and impedance plotting, and video recording and reproduction. More recently he has been engaged in the development of microwave systems and components, particularly in the field of strip transmission lines. In 1955, he was appointed consultant to the newly formed Special Systems and Components Department.

He is a member of the American Physical Society.

❖

Peter A. Rizzi (S'50–A'54–M'57) was born in Providence, R. I., on December 10, 1930. He received the B.S. degree with high honors from the University of Rhode Island in 1951, and the M.E. and D.E. degrees in electrical engineering from Yale University in 1952 and 1955. During his graduate studies, he received the Yale University Scholarship and the Charles LeGeyt Fortescue Fellowship. Since August, 1954, Dr. Rizzi has been engaged in the development of microwave components at the Missile Systems Division of the Raytheon Manufacturing Company where he is presently head of the ferrite section.

P. A. Rizzi

Dr. Rizzi is a member of Phi Kappa Phi, Sigma Xi, and Tau Beta Pi.

❖

Florian Shnurer was born on May 29, 1929, in Blakely, Pa. He entered Union College in 1946 and received the B.S.E.E. degree in 1950. In 1952, he received the M.S. degree from Northwestern University, Evanston, Ill., for which he did research in coated conductor antennas. He is a candidate for a Ph.D. from the same university.

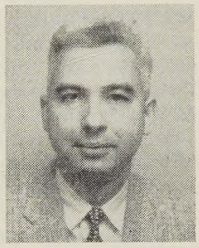

F. Shnurer

From 1950 to 1954, he was a research associate in the Microwave Laboratory at Northwestern University, where he did research in microwave antennas.

In 1954, Mr. Shnurer joined the General Electric Advanced Electronics Center at Cornell University as an engineer in the Electronic Warfare Subsection where he is presently engaged in working on special microwave circuits.

He is a member of Sigma Xi, RESA, and Eta Kappa Nu.

❖

Wallis L. Teeter (A'47–SM'53) was born in Kansas in 1923. He received the B.S. degree from Kansas State College in February, 1947.

W. L. Teeter

From 1944 to 1946, while in the Navy, he was in the Centimeter Wave Research Section at the Naval Research Laboratory in Washington, D. C. He joined the U. S. Navy Electronics Laboratory in 1947, where he was a group leader in the Radar Equipment Section in charge of uhf and microwave component design for the Radar Branch. In 1956, he joined the Palo Alto Research Laboratory of Lockheed Missile Systems Division where hs is presently a group leader in the Radar and Data Link Department.

Mr. Teeter is a registered professional engineer and a member of Eta Kappa Nu and Sigma Tau.

❖

Lucien G. Virgile was born in New York, N. Y., on January 11, 1925. He received the Bachelor degree in aeronautical engineering from the Polytechnic Institute of Brooklyn in 1944 and the M.S. degree in mechanical engineering from Stanford University in 1948. He was engaged as a materials and process engineer for the Bell Aircraft Corporation from 1944 to 1945, and as a structural design engineer for Fairchild Aircraft Corporation from 1946 to 1947. From 1948 to 1949, he was associated with the George S. May Company as a consulting engineer and subsequently was owner-manager of a design studio for four years. Since 1953, Mr. Virgile has been employed by the Sperry Gyroscope Company where he is presently product engineer responsible for mechanical engineering development and production of a wide variety of microwave systems and components.

L. G. Virgile

Mr. Virgile is a member of Tau Beta Pi.

Index to Nontechnical Subjects

INSTITUTIONAL LISTINGS

The IRE Professional Group on Microwave Theory and Techniques is grateful for the assistance given by the firms listed below, and invites application for Institutional Listing from other firms interested in the Microwave field.

COLLINS RADIO CO., Cedar Rapids, Iowa
Complete Industrial Microwave, Communication, Navigation and Flight Control Systems

HUGHES AIRCRAFT COMPANY, Culver City, California
Radar Systems, Guided Missiles, Antennas, Radomes, Tubes, Solid State Physics, Computers

MARYLAND ELECTRONIC MANUFACTURING CORPORATION, College Park, Md.
Development and Production of Microwave Antennas and Waveguide Components

MICRODOT, INC., South Pasadena, Calif.
Microminiature Coaxial Connectors, Cables, and Assemblies

MICROWAVE TUBE LAB., SYLVANIA ELECTRIC PRODUCTS, INC.
500 Evelyn Ave., Mountain View, Calif.
Traveling Wave Tubes, Backward Wave Oscillators (Helix and Oscillators), Klystrons

NATIONAL INSTRUMENT CO., INC., 23 E. 26 St., New York, N. Y.
Wide-Band Microwave Equipment, Simulated Flight Instruments, Lobe Switches, Custom Built Precision Apparatus

WEINSCHEL ENGINEERING CO. INC., Kensington, Md.
Attenuation Standards, Coaxial Attenuators and Insertion Loss Test Sets

WHEELER LABORATORIES, INC., 122 Cutter Mill Road, Great Neck, N. Y.
Consulting Services, Research & Development, Microwave Antennas & Waveguide Components

The charge for an Institutional Listing is $50.00 per issue or $140.00 for four consecutive issues. Applications for Institutional Listings and checks (made out to the Institute of Radio Engineers) should be sent to Mr. L. G. Cumming, Technical Secretary, Institute of Radio Engineers, 1 East 79th Street, New York 21, N. Y.

Call for Papers

1958 PGMTT NATIONAL SYMPOSIUM

The 1958 PGMTT National Symposium will be held on May 5-7 at Stanford University, Stanford, Calif. Authors should submit 100-word abstracts and 500-word summaries (*both in triplicate*) prior to January 15, to Dr. K. Tomiyasu, Chairman, Technical Program Committee, 601 California Avenue, Palo Alto, Calif.

1958 PGMTT NATIONAL SYMPOSIUM

The 1958 PGMTT National Symposium to be held on May 5-7 at Stanford University, Stanford, Calif., has been announced by the General Chairman, Dr. Arthur L. Aden. Papers covering the fields of microwave physics and applications, microwave components, and microwave techniques are solicited. Authors should submit 100-word abstracts and 500-word summaries (*both in triplicate*) prior to January 15, to Dr. Kiyo Tomiyasu, Chairman, Technical Program Committee, 601 California Avenue, Palo Alto, Calif.

NOTICE TO ADVERTISERS

Effective immediately the IRE TRANSACTIONS on Microwave Theory and Techniques will accept display advertising. For full details contact the Editor of these TRANSACTIONS.

STOCK DELIVERY

PROVEN...

RELIABILITY ✓

ECONOMY ✓

VERSATILITY ✓

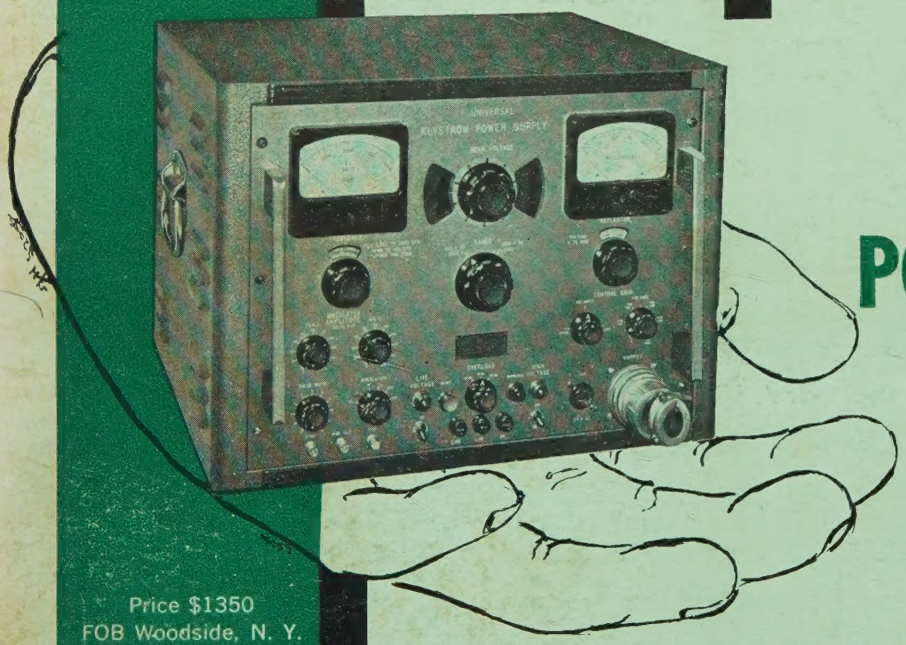

Price $1350
FOB Woodside, N. Y.

FXR Universal KLYSTRON POWER SUPPLY

Whether meter or millimeter measurements are contemplated, no microwave laboratory is complete without the FXR 'Z815B' Universal Klystron Power Supply. Unsurpassed for proven dependability and versatility, this supply incorporates the many qualities that have made FXR craftsmanship and 'know how' ...the standard in the industry.

FXR TYPE Z815B—SPECIFICATIONS

OUTPUT					MODULATION				
TYPE	VOLTAGE (volts)	CURRENT (milliamperes)	INTERNAL IMPEDENCE (ohms)	ADDITIONAL SPECIFICATIONS	TYPE	FREQUENCY RANGE (cps)	NOMINAL VOLTAGE (volts)	RISE TIME (microsecends, max.)	FALL TIME (microsecends, max.)
Beam	200 to 2000 1800 to 3600	0 to 125 0 to 100 to 2500V 250 W to 3600V	0.5 max. from 0 to 10,000 cps	Voltage Dial Accuracy: ± 1% Resolution: 0.5 volts Regulation: 0.03% from 105 to 125 volts Ripple: 3 mv rms, max.	Square Wave	250 to 2500	0 to 200	1.0	1.0
Reflector	Negative 0 to 1000		1,000,000 min.		Pulsed Wave	1 to 10 microseconds pulse width	0 to 200	1.0	1.0
Control Grid	Positive 0 to 150 Negative 0 to 300	0 to 5	0 to 30,000	Regulation: 0.03% from 105 to 125 volts Ripple: 3 mv rms, max.	Sine Wave	line frequency	0 to 200		
Filament	6.3	3 amperes		Unregulated	Saw Tooth Wave	40 to 120	0 to 200	Variable	30

DIMENSIONS (inches)	Width: 21¾ Height: 15¾ Depth: 18	OVERLOAD PROTECTION	AC Line: Fuse, 8 amperes, (both sides of line) HV Line: Fuse, 4 amperes DC HV Line: Variable overload relay 25, 65, & 125 ma or as desired by user
POWER	105 to 125 volts, 50-60 cps, 300 to 800 watts		

Data subject to change without notice.

ELECTRONICS & X-RAY DIVISION · F·R MACHINE WORKS, INC. ·

Electronics & X-Ray Division

FR MACHINE WORKS, INC.

26-12 Borough Place, Woodside 77, New York

Write Today...
for your new catalog of Precision Microwave Test Equipment.